# Developing Resilient Infrastructure for Low-Carbon Heating: Concrete Linings for Underground Thermal Energy Storage (UTES) System


**Ashraf Essa**

**Department of Civil and Environmental Engineering**

**University of Strathclyde, Glasgow**


**Thesis submitted to the Department of Civil and Environmental Engineering, University of Strathclyde, Glasgow, in fulfilment of the requirements for the degree of Doctor of Philosophy**

**March 2026**

**Declaration of Authenticity and Author's Rights**

This thesis is the result of the author's original research. It has been composed by the author and has not been previously submitted for examination, which has led to the award of a degree. The copyright of this thesis belongs to the author under the terms of the United Kingdom Copyright Acts as qualified by University of Strathclyde Regulation 3.50. Due acknowledgement must always be made of the use of any material contained in, or derived from, this thesis.

Signed:

Date: 02/03/2026

**Acknowledgements**

I would like to express my sincere gratitude to all those who contributed to the completion of this PhD.

First and foremost, I thank Dr. Shangtong Yang, my primary supervisor, for his invaluable guidance, continuous support, and constructive feedback throughout this research. His expertise and mentorship were fundamental to the development and quality of this work.

I thank the Ministry of Higher Education in Libya and the Libyan Embassy in London for their support. I also appreciate Dr. Jannik Giesekam and Dr. Huachuan Wang for their guidance.

Finally, I thank my wife and daughters for their support, patience, and encouragement, which made this journey possible.

**Abstract**

Underground thermal energy storage (UTES) systems offer a promising pathway for large-scale seasonal energy storage. However, the long-term structural performance and environmental impacts of subsurface infrastructure remain insufficiently understood. In mine-based UTES, shaft linings are subjected to combined geostatic and thermo-mechanical loading. At the same time, they influence operational heat losses. Material selection is critical for both system reliability and sustainability. This thesis investigates the mechanical, thermal, and environmental performance of concrete shaft lining materials for UTES. It places particular emphasis on a hybrid fibre-reinforced concrete incorporating basalt and polypropylene fibres.

An experimental programme characterised compressive strength, splitting tensile behaviour, crack-control response, and thermal conductivity. It is considered conventional, nominal, and hybrid fibre-reinforced concrete mixes representative of UTES shaft linings. Results show that fibre reinforcement alters failure mechanisms and cracking behaviour. This change promotes improved stress redistribution and reduces brittleness. Fibre reinforcement also influences thermal conductivity due to changes in matrix densification and interfacial bonding. These findings highlight trade-offs between mechanical performance enhancement and thermal behaviour that directly affect UTES operation.

A UTES-specific life-cycle assessment (LCA) framework was developed to assess the environmental implications of these material-level differences. The analysis used a cradle-to-operation system boundary (A1–A3 + B1). Experimentally measured thermal conductivity values were included in use-phase modelling to quantify operational heat losses from shaft linings. LCA results indicate that raw material production, particularly cement manufacture, dominates environmental impacts. Use-phase impacts are sensitive to assumptions about lining thermal performance and energy supply. The analysis reveals trade-offs between increased embodied emissions from fibre reinforcement and changes in operational energy demand.

The novelty of this research is not in developing a new LCA theory. Instead, it lies in creating a UTES-specific assessment framework that integrates experimental material performance with system-level environmental evaluation. By linking material-scale behaviour to operational and environmental outcomes, this thesis offers a stronger basis for evaluating and comparing lining materials for sustainable underground thermal energy storage systems.

## Table of Contents

**List of Figures**

**List of Tables**

## List of Symbols and Abbreviations

### Abbreviations

| | |
|---|---|
| ATES | Aquifer Thermal Energy Storage |
| BTES | Borehole Thermal Energy Storage |
| CFD | Computational Fluid Dynamics |
| GW | Global Warming |
| GWP | Global Warming Potential |
| HTC | Hydro–Thermal–Chemical |
| ICE | Inventory of Carbon and Energy |
| LCA | Life Cycle Assessment |
| LCI | Life Cycle Inventory |
| LCIA | Life Cycle Impact Assessment |
| MTES | Mine Thermal Energy Storage |
| MWh | Megawatt-hour |
| OAT | one-at-a-time |
| OPC | Ordinary Portland Cement |
| PCE | Polycarboxylate Ether |
| PCM | Phase-Change Material |
| PCMs | Phase-Change Materials |
| PV | Photovoltaic |
| ROI | Return-On-Investment |
| RMS | Raw Material Supply |
| ROW | Rest-of-World |
| SCMs | Supplementary Cementitious Materials |
| UTES | Underground Thermal Energy Storage |
| V2G | Vehicle-to-Grid |

# Chapter 1: Introduction

## 1.1 Background

As the United Kingdom increasingly shifts toward wind power, particularly in Scotland, new opportunities arise to harness surplus wind energy that would otherwise be curtailed. According to National Grid's Future Energy Scenarios (2021), the UK will require approximately 13 GW of energy storage capacity by 2030 to support a net-zero electricity system. Looking further ahead, the government's Clean Power 2030 Action Plan anticipates that between 40 and 50 GW of flexible and long-duration storage capacity will be required by 2050 to maintain system reliability during extended periods of low renewable output (National Grid ESO, 2021; HM Government, 2023).

Existing energy storage technologies, including lithium-ion batteries, hydrogen, pumped hydro, gravity-based storage, and compressed air energy storage, face a range of constraints such as high capital costs, limited geographical applicability, scalability challenges, and environmental trade-offs (Khosravani, Billings and Powell, 2026). In contrast, converting curtailed wind energy into heat and storing it underground is comparatively cost-effective, technologically simpler, and scalable to multi-gigawatt capacities (Desguers, Lyden and Friedrich, 2024). Thermal energy can be stored more economically and with fewer resource constraints than electricity, particularly when deployed on a large scale (Yang et al., 2021).

The global imperative to decarbonise energy systems has intensified in response to the acceleration of climate change (IPCC, 2018), growing geopolitical energy insecurity, and the depletion of finite fossil fuel resources (Höök & Tang, 2013).

Consequently, nations are rapidly advancing clean energy strategies to meet both immediate policy objectives and long-term climate commitments. Within this context, the United Kingdom has committed to achieving net-zero greenhouse gas emissions by 2050 (Castle & Hendry, 2024).

However, the challenge remains substantial: the built environment alone accounts for approximately 70 % of the UK's total energy consumption (Clarke et al., 2008), with an estimated 50 GW of annual energy demand dedicated to space heating and electricity across domestic, public, and commercial sectors. Alarmingly, only around 6 % of this demand is currently met through renewable sources (UK Biomass Strategy, 2023), highlighting the urgency for systemic reform and the large-scale adoption of low-carbon technologies. The rapid expansion of renewable energy generation has therefore created an urgent need for innovative energy storage solutions capable of absorbing surplus renewable electricity. Among the available options (Ergun et al. 2025), Underground Thermal Energy Storage (UTES) is increasingly recognised for its potential to enhance energy system resilience and flexibility by temporally decoupling energy supply from demand (Fry et al., 2024).

UTES technologies—namely Borehole (BTES), Aquifer (ATES), and Mine (MTES) systems—enable the seasonal storage of thermal energy by capturing excess heat during periods of low demand or high renewable output and supplying it during peak demand periods (Fry et al., 2024. This approach facilitates the integration of intermittent renewable energy sources, reduces peak loads on heating infrastructure, and decreases reliance on fossil fuels. Among these UTES variants, MTES is particularly promising in regions with extensive legacy mining infrastructure. Abandoned and flooded coal mines offer large subterranean volumes, natural insulation, and hydraulic connectivity, making them well-suited for use as large-scale thermal batteries (Turner et al., 2020).

Within this context, mine shafts offer a particularly attractive option. Shafts are typically structurally well defined, vertically oriented, and relatively isolated from surrounding rock masses, thereby reducing thermal losses (Deeming et al., 2025). According to Historic Environment Scotland records, the Barony Colliery in Scotland—one of the deepest mines in the region—contains twin shafts, each approximately 7 m in diameter and over 500 m deep

(Historic Environment Scotland, Canmore database). These shafts alone could accommodate up to 20,000 m³ of water at temperatures ranging from 10 °C to 25 °C. Heating such a volume to 40 °C, which is suitable for low-carbon heat pump systems, would require approximately 670 MWh—equivalent to only around 1/180 of the excess wind energy currently curtailed in the region.

Given that a substantial proportion of the UK's onshore wind capacity is deployed in Scotland—particularly across the Central Belt (DESNZ, 2024)—and that this region overlies the extensively mined Midland Valley coalfield containing large volumes of abandoned underground workings (Younger, 2016; Monaghan et al., 2017; BGS, 2020), the technical and geographical potential for Mine Thermal Energy Storage (MTES) deployment is considerable. Furthermore, around 25 % of the UK population resides in former mining districts, making distributed thermal storage networks a realistic option for supporting urban low-carbon heat systems. The repurposing of abandoned mines for thermal energy storage not only capitalises on existing infrastructure but also aligns with circular economy principles and regional economic regeneration objectives (Krzemień et al., 2023).

However, the long-term viability of MTES systems depends critically on the performance and integrity of concrete shaft linings, which are exposed to repeated thermal cycling, hydraulic pressure, and chemical degradation over decades of operation (Wang et al., 2025). Most existing shaft linings were originally designed for structural containment and groundwater ingress prevention rather than for thermal performance (Hentrich et al., 2019). Consequently, the combined mechanical and thermal stresses associated with cyclic heat storage may induce material fatigue, thermal cracking, and progressive deterioration, potentially compromising storage efficiency and long-term system durability. In addition, conventional cementitious materials exhibit limited thermal insulation capacity and are susceptible to degradation under prolonged exposure to fluctuating thermal and moisture conditions (Zhang, Barbhuiya & Darliev, 2024).

Beyond these engineering challenges, there remains a critical need for a comprehensive Life Cycle Assessment (LCA) to evaluate the environmental performance of emerging MTES systems. Without integrating material innovation with robust environmental impact assessment across the system life cycle, the economic viability and environmental sustainability of MTES technologies may be significantly undermined.

## 1.2 Research Significance

This study contributes to several interconnected fields, including civil engineering, energy infrastructure, materials science, and environmental assessment. From a technical perspective, it advances understanding of the behaviour of hybrid fibre-reinforced concrete under complex thermo-mechanical and environmental loading conditions. From an environmental standpoint, it supports the selection of more sustainable materials for clean energy storage applications. Strategically, the study addresses a critical barrier to the implementation of large-scale thermal energy storage and contributes to the United Kingdom's transition toward a net-zero carbon economy. By enabling long-duration thermal energy storage within mine shafts using durable lining materials, this research supports the repurposing of existing infrastructure, reduces reliance on costly new energy assets, and facilitates more effective integration of renewable electricity into district heating networks.

## 1.3 Aim and Objectives

The aim of this study is to investigate the long-term performance of lining materials used in UTES under in-situ operating conditions and to develop a LCA framework for UTES applications. Both traditional lining materials and advanced fibre-reinforced concrete linings incorporating hybrid basalt and polypropylene fibres are examined. The investigation focuses on mechanical and thermal properties relevant to resistance against repeated thermal cycling and environmental degradation typical of MTES environments. In parallel, an LCA framework is developed to evaluate the environmental performance of UTES systems, providing a quantitative analysis of carbon emissions associated with this emerging energy storage technology.

To achieve this aim, the study pursues the following specific objectives:

- To investigate the mechanical and thermal properties of traditional concrete and advanced cementitious composites reinforced with basalt fibres, polypropylene fibres, and hybrid configurations under UTES-relevant conditions.
- To compare the performance of various fibre-reinforced formulations through laboratory testing, including compressive strength, thermal conductivity, modulus of rupture, shrinkage resistance, and permeability.
- To conduct a comprehensive LCA to quantify the environmental impacts of each formulation from raw material extraction through operation, with particular emphasis on global warming potential and energy demand.
- To simulate long-term environmental exposure through accelerated ageing tests, including thermal cycling, wet–dry transitions, and environmental fatigue loading.
- To propose design guidelines for optimal material selection in MTES systems, thereby providing a practical link between materials research and engineering implementation.

## 1.4 Research Problem

Although UTES—and particularly MTES—offers a scalable and cost-effective pathway toward low-carbon heating, the large-scale deployment of such systems is constrained by material limitations associated with the concrete linings of underground shafts. Traditional lining materials are often inadequate to simultaneously meet the demands of thermal insulation, structural stability, and long-term durability under harsh subsurface conditions. Failure to address these limitations may lead to significant energy losses, safety risks, and increased maintenance costs.

Furthermore, there is a limited understanding of how advanced fibre-reinforced concrete materials perform under the coupled thermal and mechanical loading conditions relevant to UTES applications. The central challenge, therefore, lies in engineering cementitious composites that are not only thermally and mechanically robust but also environmentally sustainable and economically viable over a multi-decade service life.

Another associated problem is the absence of a standardised framework for assessing the life cycle environmental impacts of UTES systems. While several studies have examined individual technical or environmental aspects of UTES, these investigations remain fragmented and inconsistent in terms of system boundaries, impact categories, and assessment methodologies. As a result, meaningful comparison across studies is limited, and the development of environmentally optimised and economically sustainable UTES solutions is hindered. In particular, the environmental footprint of storing heat in abandoned mine shafts—especially when comparing alternative concrete lining materials—remains underexplored. There is currently no comprehensive LCA framework that captures the specific characteristics of MTES systems, including underground construction, long-term thermal cycling, and the interaction between concrete composition, energy losses, and operational emissions.

This methodological gap restricts the ability to evaluate trade-offs, identify environmental hotspots, and support material selection and policy decisions using robust sustainability data.

## 1.5 Scope of Thesis

This study is organised into six chapters:

Chapter 1 – Introduction: Presents the background and context of the study, defines the research problem, and outlines the research aim, objectives, and overall study structure.

Chapter 2 – Literature Review: Reviews state-of-the-art knowledge on UTES technologies, abandoned mine reuse, fibre-reinforced concrete behaviour under thermal and mechanical loading, and LCA methodologies. The research gaps are identified and summarised.

Chapter 3 – Methodology: Describes the mix design, experimental procedures, durability testing framework, and LCA methodology adopted in this study.

Chapter 4 – Characterisation of Physical, Material, and Mechanical Properties of UTES Linings: Presents experimental results on strength, stiffness, thermal conductivity, and expansion characteristics, alongside analysis of long-term degradation under UTES-like conditions.

Chapter 5 – Life Cycle Assessment: Evaluates the environmental trade-offs associated with the proposed lining materials, focusing on emissions, energy demand, and resource use across different UTES configurations.

Chapter 6 – Conclusions and Recommendations: Summarises the key findings, identifies limitations, and outlines directions for future research and practical implementation in MTES systems.

# Chapter 2: Literature review

## 2.1 Background

This chapter provides the background and context necessary for evaluating the performance of concrete linings used in UTES systems, with particular emphasis on shaft linings. The review begins by examining the development and durability of concrete lining materials intended to enhance the efficiency and service life of UTES infrastructure. This is followed by a discussion of the operational mechanisms of UTES systems, including temperature cycling, performance requirements, and end-user demands. A comprehensive overview of UTES functions and benefits is then presented, highlighting their capacity to store and regulate thermal energy through repeated heating and cooling cycles. The role of UTES in supporting renewable energy integration is also addressed, particularly in reducing reliance on fossil fuels and minimizing carbon emissions in district heating applications.

The chapter further explores the challenges faced by UTES systems arising from thermal fluctuations, which can compromise the integrity of concrete linings through degradation, cracking, and heat losses associated with insufficient insulation. LCA methodologies are reviewed to evaluate UTES systems from a long-term environmental and economic perspective. The chapter then compares conventional mine lining materials with advanced alternatives designed to withstand thermal and mechanical stresses, critically assessing their effectiveness in improving toughness, durability, and long-term performance. Finally, the chapter identifies key research gaps and outlines the specific research questions addressed in this study. The overall structure of the chapter is illustrated.

## 2.2 Utilising UTES systems

Heat generation currently accounts for approximately 50% of total energy consumption in the UK, with the majority still produced through the combustion of fossil-based natural gas (Gluyas et al., 2023; Gluyas, Adams and Wilson, 2020). UTES systems offer a sustainable and innovative approach to thermal energy management by exploiting the Earth's natural insulating properties [Loria, 2021; Holechek et al., 2022]. These systems store surplus heat during periods of low energy demand, such as summer months or off-peak hours, and release it during periods of higher demand, including winter seasons and peak usage periods. This process enables a more balanced and efficient energy supply (Gluyas, Adams and Wilson, 2020). Common UTES technologies include borehole thermal energy storage (BTES), Aquifer Thermal Energy Storage (ATES), and mine water–based storage systems.

In the UK, UTES systems are gaining increasing importance in response to the growing demand for energy-efficient heating and cooling solutions in buildings (Fleuchaus et al., 2018). Given that heating constitutes a substantial proportion of energy consumption across residential, public, and commercial sectors, integrating renewable energy sources such as wind and solar with UTES can significantly reduce dependence on fossil fuels (Brown et al., 2024). Such integration not only enhances energy sustainability but also contributes to the reduction of greenhouse gas emissions, thereby supporting the UK's broader decarbonisation objectives and renewable energy transition.

Matos et al. (2019) and Holechek et al. (2022) emphasised the role of UTES in mitigating the intermittency of renewable energy sources, noting that large-scale deployment requires careful reservoir selection based on hydrogeological stability and thermal conductivity. Among the various UTES technologies, BTES has emerged as a particularly effective option for seasonal heat storage. Gluyas et al. (2023) demonstrated that BTES systems operating at temperatures of approximately 70 °C can induce long-term thermal disturbances in aquifers, underscoring the importance of comprehensive environmental impact assessments. Further advancements include the incorporation of Phase-Change Materials (PCMs) to enhance space-heating performance.

Multiscale Computational Fluid Dynamics (CFD) simulations indicate that storage efficiency in such systems can vary by 10–15%, depending on geometric configuration (Bianco et al., 2024).

The deployment of UTES systems for heating and cooling can substantially reduce reliance on fossil fuels, thereby lowering the carbon footprint of buildings and industrial processes. However, studies suggest that renewable energy production must increase by six to eight times to meet a constant or 50% higher global energy demand relative to 2020 levels (Holechek et al., 2022). Limiting energy demand growth to approximately 25% by 2050 would significantly improve prospects for achieving independence from fossil fuels (Solakivi, Paimander, and Ojala, 2022). The long-term success and structural integrity of UTES systems are strongly influenced by the quality and performance of the concrete linings used in their construction. The application of advanced lining materials can markedly enhance both the thermal and mechanical performance of these systems, contributing to improved efficiency, durability, and operational reliability. Effective insulation within the lining structure is therefore essential for maintaining stable temperature conditions and ensuring efficient thermal energy storage and transfer.

### 2.3 Shaft structures and deterioration mechanisms

Maintaining shaft integrity under repeated thermal cycling represents a critical challenge in the design and long-term operation of UTES systems. Recent studies highlight the vulnerability of structural materials when exposed to cyclic thermal loading. For example, Bianco et al. (2024) reported that phase-change material (PCM)-enhanced storage tanks developed microcracks after more than 50 thermal cycles, resulting in an 8–12% reduction in heat-exchange efficiency. This finding demonstrates how relatively small-scale material degradation can lead to significant operational inefficiencies. Similarly, Fu et al. (2025) proposed a health assessment framework for pumped storage units using Kolmogorov–Arnold networks, achieving a prediction accuracy of 92% for mechanical degradation.

Although developed for hydropower applications, this approach shows strong potential for adaptation as a predictive monitoring tool for assessing UTES shaft integrity.

In terms of mitigation strategies, advanced protective coatings—such as silica aerogels capable of withstanding temperatures of up to 350 °C—have shown promise in alleviating thermal stresses in concrete structures (Li et al., 2025) [1]. However, their long-term adhesion and durability in humid and groundwater-saturated environments remain uncertain, highlighting the need for further field-based validation studies. Shaft structures form the backbone of many UTES systems, particularly those based on repurposed mine shafts. Historically, mine shafts were lined with concrete or masonry to provide structural stability, resistance to groundwater ingress, and long-term durability (Lai et al., 2013). In the UTES context, these linings acquire an additional functional role, acting as thermal and hydraulic barriers that limit conductive heat losses to surrounding rock masses and preserve storage efficiency. Typical mine shafts are cylindrical vertical excavations, ranging from a few metres to over 7 m in diameter and extending several hundred metres in depth (Fig. 1). Linings are commonly constructed using cast-in-place reinforced concrete, shotcrete (ITA-AITES, 2013) (Fig. 2), or segmental precast systems, depending on site-specific geological and hydrological conditions. In abandoned mines adapted for UTES applications, maintaining lining integrity is essential for ensuring the hydraulic stability of flooded voids and enabling safe access for monitoring, retrofitting, and long-term system operation (Monaghan et al., 2022).

In operation, shaft linings are exposed not only to conventional geotechnical stresses but also to temperature variations associated with repeated heat injection and extraction cycles. Unlike conventional mining applications, where linings are designed primarily to resist structural loads, UTES systems impose combined thermo-mechanical stresses that must be accommodated reliably over multi-decade operational timescales. Consequently, understanding and mitigating deterioration mechanisms is essential to ensuring the long-term viability of Mine Thermal Energy Storage (MTES) systems.

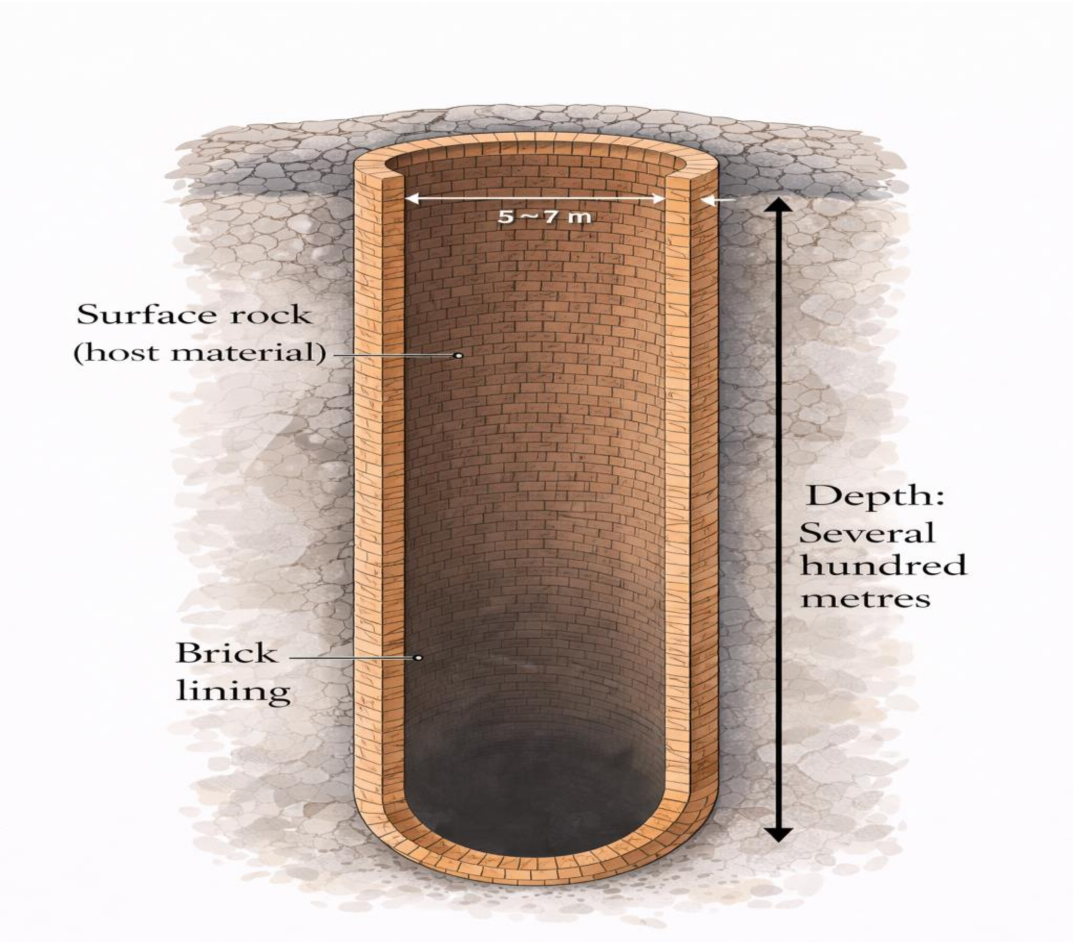


**Figure 1:** Schematic cross-section of a cylindrical vertical mine shaft typical diameter (5–7 m) (developed by the author).

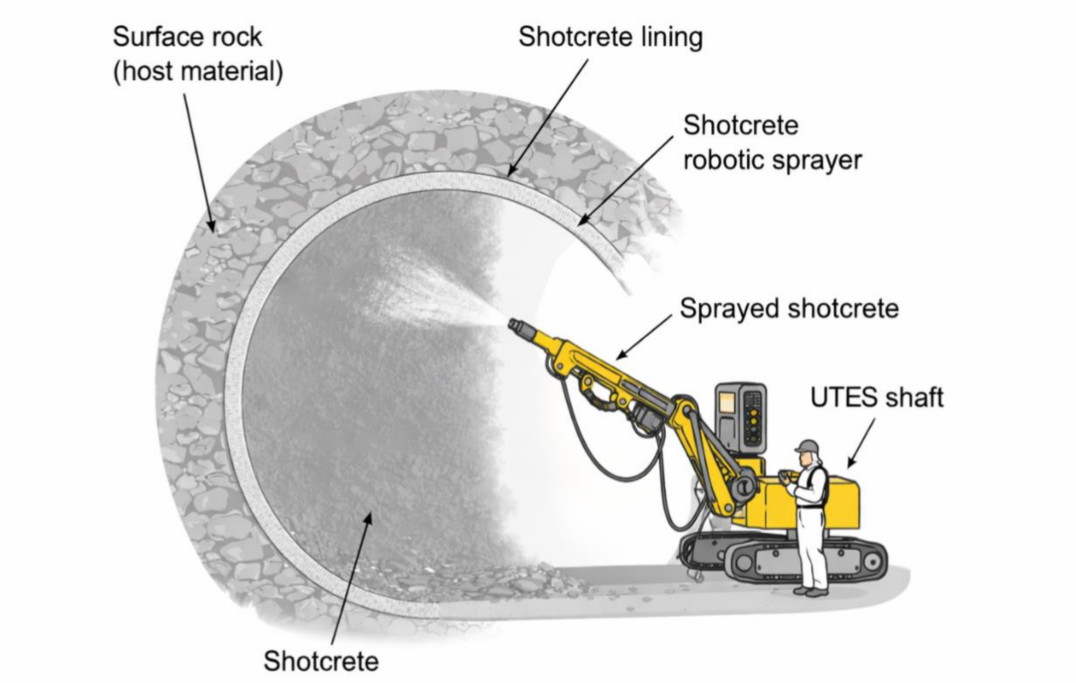


**Figure 2:** Schematic diagram of shotcrete application (adapted from Epiroc, 2023).

Thermal cycling: Repeated heating and cooling between approximately 10 and 40 °C induce differential expansion and contraction within the cementitious matrix. Over time, this process leads to microcrack formation, strength degradation, and reduced fracture toughness (Yao et al., 2020). This mechanism is particularly critical in mine water UTES systems, where seasonal thermal fluctuations are frequent and sustained.

Moisture and wet–dry cycling: Alternating saturation and drying conditions generate shrinkage–swelling stresses within the pore structure, progressively weakening the cement matrix and increasing porosity. This degradation pathway not only reduces mechanical strength but also accelerates the ingress of aggressive chemical agents.

Chemical attack: Abandoned mine environments often contain groundwater enriched with sulphates, chlorides, or acidic constituents. These species can react with cement hydration products, leading to sulphate attack, reinforcement corrosion, and secondary ettringite formation. Such reactions result in volumetric expansion, cracking, and surface spalling of the lining (RILEM, 2007).

Permeability increase: The combined effects of microcracking, leaching, and chemical alteration progressively increase lining permeability. Enhanced permeability facilitates ion transport, accelerates material degradation, and reduces the thermal insulation capacity of the lining, thereby directly diminishing storage efficiency (Park & Kim, 2012).

Freeze–thaw cycling in shallow shafts: In cold climates, tunnels are vulnerable to frost problems arising from seasonal freezing and thawing of the surrounding ground, and the freezing depth influences thermal stability, which is a key factor in design and durability of cold-region underground structures (Zhou et al., 2023). Freeze-thaw deterioration originates when water in concrete pores freezes and expands, producing expansive hydraulic pressures; if the pore system cannot relieve these stresses, internal cracking, scaling, and spalling occur (Liu et al., 2024). Collectively, these deterioration mechanisms compromise both the structural integrity and thermal efficiency of UTES shafts. Concrete with high permeability and poor pore structure is more susceptible to freeze–thaw deterioration, as internal water can freeze and generate damaging pressures more readily; brittle failure behaviour exacerbates crack propagation (Liu et al., 2024). Consequently, advanced fibre-reinforced concretes and admixture-modified cementitious systems have been proposed to enhance crack resistance, improve toughness, and extend service life. These materials represent a promising research direction for the reliable and durable deployment of UTES systems in mine shaft applications.

### 2.4 Lining Materials in UTES

The performance of shaft lining materials is central to the successful operation of UTES systems, particularly those based on repurposed mine shafts. Unlike conventional mining linings, which are designed primarily to provide structural stability, UTES linings must function as multifunctional barriers that deliver structural integrity, thermal regulation, hydraulic sealing, and durability over multi-decade service lives. The following subsections synthesise the technical roles and challenges associated with shaft linings in UTES applications. These coupled functional roles of UTES shaft linings are schematically illustrated in Figure 3.

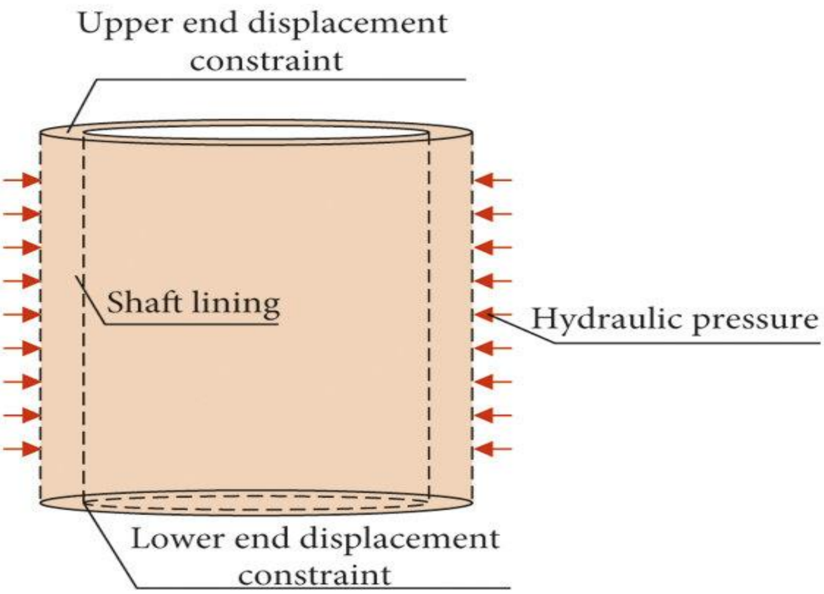


**Figure 3:** Conceptual illustration of the multifunctional roles of UTES shaft linings, showing structural load resistance, hydraulic sealing against groundwater ingress, thermal regulation limiting heat loss, and long-term durability (developed by the author).

### 2.4.1 Structural and Mechanical Performance

Shaft linings must ensure long-term structural stability under combined geotechnical and hydrostatic loading conditions. These include vertical overburden pressures, lateral in-situ stresses, and groundwater pressure from surrounding strata. In abandoned mine shafts, degraded or weakened linings pose risks of collapse or uncontrolled water ingress, both of which threaten system operability and safety. Conventional concrete, while generally adequate under static loading, often lacks the tensile toughness and crack resistance required to withstand cyclic thermal and hydraulic stresses (Lai et al., 2013; Liu et al., 2020). Reinforced and fibre-modified concretes therefore play a critical role in enhancing compressive strength, flexural capacity, and post-cracking behaviour, thereby maintaining shaft stability during UTES operation.

### 2.4.2 Thermal Regulation and Insulation

In addition to their structural function, shaft linings act as thermal barriers that regulate heat transfer between the storage medium, typically mine water, and the surrounding rock mass. Conductive heat losses through the lining reduce storage efficiency and limit the capacity of UTES systems to provide intra-seasonal energy balancing. Although concrete exhibits relatively low thermal conductivity, its insulating performance can deteriorate as microcracking and permeability increase under repeated thermal cycling. Enhancing linings with Supplementary Cementitious Materials (SCMs) and fibre reinforcement has been shown to limit crack development and maintain lower effective thermal conductivity, which is critical for preserving long-term thermal efficiency (Cabeza et al., 2015; Yao et al., 2020).

### 2.4.3 Hydraulic Integrity

Hydraulic performance is a fundamental function of column linings in geothermal energy storage systems. The cement sheath and casing linings act as low-permeability hydraulic barriers, essential for establishing zonal isolation and preventing undesired fluid communication between the wellbore and surrounding formations (Wu, 2020). These linings are designed to minimise seepage of stored geothermal fluids, thereby protecting usable storage capacity and supporting long-term system integrity (Alsubaih, 2025). In enhanced geothermal systems, maintaining such hydraulic barriers is central to preserving well integrity and preventing leakage into adjacent geological formations (EGS Well Integrity overview, 2025). Experimental studies indicate that thermal cycling and wet–dry exposure can significantly increase permeability in Ordinary Portland Cement (OPC)-based concretes through microcrack development, thereby undermining hydraulic sealing performance (Park & Kim, 2012). In contrast, advanced fibre-reinforced concretes can effectively restrict crack widths and maintain lower permeability, improving long-term hydraulic integrity (Figure 4).

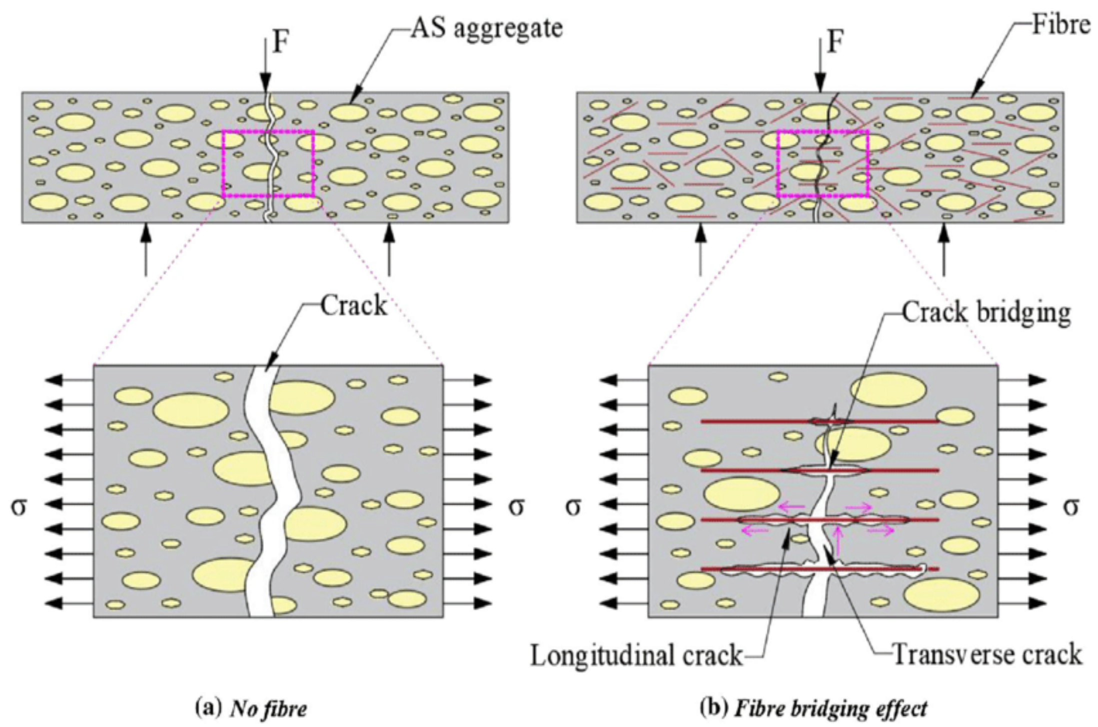


**Figure 4:** Crack-bridging mechanism in fibre-reinforced concrete showing restriction of crack width and reduced permeability, contributing to improved long-term hydraulic integrity under thermo-mechanical loading (developed by the author).

### 2.4.4 Durability under Harsh Conditions

UTES linings are subjected to aggressive operational environments characterised by the combined action of thermal, hydraulic, and chemical stresses (Figure 5). Groundwater in abandoned coal mines frequently contains elevated concentrations of sulphates, chlorides, or acidic species, which can react with cement hydration products, leading to sulphate attack, reinforcement corrosion, and secondary ettringite formation.

These degradation mechanisms result in expansion, cracking, and surface spalling, further exacerbating permeability and thermal losses (RILEM, 2007; Lai et al., 2013). In addition, freeze–thaw cycling in shallow shaft sections can cause surface scaling and internal microcracking. The ability of lining materials to withstand these coupled deterioration processes is therefore a decisive factor in determining the long-term performance and reliability of UTES systems.

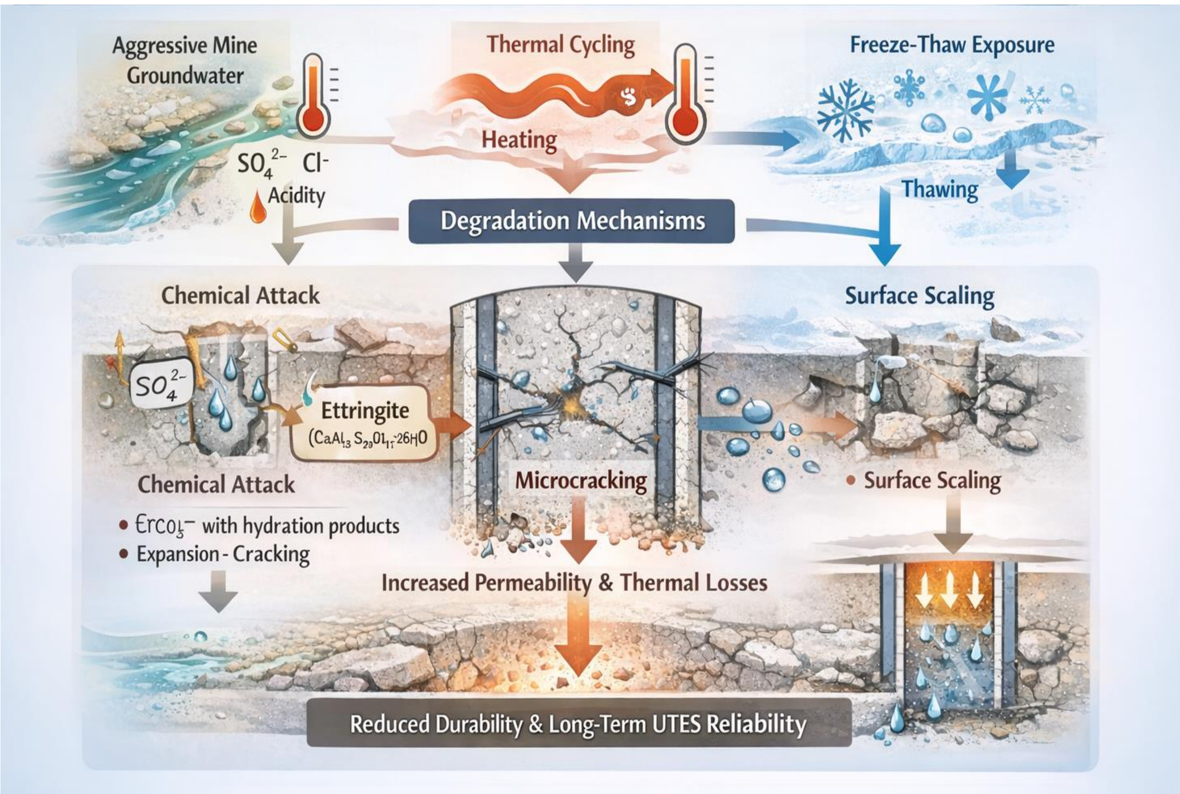


**Figure 5:** Conceptual Framework of Coupled Durability Degradation Mechanisms in UTES Shaft Linings under Harsh Thermo–Hydro–Chemical Conditions (developed by the author).

### 2.4.5 Integration with Thermal Systems

Finally, shaft linings interact directly with heat exchangers, heat pump systems, and embedded thermal components. Their mechanical, thermal, and microstructural properties influence both heat transfer efficiency and the structural stability of embedded infrastructure. Cracking, increased permeability, or chemical degradation can compromise exchanger performance, reduce heat transfer efficiency, and diminish overall system reliability (Sommer et al., 2015).

To ensure effective integration, lining materials must retain stable mechanical and thermal properties under repeated operational cycles while maintaining compatibility with associated thermal system components.

## 2.5 Conventional vs. Advanced Materials

OPC–based concretes, although widely used, are vulnerable to the combined deterioration mechanisms prevalent in UTES environments (Zeng et al., 2022). Their inherent brittleness, susceptibility to microcracking, and relatively high permeability limit their capacity to withstand repeated thermal cycling, hydraulic loading, and thermo-mechanical stresses. Elevated temperatures and moisture fluctuations further accelerate chemical degradation processes, such as leaching and delayed ettringite formation, thereby compromising long-term durability.

In contrast, advanced concretes incorporating SCMs, nanomaterials, and fibre reinforcements have demonstrated superior performance under such demanding conditions. SCMs such as fly ash, silica fume, and ground granulated blast furnace slag refine pore structure, reduce permeability, and enhance resistance to thermal cracking by improving matrix density and interfacial bonding (Mehta & Monteiro, 2014; Neville, 2011). At the nanoscale, additives such as nano silica further promote pozzolanic reactions and strengthen the cementitious matrix, leading to improved thermal stability and mechanical resilience.

Fibre-reinforced concretes provide additional performance benefits. Basalt fibres enhance tensile strength and maintain structural integrity at elevated temperatures due to their high thermal resistance, while polypropylene fibres improve crack-bridging capacity, energy absorption, and post-cracking toughness. When used in combination, these fibres exhibit synergistic effects that limit crack initiation and propagation, reduce permeability, and preserve thermal resistance under cyclic loading conditions (Afroughsabet & Ozbakkaloglu, 2015; Zhang et al., 2017). While a wide range of advanced cementitious systems has been proposed, fibre-reinforced concretes incorporating basalt and polypropylene fibres represent a practical compromise between performance enhancement, scalability, and life-cycle impact — motivating their selection in the present study. Collectively, these advanced material systems offer a viable pathway toward more durable, efficient, and sustainable UTES linings capable of long-term service in aggressive subsurface thermal environments. Despite these advances, few studies evaluate how such material-level improvements translate into reduced thermal losses, extended service life, or measurable life-cycle environmental benefits in UTES applications.

## 2.6 Thermal Cycling and Material Resilience

Thermal cycling represents a critical durability challenge for UTES systems, particularly those embedded within concrete-lined mine shafts. Repeated expansion and contraction under fluctuating thermal loads can induce microcracking, interfacial debonding, and progressive mechanical degradation. Understanding and enhancing the thermal resilience of construction and containment materials is therefore essential to ensure long-term system performance and minimise maintenance requirements. Recent developments in energy storage materials provide relevant analogues. Jiang et al. (2024) demonstrated that supercapacitor devices incorporating ionic liquids retained approximately 85% of their capacitance after 5,000 cycles at 200 °C.

Although developed for electrochemical applications, these findings indicate the potential for incorporating ionic liquid-based additives or phase-change materials into cementitious systems to buffer thermal stresses. Such approaches could mitigate crack initiation and propagation, thereby preserving the structural integrity of UTES lining materials during repeated heating and cooling cycles.

In large-scale mechanical systems, the influence of thermal gradients on material fatigue is well established. Lund and Madsen (2024) reported that fracture propagation rates in wind turbine blades increased by approximately 40% when thermal gradients exceeded 30 °C/mm. Comparable thermal gradients may occur in UTES environments, particularly during rapid charge and discharge cycles. This raises concerns regarding the long-term performance of steel reinforcement, liners, and embedded monitoring components. Tailoring thermal conductivity and stress distribution through fibre reinforcement or functionally graded composites may offer effective strategies to reduce thermally induced fatigue.

Environmental interactions further compound these challenges. Meng et al. (2021) examined the effects of BTES on subsurface hydrology and found that sustained thermal plumes altered groundwater flow and solute migration rates by 15–25%. These findings highlight the importance of advanced coupled hydro–thermal–chemical modelling to assess both long-term environmental impacts and material degradation mechanisms in UTES systems. Heat-induced changes in groundwater pathways may, for example, accelerate corrosion of metallic components or enhance leaching of degradation products from concrete linings.

Overall, achieving thermal resilience in UTES systems subjected to repeated thermal cycling requires a multidisciplinary design approach. Material innovations informed by advances in electrochemical and renewable energy technologies, combined with predictive thermo-mechanical and environmental modelling, are essential for developing robust, long-life underground thermal energy storage infrastructure.

## 2.7 Integration with Renewable Energy Systems

The successful decarbonisation of energy systems increasingly depends on the effective integration of thermal energy storage with intermittent renewable energy generation. UTES offers a promising solution for addressing short-term supply–demand mismatches and enhancing the operational efficiency of hybrid renewable energy systems.

Hybrid UTES–photovoltaic (PV) configurations have demonstrated system-level energy efficiencies of approximately 60–64% in net-zero energy communities (Liu et al., 2023). However, these performance levels are highly dependent on temporal alignment between energy supply and demand, as well as the availability of intelligent grid interaction strategies. Demand-side management, dynamic pricing mechanisms, and vehicle-to-grid (V2G) integration can significantly enhance the economic viability of such systems, particularly in urban and semi-urban retrofit contexts.

Beyond PV integration, UTES has also been explored in conjunction with other renewable energy infrastructures. Zhou et al. (2023) modelled ocean thermal energy systems integrated with power generation infrastructure and reported renewable energy penetration levels of up to 86%. These findings highlight the scalability and adaptability of UTES across diverse geophysical and infrastructural settings, including coastal regions and industrial clusters. Similarly, Ayub et al. (2024) conducted a techno-environmental assessment of hydrogen production pathways and found that wind-driven UTES integration reduced the carbon intensity of blue hydrogen production by approximately 30% compared with conventional solar–grid hybrid systems. This evidence suggests that UTES not only enhances system resilience but also plays a critical role in reducing life-cycle greenhouse gas emissions of coupled energy technologies.

Despite these advances, storage duration and dispatchability remain significant challenges. Li et al. (2023) observed that the temporal variability of renewable energy sources, particularly wind and solar, has introduced uncertainty into hydropower investment models due to their reliance on predictable energy inflows. The authors advocate targeted policy instruments, including performance-based subsidies and capacity credit mechanisms, to incentivise UTES deployment as a long-duration buffering solution. Such measures could stabilise Return-On-Investment (ROI) timelines and reduce investor risk, particularly in grid-constrained or low-inertia energy markets.

### 2.8 Life Cycle Assessment (LCA) Methodologies

LCA is a systematic, science-based methodology used to evaluate the environmental impacts associated with a product, process, or system throughout its entire life cycle, from raw material extraction and processing to construction, operation, maintenance, and end-of-life management (ISO 14040, 2006; ISO 14044, 2006) the general life-cycle stages considered in LCA for UTES infrastructure are conceptually illustrated (Figure 6).

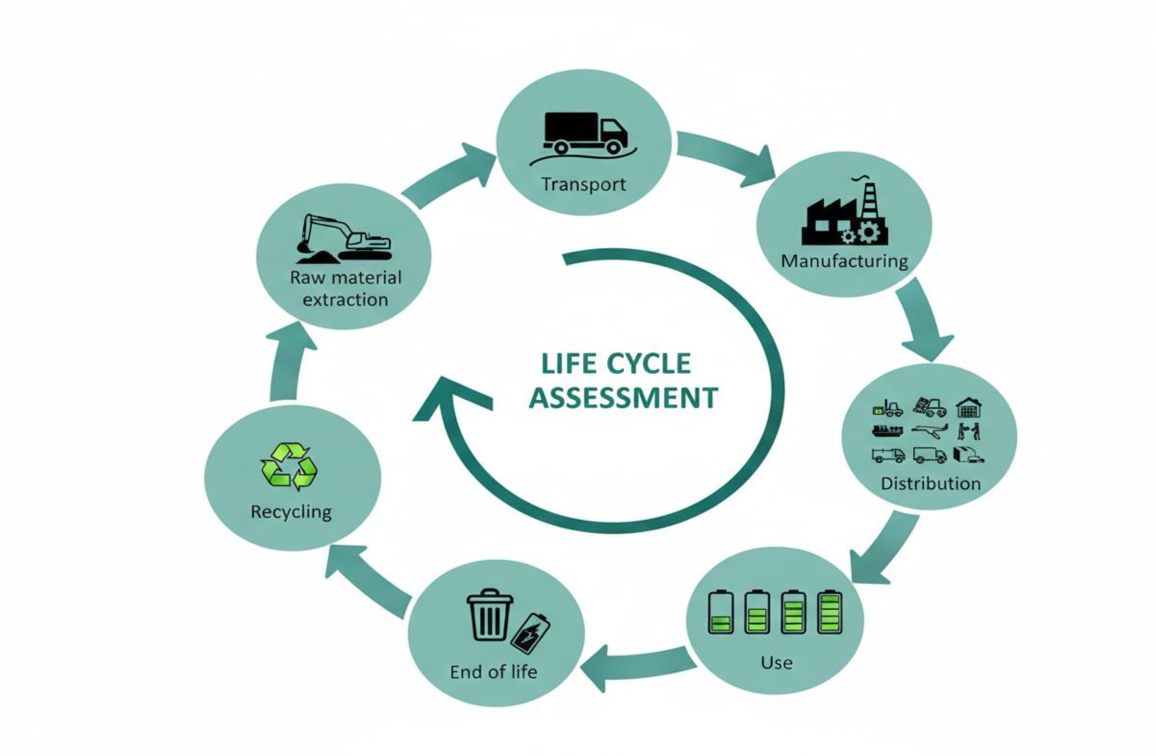


**Figure 6**: Conceptual system boundary of Life Cycle Assessment (LCA) for UTES infrastructure, illustrating cradle-to-grave stages (developed by the author).

Commonly described as a cradle-to-grave approach, LCA is designed to identify environmental trade-offs across different life-cycle stages and to prevent the shifting of environmental burdens from one stage, geographic location, or impact category to another (Finnveden et al., 2009; Hellweg and Canals, 2014). Over the past three decades, LCA has become a cornerstone of sustainability assessment within the construction sector, energy systems, and large-scale infrastructure development. In the context of UTES and LCA plays a particularly important role due to the long service life, material-intensive nature, and site-specific operating conditions of these systems. UTES technologies, including BTES and MTES, are frequently promoted as low-carbon or climate-positive solutions because they enable the storage and reuse of surplus thermal energy.

This, in turn, reduces reliance on fossil fuels and supports the integration of intermittent renewable energy sources (Dincer and Rosen, 2011; Cabeza et al., 2014). However, these operational benefits must be evaluated alongside the embodied environmental impacts associated with shaft excavation, lining construction, material production, installation, maintenance, and eventual decommissioning. LCA provides the analytical framework required to quantify such trade-offs in a transparent and systematic manner.

Despite its clear relevance, the application of LCA to UTES systems remains limited and methodologically fragmented. Existing studies often prioritise operational energy efficiency or direct carbon savings, while giving insufficient attention to the embodied emissions of construction materials and the environmental implications of long-term durability, repair, and maintenance. Consequently, there is currently no comprehensive or standardised LCA framework specifically tailored to UTES infrastructure, particularly with respect to shaft linings constructed from advanced or modified cementitious composites

### 2.8.1 General LCA Framework and Methodological Phases

According to ISO 14040 and ISO 14044, an LCA study consists of four interrelated phases: (i) goal and scope definition, (ii) life-cycle inventory (LCI) analysis, (iii) LCIA, and (iv) interpretation (ISO 14040, 2006; ISO 14044, 2006). These phases are iterative rather than strictly linear, and methodological choices made in the early stages strongly influence the robustness, transparency, and policy relevance of the results (Finnveden et al., 2009).

#### 2.8.1.1 Goal and Scope Definition

The goal and scope phase establishes the purpose of the study, the intended audience, and the decision context in which the results will be applied. In UTES-related LCAs, goals may include comparing alternative shaft lining materials, evaluating the environmental implications of extending service life through advanced concretes, or assessing trade-offs between embodied emissions and operational carbon savings. Scope definition involves specifying system boundaries, functional units, impact categories, assumptions, and limitations.

Clear articulation of the goal and scope is particularly important for UTES because system performance is highly dependent on local geological, thermal, and hydrochemical conditions. Without careful scoping, LCA results may be misleading or difficult to compare across studies, especially when extrapolating from laboratory-scale or short-term assessments to multi-decade operational lifetimes (Bare et al., 2012; Hellweg and Canals, 2014).

#### 2.8.1.2 Life Cycle Inventory (LCI) Analysis

The LCI phase quantifies all relevant material and energy inputs, as well as emissions and waste outputs, associated with each process within the defined system boundary (ISO 14044, 2006). For UTES shaft linings, this includes cement production, aggregate extraction, fibre or additive manufacturing, transportation, construction activities, operational energy use (e.g., pumping and heat exchange), maintenance interventions, and end-of-life treatment.

Inventory data are commonly sourced from established LCA databases such as EcoInvent or the Inventory of Carbon and Energy (ICE) (Wernet et al., 2016; Hammond and Jones, 2011). However, these datasets are typically generic and may not accurately represent site-specific conditions encountered in mine shafts, such as prolonged water saturation, chemical attack, or repeated thermal cycling. Consequently, the LCI phase represents a major source of uncertainty in UTES and LCAs, particularly when assessing long-term durability and maintenance requirements (Li et al., 2019).

#### 2.8.1.3 Life Cycle Impact Assessment (LCIA)

The LCIA phase translates inventory flows into environmental impact indicators, such as global warming potential, acidification, eutrophication, freshwater ecotoxicity, and resource depletion (Bare et al., 2012). In UTES assessments, climate change impacts are often prioritised due to their relevance to decarbonisation strategies. However, other impact categories remain important given the material intensity of shaft linings and reinforcement systems, particularly where resource extraction, toxicity, or long-term land-use impacts are significant (Finnveden et al., 2009).

#### 2.8.1.4 Interpretation

The interpretation phase involves analysing results, identifying key contributors to environmental impacts, evaluating uncertainty and sensitivity, and drawing conclusions consistent with the study's goal and scope. For UTES systems, interpretation must explicitly consider the interaction between material durability, thermal performance, and maintenance frequency, as these factors directly influence both environmental and technical performance over the system lifetime.

### 2.8.2 System Boundaries and Data Quality

One of the most critical methodological challenges in applying LCA to the built environment and energy infrastructure is the definition of system boundaries. System boundaries determine which processes and life-cycle stages are included in the assessment, such as raw material extraction, material production, transportation, construction, operation, maintenance, and end-of-life disposal or recycling (ISO 14044, 2006).

Li et al. (2019) demonstrated that uncertainties in maintenance schedules, emission factors, and end-of-life scenarios can significantly influence LCA results in building applications. For UTES systems, boundary definition is further complicated by long operational lifetimes and gradual performance degradation. Excluding maintenance or repair activities may underestimate environmental impacts, while neglecting operational benefits may overstate embodied emissions (Hammond and Jones, 2011; Levasseur et al., 2010).

For UTES shaft linings, it is essential to clearly distinguish between life-cycle modules: A1–A3 (raw material extraction and production), A4–A5 (transportation and construction/installation), and B1–B7 (use phase, including thermal losses, pumping energy, inspection, maintenance, and repair), in accordance with EN 15978 (CEN, 2011). End-of-life modules (C1–C4) and potential benefits beyond the system boundary (module D) may also be relevant, particularly when material recycling or reuse is considered.

Data quality is closely linked to boundary definition. Hammond and Jones (2011) emphasised that poor-quality or outdated inventory data can dominate LCA outcomes, potentially leading to erroneous conclusions. Levasseur et al. (2010) further highlighted the importance of temporal consistency, noting that emissions occurring at different times should be treated appropriately, particularly in climate change impact assessments. This temporal dimension is especially relevant for UTES, where upfront construction emissions occur decades before operational carbon savings are realised.

### 2.8.3 Standardisation and Functional Units

A major methodological challenge in LCA research is the lack of consistent functional units, which significantly limits comparability across studies. Tang et al. (2018) demonstrated that LCA results can vary substantially depending on how the functional unit is defined, even when evaluating the same system.

In construction-related LCAs, functional units are often expressed on a mass basis (e.g., per kilogram of concrete). While convenient, such units fail to capture differences in durability, service life, and performance. In UTES applications, this limitation is particularly significant because shaft linings serve not only as structural elements but also as thermal containment systems, whose performance evolves over time.

Service-based functional units are therefore more appropriate for UTES LCAs. Examples include “1 meter square (1 $m^2$) of shaft lining providing thermal containment over 30 years” or “the storage and release of 1 MWh of thermal energy over the system lifetime.” Finnveden et al. (2009) argue that functional units should reflect the service delivered rather than the physical product, particularly when comparing fundamentally different technologies.

### 2.8.4 Adaptable Protocols and Application to UTES

Given the complexity and variability of infrastructure systems, several researchers have advocated for adaptable LCA frameworks that maintain methodological rigour while allowing contextual flexibility. Gong et al. (2012), in their study of wastewater reuse systems, proposed a phased LCA methodology that explicitly separates infrastructure impacts from operational impacts. This approach is directly applicable to UTES, where shaft construction and lining installation represent significant upfront impacts, while operational impacts accrue gradually over decades.

Bare et al. (2012) and Hellweg and Canals (2014) further emphasise the importance of transparency, sensitivity analysis, and context-specific modelling in LCA, particularly for long-lived infrastructure. For UTES, adaptable LCA protocols must integrate technical performance indicators, such as thermal conductivity stability, fracture resistance, and service life extension, into the environmental assessment to ensure accurate and relevant results.

### 2.8.5 Relevance and Research Gap for UTES

While LCA has been widely applied in the building and energy sectors (Cabeza et al., 2014; Blengini and Di Carlo, 2010), its direct application to UTES remains limited. Existing studies often focus narrowly on operational energy savings or carbon payback periods, with limited consideration of embodied emissions from materials such as cement, aggregates, fibres, and reinforcement used in shaft linings.

Moreover, most LCAs rely on generic datasets that do not adequately represent the harsh environmental conditions of mine shafts, including prolonged water saturation, chemical attack, and repeated thermal cycling. This highlights a critical research gap: there is currently no established LCA framework specifically tailored to UTES that integrates material durability, thermal performance, and environmental impact over multi-decade service lifetimes. Addressing this gap is essential for providing holistic, evidence-based guidance on the adoption of advanced cementitious materials in mine thermal energy storage systems and for enhancing the environmental credibility and public acceptance of UTES technologies.

## 2.9 Research Gap

Despite significant advances in underground thermal energy storage (UTES) technologies over the past two decades, the existing literature reveals persistent and interconnected gaps that constrain large-scale deployment, long-term reliability, and environmental credibility. UTES is increasingly recognised as a critical component of low-carbon energy systems, particularly for balancing seasonal heat demand and integrating intermittent renewable energy sources. However, unresolved challenges remain in material durability, component fatigue, coupled subsurface processes, and system-level integration with renewable energy and policy frameworks. These challenges are especially pronounced in mine thermal energy storage (MTES) and deep BTES systems, where infrastructure is exposed to complex thermal, hydraulic, and chemical environments over multi-decade operational lifetimes.

While individual studies have addressed isolated aspects of UTES performance, the literature remains fragmented, with limited cross-disciplinary integration between materials science, geomechanics, hydrogeology, and environmental assessment. Consequently, design practices often rely on assumptions derived from conventional underground structures rather than UTES-specific evidence. A critical synthesis of the state-of-the-art identifies four principal research gaps that collectively hinder the technical robustness, environmental acceptance, and economic viability of UTES systems. These gaps form the conceptual foundation of the present research.

### 2.9.1 Material Innovation under Thermal Stress

Concrete remains the dominant construction material for UTES shaft linings due to its structural capacity, availability, and cost-effectiveness (Barbhuiya, Da & Idrees, 2024). Nevertheless, conventional concretes exhibit well-documented vulnerabilities when exposed to repeated thermal–mechanical loading and chemically aggressive groundwater environments. Cyclic heating and cooling induce differential thermal expansion between cement paste, aggregates, and reinforcement, promoting microcracking, increased permeability, and progressive mechanical degradation. The mechanisms of thermal stress development and resulting crack patterns under different restraint conditions are conceptually illustrated in Figure 7.

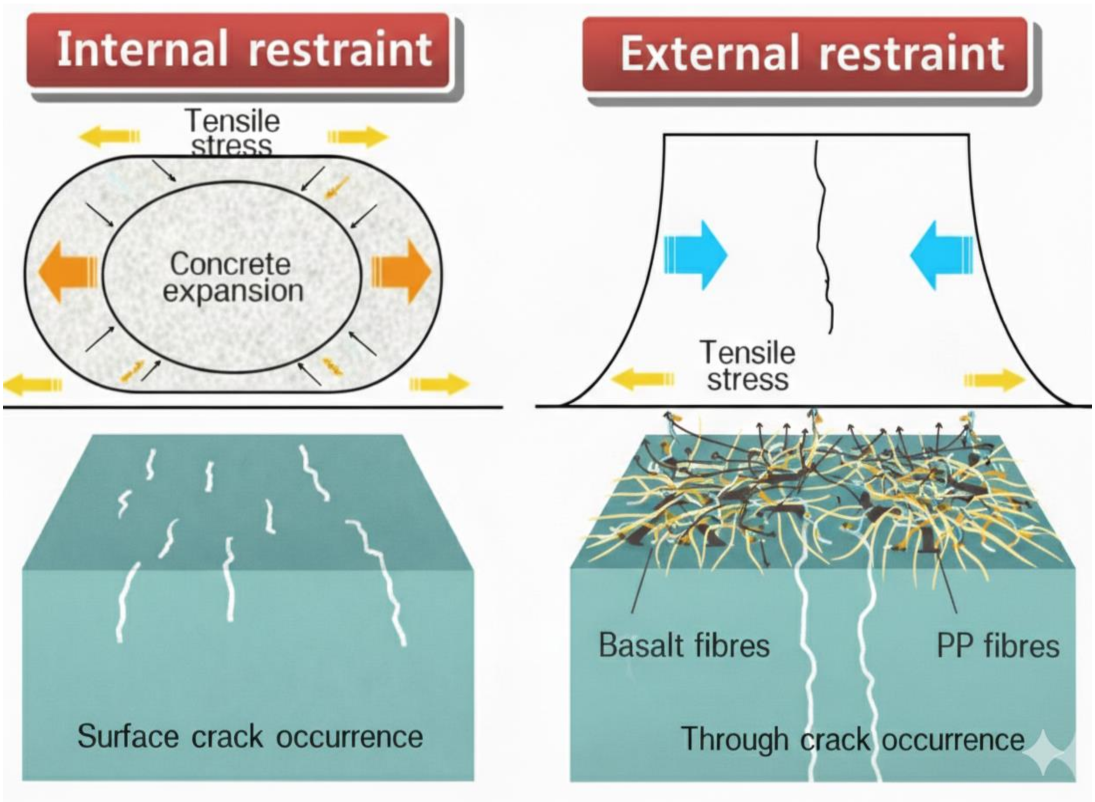


**Figure 7**: Schematic illustration of thermal stress-induced cracking in concrete under internal and external restraint conditions, showing surface crack formation due to restrained expansion and through-crack development under externally imposed tensile stresses (developed by the author).

These effects are exacerbated under saturated conditions, where moisture transport accelerates leaching, sulphate attack, and freeze–thaw–like damage mechanisms (Park & Kim, 2012; Yao et al., 2020). Over time, such degradation compromises both structural integrity and thermal containment efficiency, directly affecting system performance and lifespan.

Recent research has explored advanced cementitious composites as potential next-generation lining materials. Graphene- and graphene oxide-enhanced concretes have attracted considerable attention due to graphene's exceptional mechanical strength, high surface area, and ability to refine pore structure.

Experimental studies have demonstrated improvements in tensile and compressive strength, fracture toughness, crack-bridging capacity, and interfacial bonding between hydration products and aggregates (Montazerian et al., 2023; Alateah et al., 2023; Wang et al., 2022). These enhancements are particularly relevant for UTES, where limiting crack propagation is essential for maintaining thermal efficiency and preventing groundwater ingress.

Similarly, self-healing concretes incorporating microbial encapsulation, mineral admixtures, or capsule-based healing agents have shown promising potential to autonomously seal microcracks, reduce permeability, and extend service life (Cappellesso et al., 2023; Li et al., 2025). Recent developments indicate that certain self-healing systems can partially recover mechanical and transport properties even after severe thermal exposure, such as fire damage, suggesting resilience under extreme thermal events (Vedrtnam et al., 2025). These characteristics indicate that self-healing concretes could play a transformative role in reducing maintenance demands and life cycle impacts of UTES infrastructure.

Despite these advances, a fundamental research gap persists in validating these materials under UTES-relevant conditions. Most studies rely on short-term laboratory tests under static or simplified loading regimes, often neglecting the coupled thermal, hydraulic, and chemical stresses present in operational systems. Most existing studies have investigated the deterioration of concrete under either elevated temperature or corrosive environments in isolation; research addressing their combined long-term effects remains limited, especially under high-temperature geochemical conditions such as those in shallow (10–45 °C) and deeper (>60 °C) geothermal or mine water settings (Yunpeng et al., 2025).

#### 2.9.1.1 Critical unresolved questions include:

The long-term fracture resistance and fatigue behaviour of graphene- or fibre-reinforced concretes under cyclic thermal–mechanical loading.

The durability, repeatability, and exhaustion mechanisms of self-healing agents in saturated and chemically aggressive environments.

The stability of thermal conductivity and heat transfer performance in modified concretes subjected to prolonged moisture exposure and temperature variation.

Without systematic experimental evidence and validated predictive models, the applicability of advanced cementitious composites to UTES shaft linings remains uncertain. This represents a core research gap in linking material innovation to long-term functional performance and system reliability under realistic operating conditions.

### 2.9.2 Component Fatigue at Elevated Temperatures

While UTES research has traditionally focused on subsurface heat transfer, storage efficiency, and fluid–rock interactions, comparatively little attention has been paid to the fatigue behaviour of structural and metallic components embedded within these systems. Shaft linings, steel reinforcement, connectors, heat exchangers, and auxiliary components are exposed to repeated thermal gradients, mechanical constraints, and chemically aggressive mine-water environments. Together, these conditions promote fatigue accumulation, corrosion-assisted cracking, creep, and fracture propagation.

Insights from adjacent research fields underscore the importance of addressing this gap. For instance, studies on high-temperature supercapacitors demonstrate that tailored material systems and electrolytes can significantly enhance endurance under elevated thermal conditions (Jiang et al., 2024). However, analogous investigations into the electrochemical–mechanical resilience of UTES structural components are largely absent.

Metals exposed to cyclic thermal loading and corrosive groundwater are particularly susceptible to accelerated degradation, potentially compromising both safety and operational continuity (Lund & Madsen, 2024).

Current UTES design practices often extrapolate durability expectations from conventional underground structures, such as tunnels or shafts, without explicitly accounting for the unique cyclic thermal loads imposed by seasonal heat injection and extraction. Consequently, there is a lack of:

- Mechanistically informed fatigue models for reinforced concrete linings under UTES-specific thermal gradients.
- Accelerated laboratory testing protocols capable of simulating decades of seasonal thermal cycling within feasible timescales.
- Integrated modelling approaches that couple electrochemical corrosion processes with mechanical fatigue and crack evolution.

This gap introduces uncertainty in predicting service life, inspection intervals, maintenance requirements, and safety margins for UTES infrastructure. Addressing it requires a cross-disciplinary approach that integrates materials science, structural engineering, corrosion science, and thermo-mechanical modelling.

### 2.9.3 Coupled Hydro–Thermal–Chemical Dynamics

Most existing UTES simulation studies conceptualise thermal energy storage as a predominantly physical process, often decoupled from hydrogeological and geochemical interactions. Heat injection and extraction alter groundwater density, viscosity, and flow regimes, influencing solute transport, geochemical equilibria, and microbial activity.

These interactions are particularly complex in heterogeneous subsurface environments, such as abandoned mines and fractured rock systems. Meng et al. (2021) demonstrated that long-term thermal plumes in borehole thermal energy storage systems increased subsurface contaminant migration by 15–25%, highlighting the potential for UTES operations to alter groundwater quality and contaminant pathways. In mine-based UTES systems, where shafts intersect chemically diverse aquifers and legacy mine drainage networks, such effects may be amplified. Thermal cycling can:

- Alter pH and mineral solubility, enhancing mobilisation of metals and other contaminants.
- Modify redox conditions, influencing corrosion rates, microbial metabolism, and mineral precipitation.
- Induce density-driven flow and thermal convection, redistributing contaminants beyond the immediate storage zone.
- Despite these risks, integrated Hydro–Thermal–Chemical (HTC) models remain underdeveloped.

Most existing models assume homogeneous aquifer properties, neglect multiphase flow, or exclude reactive transport processes altogether. The lack of validated HTC frameworks limits the ability to predict long-term environmental impacts, undermines regulatory confidence, and poses a barrier to social acceptance of UTES projects, particularly in environmentally sensitive or post-mining regions.

### 2.9.4 Integration with Intermittent Renewable Sources

UTES is frequently promoted as a strategic enabler for integrating intermittent renewable energy sources, such as wind and solar, by storing surplus energy as heat for later use. Hybrid UTES–renewable systems have demonstrated promising performance, with reported overall efficiencies of 60–64% in net-zero and low-carbon building applications (Liu et al., 2023). However, large-scale deployment remains constrained by economic, regulatory, and market uncertainties.

Key challenges include the absence of standardised market mechanisms for valuing long-duration and seasonal thermal storage. Unlike electrochemical batteries, which benefit from well-defined revenue streams and policy support, UTES often lacks clear financial incentives. Existing policy frameworks tend to prioritise short-term grid balancing, offering limited recognition of the strategic value of seasonal heat storage. Moreover, UTES economics are highly region-specific, depending on local energy prices, heat demand density, geological suitability, and grid flexibility (Li et al., 2023).

Additionally, limited research has addressed business models capable of integrating UTES with district heating networks, renewable energy producers, and grid services. This disconnects between technical potential and market readiness represents a critical barrier to investment and deployment.

### 2.9.5 Synthesis of the Research Gap

Collectively, these gaps demonstrate that while UTES is technically promising, its long-term deployment is constrained by insufficient understanding of material durability, component fatigue, coupled subsurface processes, and system-level integration. Critically, there is a lack of integrated research frameworks connecting advanced cementitious material performance with structural resilience, environmental impact, and operational efficiency over multi-decade lifetimes.

Addressing these interconnected challenges is essential to improving the reliability, sustainability, and societal acceptance of UTES systems. The present research directly responds to these gaps by advancing knowledge at the intersection of material innovation, durability under thermal stress, and environmental performance in underground thermal energy storage infrastructure.

### 2.10 Summary of Research Gaps

A critical synthesis of the literature identifies four interrelated research gaps that collectively limit the technical robustness, environmental credibility, and large-scale deployment of UTES systems.

First, material innovation under thermal stress remains insufficiently validated for UTES applications. Although advanced cementitious materials—including graphene-enhanced, fibre-reinforced, and self-healing concretes—have demonstrated promising improvements in strength, crack control, and durability under laboratory conditions, their long-term behaviour under UTES-relevant environments is largely unknown. Systematic evidence is lacking on their fracture resistance, thermal conductivity stability, and durability under repeated thermal cycling, continuous water saturation, and chemically aggressive mine-water exposure over multi-decade lifetimes.

Second, component fatigue at elevated and cyclic temperatures represents a major but underexplored vulnerability in UTES infrastructure. Structural and metallic components, such as reinforced linings, steel elements, connectors, and heat exchangers, are subjected to repeated thermal gradients, mechanical restraint, and corrosion-prone environments. Current UTES design practices rely heavily on assumptions derived from conventional underground structures, in the absence of UTES-specific fatigue models, accelerated testing methodologies, or coupled corrosion–fatigue frameworks capable of predicting long-term performance and safety margins.

Third, coupled HTC dynamics remain inadequately represented in UTES modelling and environmental assessment. Existing studies frequently treat thermal storage as a purely physical process, neglecting interactions with groundwater flow, solute transport, geochemical reactions, and microbial activity.

Evidence that thermal plumes can significantly alter contaminant migration highlights the need for integrated HTC models capable of assessing long-term environmental risks, regulatory compliance, and public acceptability—particularly in mine-based and post-industrial settings.

Finally, integration with intermittent renewable energy systems is constrained by economic, regulatory, and market barriers. While hybrid UTES–renewable systems have demonstrated encouraging efficiencies, the absence of standardised valuation mechanisms for long-duration and seasonal thermal storage, combined with region-specific policy frameworks, limits investment and large-scale implementation.

This gap is compounded by limited research into viable business models that link UTES with district heating networks, renewable energy generators, and grid services.

Taken together, these gaps reveal a systemic lack of integrated, interdisciplinary research frameworks connecting material-level innovation with structural durability, environmental performance, and system-level functionality over realistic operational lifetimes. For UTES to transition from demonstration projects to scalable infrastructure, advances in advanced lining materials must be supported by robust durability testing, life-cycle-based environmental evaluation, and design methodologies that explicitly account for cyclic thermal loading.

This study directly addresses the first two gaps by systematically investigating the mechanical, thermal, and durability performance of advanced fibre-reinforced cementitious composites under UTES-relevant thermal–mechanical loading conditions, while situating these findings within a broader sustainability and LCP context.

# Chapter 3: Methodology

## 3.1 Introduction

This chapter presents the research methodology adopted to address the research gaps identified in Chapter 2 and to achieve the objectives of the study through a systematic, transparent, and scientifically robust approach. In response to the increasing demand for sustainable construction materials and the growing concern over the environmental impacts of cement-based products, this research adopts an integrated methodological framework designed to generate reliable, comparable, and evidence-based findings. The chapter focuses on evaluating the performance and environmental implications of conventional and hybrid fibre-reinforced concrete linings for Underground Thermal Energy Storage (UTES) shafts.

To achieve this aim, the study employs a mixed-method approach that combines experimental testing with life cycle assessment (LCA) modelling. This integrated framework ensures that the mechanical and hygrothermal properties of the concrete linings, measured under controlled laboratory conditions, are directly linked to their environmental performance. By coupling experimental results with environmental assessment, the methodology provides a comprehensive evaluation of both material functionality and sustainability outcomes, thereby strengthening the relevance of the findings for engineering and environmental decision-making.

Life cycle assessment serves as the principal analytical tool for evaluating environmental impacts and is conducted in accordance with internationally recognised standards (ISO 14040 and ISO 14044). LCA is widely regarded as one of the most robust methods for assessing the environmental performance of construction materials across their life cycle, from raw material extraction to the defined use stage. In this study, the LCA framework is specifically structured to assess and compare three concrete mix scenarios—Conventional, Hybrid, and Nominal—

allowing for a clear examination of the environmental trade-offs associated with fibre incorporation and mix design choices.

This chapter outlines the overall research design, including the definition of the LCA goal and scope, the functional unit, and the system boundaries adopted for the analysis. Attention is given to the selection of life cycle stages most relevant to the research objectives, namely modules A1–A3 (raw material supply, transport, and manufacturing) and module B1 (use phase). The integration of the foreground system with a recognised background database is described to ensure methodological consistency and data reliability.

Furthermore, the chapter details the data sources, assumptions, and modelling procedures implemented using OpenLCA software in conjunction with the ecoinvent background database under the cut-off allocation model. The rationale for the selected impact assessment methods is explained, alongside the procedures adopted to ensure data quality, comparability, and reproducibility. The chapter also addresses methodological limitations and outlines the measures taken to minimise uncertainty and enhance the robustness of the results. By clearly defining the methodological framework, this chapter provides a solid foundation for the analysis and interpretation of results presented in the subsequent chapters.

### 3.2 Experimental Programme

The experimental component of the study focused on the design, preparation, and testing of three concrete mixes. These comprised:

(i) a conventional control mix with a cement: sand: aggregate ratio of 1:2:4.

(ii) a hybrid mix of identical proportions incorporating basalt and polypropylene (PP) fibres together with a polycarboxylate ether (PCE)-based water-reducing admixture; and

(iii) a nominal 1:2:3 mix representing an upper-bound strength configuration.

Each mix was characterised in terms of compressive and tensile strength, as well as thermal conductivity under both dry and saturated conditions. All experimental procedures were conducted in accordance with the relevant British Standards (BS EN 12390 series and BS EN ISO 10456), ensuring consistency, repeatability, and traceability. Table 1 below summarises the compositions of the concrete mixes considered in these scenarios

### 3.3 Materials Selection and Mix Design

This study evaluated three concrete mix designs with the aim of assessing how hybrid fibre reinforcement affects the mechanical and thermal properties of concrete linings in Underground Thermal Energy Storage (UTES) applications. While fibre-reinforced concrete has been extensively studied in general, its performance in deep-shaft UTES environments remains largely unexamined. Therefore, this investigation provides new insights into the behaviour of these materials under the specific thermal and structural demands of such applications. The experimental component of the study focused on the design, preparation, and testing of three concrete mixes (Table 1)

A conventional control mix using a 1:2:4 proportion of cement: sand: aggregate,

A hybrid mixes with identical proportions enhanced with basalt and polypropylene (PP) fibres and incorporating a polycarboxylate ether (PCE)-based water-reducing admixture,

A nominal 1:2:3 mix, representing an upper-bound strength configuration.

.

Table 1: Summary of Concrete Mix Scenarios and Their Research Roles

| Scenario | Scenario 1 Conventional | Scenario 2 Hybrid | Scenario 3 Nominal |
|---|---|---|---|
| Mix Ratio (C:S: A) | 1:2:4 | 1:2:4 | 1:2:3 |
| Water–Cement Ratio (w/c) | 0.45 | 0.45 | 0.45 |
| Additives / Fibres | None | Basalt fibre (1% of cement weight), PP fibre (0.2% of volume), PCE water reducer (1% of cement weight) | None |
| Measured Thermal Conductivity (k, $W \cdot m^{-1} \cdot K^{-1}$) | 1.90 | 2.41 | 2.00 |
| Expected Strength (MPa) | -50 | -65 | -70 |
| Primary Purpose in Study | Baseline control to evaluate effect of fibres/admixture; representative of standard concrete used in underground applications | Evaluate combined effect of fibres and admixture on strength, crack control, and heat transfer | Benchmark high cement mix for sensitivity testing; isolates effect of binder enrichment alone |

### 3.3.1 Materials Selection and Mix Scenarios

Three concrete mix scenarios were designed and evaluated to investigate the influence of fibre reinforcement and binder content on the mechanical, thermal, and environmental performance of concrete shaft linings for Underground Thermal Energy Storage (UTES) applications. The selected mixes enabled systematic comparison between a conventional reference mix, a fibre-reinforced hybrid mix, and a higher-strength nominal mix, while maintaining consistent testing and assessment conditions.

#### 3.3.1.1 Scenario 1: Conventional Mix (1:2:4)

Scenario 1 employed a conventional 1:2:4 concrete mix consisting of Ordinary Portland Cement (CEM I 52.5N), AGSTB005 sharp concreting sand, and AGSTB006 Jewson gravel (shingle) with a nominal maximum aggregate size of 10 mm. This standard mix was selected as the baseline control and did not incorporate fibres or chemical admixtures. Its primary purpose was to isolate the effects of fibre reinforcement and admixture addition on the mechanical and thermal properties of concrete.

Although BS EN 206 and BS 8500 specify performance-based designed mixes for structural concrete, a nominal 1:2:4 mix was adopted exclusively for laboratory control purposes. This approach is consistent with established research practice, where a 1:2:4 mix is frequently used as a reference configuration while fibre content and admixtures are varied (Li, 2018). The use of this mix simplified specimen preparation and supported transparent life cycle assessment (LCA) modelling.

The mix utilised a water-to-cement ratio of 0.45 and incorporated 10 mm coarse aggregate, resulting in moderate compressive strength and a typical saturated thermal conductivity of approximately 1.90 $W \cdot m^{-1} \cdot K^{-1}$. This scenario established the B1 reference condition for comparative analysis across production (A1–A3) and operational stages, thereby ensuring consistency with UK LCA datasets and supporting the overall validity of the study.

#### 3.3.1.2 Scenario 2: Hybrid Mix (1:2:4 with Fibres and Water-Reducing Admixture)

Scenario 2 utilised the same base materials as Scenario 1 but incorporated fibre reinforcement and a chemical admixture to enhance mechanical performance and thermal stability. Advanced cementitious composites were designed using basalt fibres, polypropylene (PP) fibres, and a hybrid combination of basalt and PP fibres to improve crack resistance, post-cracking behaviour, and thermal conductivity.

Fibre dosages were selected based on existing literature (Afroughsabet et al., 2015; Ozbakkaloglu, 2015; Yao et al., 2020) and optimised for shaft lining applications. The hybrid mix incorporated basalt fibres at 1% by cement mass and polypropylene fibres at 0.2% by concrete volume. A polycarboxylate ether (PCE)-based water-reducing admixture was added at 1% by cement mass to maintain workability at a constant water-to-cement ratio of 0.45 without adversely affecting durability.

All constituent materials complied with BS EN 206, BS 8500, and BS EN 934-2. Laboratory testing demonstrated that the hybrid mix exhibited enhanced mechanical strength and increased thermal conductivity compared to the control mix, with a measured thermal conductivity of 2.41 $W \cdot m^{-1} \cdot K^{-1}$. From an LCA perspective, this scenario enabled evaluation of the trade-off between increased embodied environmental impacts during material production (A1–A3) and reduced energy demand during the operational phase (B1). As such, it supported both technical performance requirements and sustainability objectives within UTES applications.

#### 3.3.1.3 Scenario 3: Nominal High-Strength Mix (1:2:3)

Scenario 3 employed a nominal 1:2:3 concrete mix with increased cement content and served as a benchmark representing higher-grade concrete. The same water-to-cement ratio (0.45) was maintained, and fibres and chemical admixtures were excluded to isolate the effect of binder enrichment on concrete performance. This mix functioned as a high-strength, high-density reference case for both experimental testing and LCA analysis. It represented an upper boundary of embodied environmental impact while delivering improved compressive strength and moderate thermal conductivity ($k = 2.00\ W \cdot m^{-1} \cdot K^{-1}$).

The inclusion of this scenario enabled direct comparison between material densification and fibre reinforcement as alternative strategies for enhancing the performance of UTES shaft linings across mechanical, thermal, and environmental dimensions.

### 3.3.2 Materials Compliance and Experimental Documentation

All materials conformed to BS EN 206:2013+A2:2021, and their properties were verified through standard laboratory testing. The basalt fibres had dimensions of 1 × 6 mm, a tensile strength of approximately 4,800 MPa, and a modulus of elasticity of 90 GPa.

The polypropylene fibres comprised fibrillated strands with a density of 910 kg·m$^{-3}$ and a tensile strength in the range of 400–600 MPa. A polycarboxylate ether (PCE)-based superplasticiser was used to improve fibre dispersion and to maintain workability at the specified water-to-cement ratio.

**Figure 8**: The types of fibres.

The fibre types employed in the experimental programme are illustrated in Figure 3.1, while the laboratory mixing and moulding setup is presented in Figure 8. Together, these figures and the defined mix scenarios enhance methodological transparency, ensure reproducibility, and allow for robust comparison across both the experimental programme and the life cycle assessment framework.

### 3.4 Mixing and Casting Procedure

A standardised and repeatable mixing and casting procedure was adopted to ensure material homogeneity and uniform fibre dispersion across all concrete batches. The procedure was applied consistently to minimise variability and enhance the reliability of experimental results.

Initially, dry materials comprising cement, fine aggregate (sand), and coarse aggregate (gravel) were placed in the mixer and dry-blended for approximately two minutes until a uniform consistency was achieved. Subsequently, basalt and polypropylene fibres were gradually introduced into the dry mixture and blended for an additional two minutes to promote even fibre distribution within the cementitious matrix.

Water was then added progressively during mixing to facilitate uniform hydration and to reduce the risk of fibre agglomeration. Following this, the polycarboxylate ether (PCE)-based water-reducing admixture was introduced, and mixing was continued for a further five minutes using the mechanical mixer illustrated in Figure 3.2 to ensure complete dispersion of fibres and admixture.

For casting, fresh concrete was placed into 100 mm cube moulds, as shown in Figure 9, in two equal layers. Each layer was compacted using a vibrating table in accordance with BS EN 12390-2:2019. Immediately after casting, the specimens were covered with plastic sheets to prevent moisture loss. After 24 hours, specimens were demoulded and transferred to a curing tank maintained at 20 ± 2 °C. Mechanical and thermal testing were conducted at curing ages of 7 and 28 days. Visual inspection confirmed consistent workability and uniform fibre dispersion, with no evidence of fibre balling or clustering.

**Figure 9**: The laboratory mixing machine and model cubes (author's own photo).

### 3.4.1 Calculation of the Mix

Each concrete specimen measured 100 mm on each side, corresponding to a volume of 0.001 $m^3$. A total of twelve specimens were prepared for each mix, resulting in an overall batch volume of 0.012 $m^3$. Mix proportion calculations were therefore performed based on this total volume, using a nominal mix ratio of 1:2:3 and a water-to-cement ratio of 0.45. The calculated material quantities were subsequently verified through trial batching to confirm adequate workability and consistency prior to full specimen production. The final mix quantities and proportions are summarised in Table 2.

**Table 2:** Summarises the calculated quantities for a 0.012 m³ batch. For life-cycle inventory (LCI) modelling, the quantities were normalised to 1 m³ of concrete for each scenario

| Material | Basis | Density ($kg/m^3$) | Volume ($m^3$) | Mass (kg) | Notes / Assumptions |
|---|---|---|---|---|---|
| Cement (CCASCEM2) | 1 part | 1440 | 0.0020 | 2.88 | Base 1:2:3 mix ratio |
| Sand (AGSTB005) | 2 parts | 1600 | 0.0040 | 6.40 | Sharp concreting sand |
| Gravel (AGSTB006, 10 mm) | 3 parts | 1500 | 0.0060 | 9.00 | Jewson gravel/shingle |
| Basalt fibre | 1% of cement mass | 2600 | – | 0.0288 | 28.8 g |
| Polypropylene (PP) fibre | 0.2% of volume | 910 | 0.0000024 | 0.00218 | 2.18 g |
| Water | w/c = 0.45 | 1000 | – | 1.296 | 1.296 L |
| Water reducer (PCE) | 1% of cement mass | – | – | 0.028 | 28 g |

### 3.5 Mechanical Testing

Mechanical performance testing was undertaken to evaluate the strength and structural reliability of the developed concrete mixes under compressive, flexural, and tensile loading conditions. These tests were designed to quantify the mechanical contributions of basalt and polypropylene fibre reinforcement and to compare their performance against that of the conventional control mix.

Such evaluation is essential for determining the suitability of the proposed concrete mixtures for Underground Thermal Energy Storage (UTES) shaft lining applications, where mechanical strength, durability, and resistance to cracking are critical performance requirements (Wang et al., 2025)

All mechanical tests were conducted after a standard curing period of 28 days, which corresponds to the reference age commonly adopted for hardened concrete testing. This approach ensured consistent hydration and strength development across all specimens and allowed direct comparison between mixes. Specimen preparation, curing, and testing procedures were carried out under controlled laboratory conditions in strict accordance with the relevant British Standards, including the BS EN 12390 series (BSI, 2020; SIST EN 12390-12, 2020), thereby ensuring reliability, repeatability, and traceability of results.

Compressive strength tests were performed to assess load-bearing capacity, while flexural and tensile tests were conducted to evaluate crack resistance and post-cracking behaviour, which are particularly relevant for fibre-reinforced systems. The resulting data provided a comprehensive assessment of mechanical performance across the different mix scenarios.

All recorded test results were subjected to statistical analysis to determine the mean values, standard deviations, and coefficients of variation for each mechanical property. These statistical measures enabled the evaluation of data consistency and facilitated comparison between mixes with varying fibre contents and compositions. The analysed results were subsequently used to relate mechanical performance to fibre reinforcement mechanisms and mix design parameters. Furthermore, the mechanical performance data served as key input parameters for the life cycle assessment (LCA), establishing a direct link between structural performance and sustainability outcomes for UTES shaft lining applications.

### 3.5.1 Compressive Strength Testing

Compressive strength evaluations were conducted in accordance with BS EN 12390-3:2019 using a calibrated 2000 kN compression testing machine (Controls Automax 5, Model 65-L27A05).

Figure 10 shows the experimental setup for the compressive strength testing. A controlled loading rate of 0.6 ± 0.2 $MPa \cdot s^{-1}$ was applied to ensure uniform stress distribution and to minimise the risk of premature failure. For each concrete mix design, 12 cube specimens with dimensions of 100 mm were tested, providing a robust statistical basis for evaluating compressive strength performance. Prior to testing, the bearing surfaces of the specimens were carefully inspected, aligned, and cleaned to eliminate surface irregularities and reduce stress concentrations, thereby ensuring accurate and repeatable measurements. The mean compressive strength, standard deviation, and coefficient of variation were subsequently calculated for each mix to assess both strength development and result consistency.

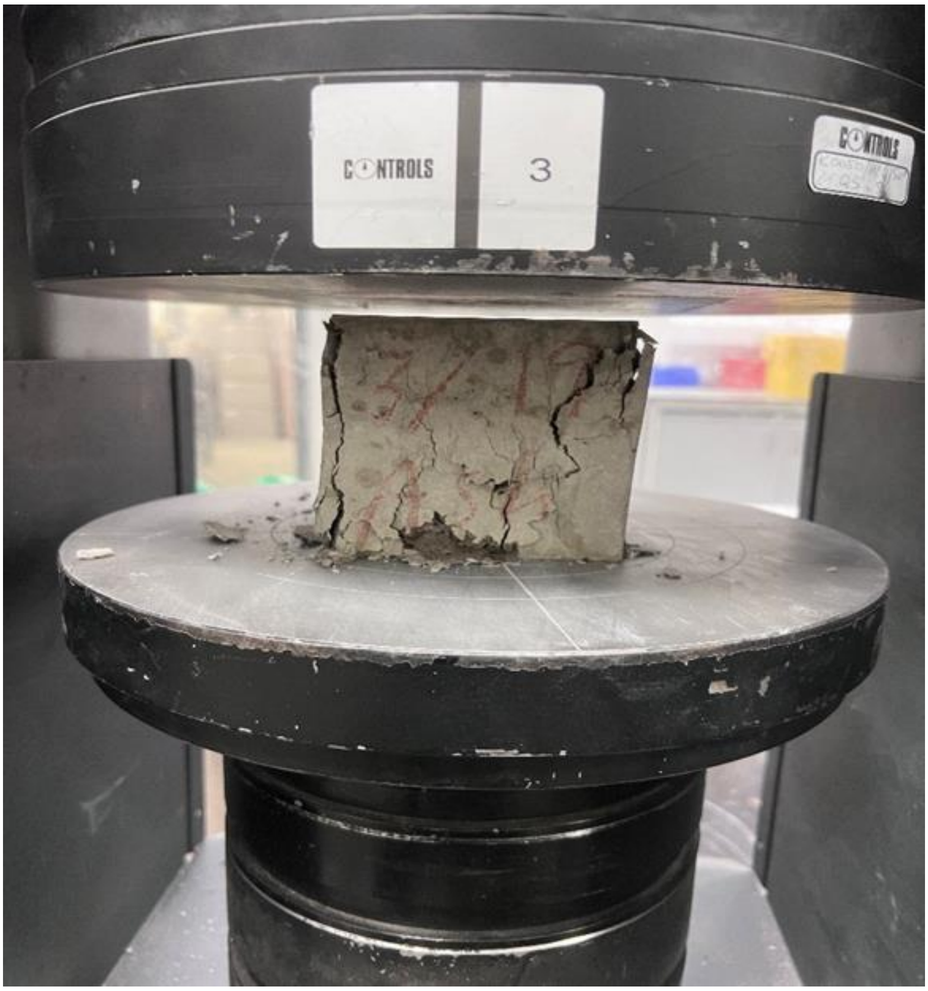


**Figure 10**: Compressive strength test (author's own photo).

The indirect tensile strength, commonly referred to as splitting tensile strength, was assessed in accordance with BS EN 12390-6:2009 using 100 mm cube specimens. Each specimen was positioned horizontally between two steel loading strips and subjected to a diametral compressive load applied at a constant rate until failure occurred along the vertical plane. The splitting tensile strength was calculated based on the maximum load recorded at failure, providing a reliable indicator of the tensile capacity of the concrete. This test was particularly relevant for evaluating the contribution of fibre reinforcement to crack control and post-cracking behaviour under tensile stress conditions. Figure 3.3 illustrates the experimental setup used for the compressive strength testing.

All mechanical testing equipment employed in this study was calibrated on 31 July 2025 to ensure measurement accuracy and compliance with the required precision standards. The corresponding calibration certificates and verification records are provided in Appendix B. The results obtained from these tests formed a key component of the comparative analysis presented in Chapter 4, enabling quantitative assessment of the mechanical performance improvements achieved through the incorporation of hybrid fibre reinforcement in the developed concrete mixes.

### 3.5.2 Tensile Strength Test

The flexural tensile strength of the concrete mixtures was evaluated using a three-point bending test in accordance with BS EN 12390-5:2019 – Testing hardened concrete: Flexural strength of test specimens. This assessment aimed to determine the tensile capacity of the concrete under bending and to analyse the influence of fibre reinforcement on crack initiation, propagation, and post-cracking load-bearing behaviour, which are critical for Underground Thermal Energy Storage (UTES) shaft lining applications. Cubic specimens measuring 100 × 100 × 100 mm were prepared for each mix. After casting, the specimens were compacted on a vibrating table to eliminate trapped air and ensure uniform density. The cubes were demoulded after 24 hours and cured in water at 20 ± 2 °C for 28 days to promote consistent hydration and strength development.

Although BS EN 12390-5 generally prescribes prismatic beam specimens (100 × 100 × 500 mm) for flexural testing, 100 mm cube specimens were employed due to laboratory space and equipment constraints. The testing setup was adjusted to maintain a span-to-depth ratio of approximately 4:1, ensuring comparable stress distribution and bending conditions to those outlined in the standard.

Testing was performed using a servo-controlled universal testing machine equipped with a three-point bending fixture, as shown in Figure 11.

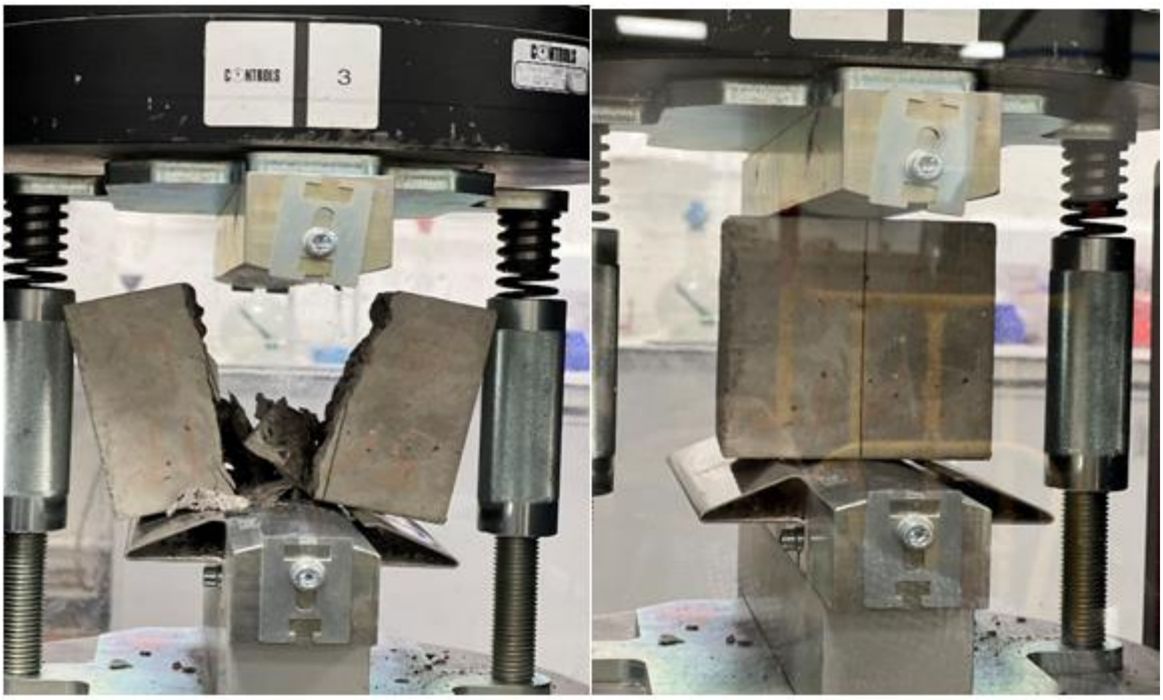


**Figure 11**: Tensile strength test (author's own photo).

Each specimen was positioned horizontally on two steel supports, and a central load was applied at a constant rate of 0.05 ± 0.01 MPa·s$^{-1}$ until failure occurred. The applied flexural load induced tensile stress along the bottom face of the specimen, leading to vertical cracking originating at mid-span. The recorded maximum load was used to calculate the flexural tensile strength, enabling quantitative comparison of the effect of fibre reinforcement across the different concrete mixtures.

#### 3.5.2.1 Flexural Tensile Strength Testing

The flexural tensile strength of the concrete mixtures was determined using a three-point bending test conducted in accordance with BS EN 12390-5:2019 (Testing hardened concrete: Flexural strength of test specimens). This method was selected to characterise the tensile behaviour of concrete subjected to bending, which is particularly relevant for Underground Thermal Energy Storage (UTES) shaft linings, where tensile stresses govern crack initiation, crack propagation, and post-cracking performance under combined thermal and mechanical loading conditions.

For fibre-reinforced concrete systems, flexural testing provides a more representative assessment of tensile performance than direct tensile tests, as it captures the composite interaction between fibres and the cementitious matrix (Anh-Thang Le & An Le Hoang, 2023). This includes crack-bridging mechanisms, stress redistribution after matrix cracking, and enhanced energy absorption, all of which contribute to improved structural resilience (Zhao, Zhang & Li, 2025).

Cubic specimens measuring 100 × 100 × 100 mm were prepared for each concrete mixture. After casting, the specimens were compacted using a vibrating table to remove entrapped air and ensure uniform fibre dispersion. The specimens were demoulded after 24 hours and cured in water at 20 ± 2 °C for 28 days in accordance with BS EN 12390-2, ensuring consistent hydration and strength development.

During testing, each specimen was subjected to a central point load applied at a constant rate until failure. The flexural tensile strength, $f_{ct,fl}$, was calculated using the standard bending equation:

$$f_{ct,fl} = \frac{3FL}{2bd^2}$$

where $F$is the maximum applied load at failure (N), $L$is the span length between supports (mm), $b$is the specimen width (mm), and $d$is the specimen depth (mm). This formulation assumes linear elastic behaviour up to cracking and a uniform stress distribution across the tensile zone. The calculated values enabled direct comparison of tensile performance across the different mix designs and provided quantitative insight into the effectiveness of fibre reinforcement in enhancing flexural behaviour.

#### 3.5.2.2 Theoretical Framework and Calculation of Flexural Tensile Strength

During three-point bending, the applied load generated a bending moment that induced tensile stresses along the lower fibre of the specimen and compressive stresses at the upper surface. Failure occurred when the maximum tensile stress exceeded the tensile capacity of the concrete. The flexural tensile strength, $f_{ct,fl}$, was calculated using classical elastic bending theory for rectangular cross-sections, based on the maximum applied load at failure.

$$f_{ct\cdot fl} = \frac{3fL}{2bd^2}$$

where:

$F$= maximum applied load at failure (N),

$L$= span length between supports (mm),

$b$= specimen width (mm),

$d$= specimen depth (mm).

For the cube specimens used in this study, $b = d = 100$mm, and the span length $L$was adjusted accordingly to satisfy the target span-to-depth ratio.

This equation was derived from linear elastic beam theory, if plane sections remained plane and that tensile failure governed the ultimate capacity. This assumption was considered valid for fibre-reinforced concrete up to first cracking. Beyond this stage, the fibres contributed to post-cracking load transfer, thereby enhancing ductility and residual load-bearing capacity.

#### 3.5.2.3 Evaluation of Configuration and Altered Geometry

Although BS EN 12390-5 specifies the use of prismatic beam specimens, typically measuring 100 × 100 × 500 mm, for flexural strength testing (British Standards Institution 2019). Cube specimens were employed in this study due to limitations in laboratory space and available testing equipment. To ensure mechanical equivalence with the standard testing configuration, the loading arrangement was modified to maintain a span-to-depth ratio of approximately 4:1. This ratio is widely recognised in the literature as sufficient for reproducing comparable bending stress distributions and failure modes when non-standard specimen geometries are adopted.

Flexural evaluations were conducted using a servo-controlled universal testing machine fitted with a three-point bending apparatus. Each cube specimen was positioned horizontally on two steel roller supports, and a concentrated load was applied at mid-span at a controlled stress rate of 0.05 ± 0.01 $MPa \cdot s^{-1}$ until failure occurred. This configuration ensured stable loading conditions and consistent stress application across all specimens.

#### 3.5.2.4 Failure Mode and Relevance to UTES Applications

Flexural loading produced a dominant tensile crack that initiated at the bottom surface near mid-span and propagated vertically towards the compression zone. In fibre-reinforced specimens, crack development was visibly restrained, and load-carrying capacity was maintained beyond first cracking due to fibre-bridging and pull-out mechanisms. This response is particularly relevant for underground thermal energy storage (UTES) shaft linings, where tensile stresses generated by thermal gradients and cyclic heating–cooling can promote crack formation. Improved flexural tensile strength and enhanced post-cracking resistance contribute to effective crack control, reduced permeability, and increased long-term durability of underground thermal storage structures (Wu & Li, 2021).

#### 3.5.2.5 Justification of the Modified Cube-Based Flexural Method

Although BS EN 12390-5:2019 specifies prismatic beam specimens for the determination of flexural tensile strength, numerous studies have demonstrated that non-standard specimen geometries, including cubes and short beams, can produce reliable and comparable results, provided that appropriate span-to-depth ratios and loading configurations are applied (Federal Highway Administration FHWA, 2017). Previous experimental investigations have shown that maintaining a span-to-depth ratio within the range of 3.5–4.5 promotes a bending-dominated stress state and generates tensile stress distributions at the extreme fibre that are comparable to those obtained using standard prismatic beams (RILEM TC 162-TDF; Mindess et al., 2003; Banthia and Gupta, 2006).

Cube-based flexural testing has therefore been widely adopted in fibre-reinforced concrete research, particularly where material availability, laboratory equipment, or experimental constraints limit the use of conventional beam specimens. This approach preserves the fundamental tensile failure mechanism, with crack initiation occurring at the tension face near mid-span, consistent with classical elastic beam theory (Neville, 2011; Bentur and Mindess, 2007).

The primary objective of this study was to evaluate the comparative performance of different concrete mixes rather than to establish absolute design values. Consequently, the use of cube-based flexural testing was considered methodologically appropriate and sufficiently robust for identifying relative differences in tensile resistance, crack control, and post-cracking behaviour, while ensuring consistency and repeatability across all test scenarios.

#### 3.5.2.6 Relevance of Flexural Tensile Strength to UTES Shaft Lining Performance

Flexural tensile strength represents a critical mechanical parameter for underground thermal energy storage (UTES) shaft linings, as their structural behaviour is predominantly governed by tensile stresses generated by restrained thermal deformation rather than by pure compressive loading (Schmidt et al. 2024). During thermal charging and discharging cycles, temperature gradients develop across the lining thickness, inducing bending moments and associated tensile stresses that may exceed the direct tensile capacity of plain concrete, thereby initiating cracking.

The flexural tensile strength evaluated in this study served as a reliable indicator of the concrete's resistance to thermally induced cracking under bending-dominated stress conditions representative of in-service shaft linings. In fibre-reinforced concrete, the presence of fibres enhanced tensile performance by bridging both micro- and macro-cracks, redistributing stresses, and delaying crack localisation and propagation. These mechanisms contributed to improved post-cracking load-bearing capacity and increased ductility under thermal and mechanical loading.

Enhancements in flexural tensile strength and post-cracking behaviour directly reduced crack widths during repeated thermal cycling, thereby limiting potential leakage pathways and preserving the functional integrity of the shaft lining. Reduced crack widths also improved watertightness, mitigating the risk of groundwater ingress and limiting exposure to aggressive chemical environments.

Furthermore, improved flexural performance increased durability under cyclic thermal loading, reducing the likelihood of progressive damage and decreasing long-term maintenance requirements. Collectively, these benefits enhanced the operational reliability and safety of UTES systems by minimising the risk of structural degradation or failure during service. Flexural tensile testing therefore, provided a robust and application-relevant basis for assessing the suitability of fibre-reinforced concrete linings for UTES shafts, capturing key performance attributes related to cracking resistance, durability, and long-term structural integrity.

## 3.6 Thermal Testing

### 3.6.1 Assessment of Thermal Conductivity

Thermal conductivity testing was performed to evaluate the heat-transfer characteristics of the developed concrete mixes. This property is particularly important for Underground Thermal Energy Storage (UTES) applications (Colangelo et al. 2017), as efficient heat transfer through shaft lining materials directly affects system performance, energy efficiency, and long-term structural reliability. The thermal conductivity of the concrete specimens was measured using a Hot Disk Thermal Constants Analyser (Model TPS 2500 S, Sweden), as shown in Figure 12 and summarised in Table 3. The instrument operates based on the Transient Plane Source (TPS) method. It complies with the requirements of BS EN ISO 10456:2007 + A1:2009, which specifies standard procedures for determining the thermal properties of construction materials.

The TPS method employs a thin nickel double-spiral sensor that functions simultaneously as a heat source and a temperature sensor.

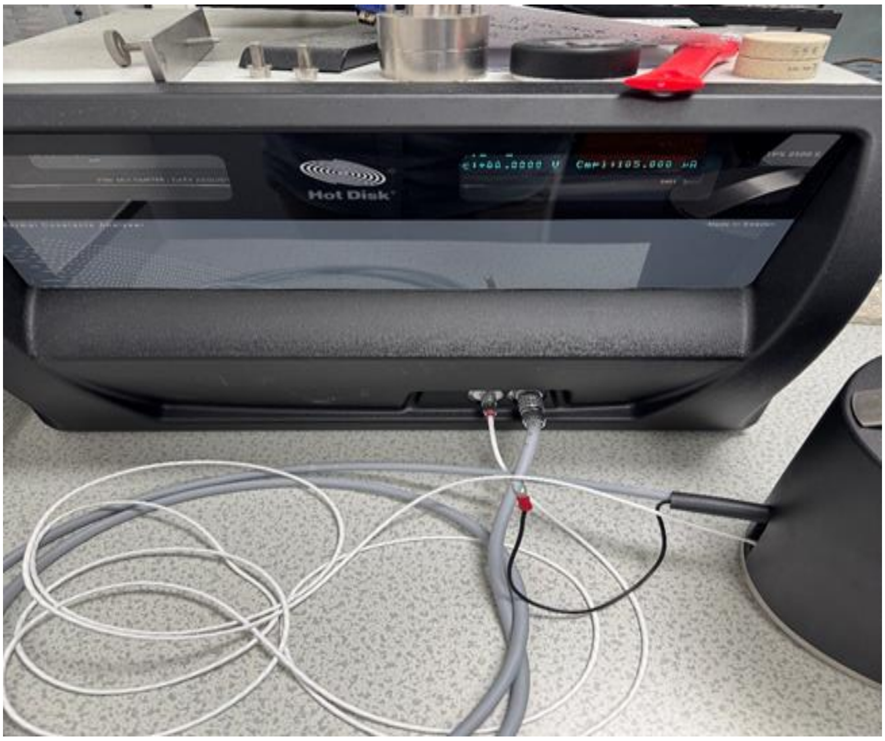


**Figure 12:** Hot Disk Thermal Constants Analyser (Model TPS 2500 S) (author's own photo).

**Table 3**: Thermal Conductivity Testing Setup and Measurement Framework

| Label | Description |
|---|---|
| A | Hot Disk TPS 2500 S device used for measuring thermal conductivity |
| B | Sensor positioned between concrete specimen halves during testing |
| C | Data acquisition and analysis process using Hot Disk software |

During testing, the sensor was positioned between two halves of each concrete specimen. A controlled electrical pulse was applied to generate a transient heat flow, and the resulting temperature rise was recorded over time. Thermal conductivity (k) and thermal diffusivity (α) were subsequently calculated using transient heat transfer equations embedded within the analysis software.

All specimens were prepared as 100 × 100 × 100 mm cubes, consistent with those used for mechanical testing, to ensure comparability across test methods. Before measurement, specimens were conditioned to a saturated surface-dry state to replicate the moisture conditions typically encountered in subterranean environments. Measurements were conducted at ambient temperature under controlled laboratory conditions.

Each concrete mix was tested in triplicate to improve the reliability, and mean values were used for subsequent analysis. Instrument calibration was verified prior to testing using a reference material with known thermal conductivity (Pyrex standard), ensuring measurement accuracy and compliance with manufacturer specifications.

The recorded temperature–time data were analysed using Hot Disk software, which automatically fitted the experimental results to the theoretical heat-transfer model. The derived thermal conductivity values were statistically validated and incorporated into the comparative performance assessment presented in Chapter 4 (Results and Discussion).

In the Hot Disk Transient Plane Source (TPS) method, the sensor was supplied with a constant electrical power, and the resulting average temperature rise was recorded over time. For an isotropic and homogeneous material of sufficiently large extent, the theoretical temperature response of the sensor embedded within the specimen can be expressed as:

$$\Delta T(t) = \frac{P}{\pi^{3/2} r^2 k} D(\tau)$$

Where is the total heating power applied to the sensor (W), is the thermal conductivity of the specimen (W·m$^{-1}$·K$^{-1}$), and is a dimensionless time-dependent function defined by the TPS analytical model.

The dimensionless time is given by:

$$\tau = \frac{at}{r^2}$$

where is the thermal diffusivity of the material (m$^2$·s$^{-1}$),

is the heating time (s) and is the sensor radius (m).

The slope and overall shape of the measured curve were used to determine both the thermal conductivity and thermal diffusivity of the concrete specimens.

Thermal conductivity primarily governed the magnitude of the temperature rise, such that materials with higher thermal conductivity exhibited faster heat dissipation and consequently lower temperature increases for a given power input.

In contrast, thermal diffusivity controlled the rate of heat propagation through the material, thereby influencing the temporal response of the temperature curve.

In addition to thermal conductivity and diffusivity, the volumetric heat capacity or specific heat capacity was estimated using the following relationship:

$$a = \frac{k}{\rho c_p} \Rightarrow c_p = \frac{k}{\rho a}$$

The combined evaluation of thermal conductivity, thermal diffusivity, and specific heat capacity enabled a comprehensive interpretation of the thermal behaviour of the concrete lining materials. These properties are particularly relevant for Underground Thermal Energy Storage (UTES) applications, as they govern both heat transfer efficiency and thermal response time, thereby influencing system performance and long-term operational stability.

### 3.6.2 Method requirements and limitations

The Transient Plane Source (TPS) method relies on several theoretical assumptions, including local homogeneity and isotropy of the measured region (Gustafsson, 1991; He et al., 2007). To satisfy the semi-infinite boundary condition, the specimen dimensions were required to exceed the sensor radius several times (ISO 22007-2:2015; Hot Disk AB, 2018). Good thermal contact between the sensor and the specimen surfaces was ensured to minimise contact resistance, which can otherwise lead to underestimation of thermal conductivity (He, 2005; Dickens et al., 2007). Heating power was kept low to produce a small and controlled temperature rise, maintaining effectively constant thermal properties during testing (Gustafsson, 1991; Hakansson & Gustafsson, 2016).

The TPS method measures the transient temperature increase of a sensor embedded between two specimen halves. Thermal conductivity (k) and diffusivity (α) were calculated by fitting the temperature–time response to the theoretical heat transfer model based on Fourier's law. Limitations of the method include sensitivity to surface roughness, moisture variability, and deviations from isotropy, which were mitigated by conditioning specimens to a stable saturated surface-dry (SSD) state in accordance with ISO 10456:2007+A1:2009.

## 3.7 Quality and Uncertainty of Data

Ensuring the reliability, accuracy, and reproducibility of all experimental results was a primary consideration throughout this study. All testing procedures were conducted in strict accordance with the relevant British Standards, including the BS EN 12390 series for mechanical testing and BS EN ISO 10456:2007 +A1:2009 for thermal property assessment. These standards define recognised testing methodologies, calibration requirements, and data reporting protocols, thereby providing a consistent and validated framework for experimental evaluation.

To achieve a high level of data quality, all measurements were obtained using calibrated, traceable, and certified laboratory instruments. Calibration of the primary testing equipment, including the 2000 kN compression testing machine and the Hot Disk TPS 2500 S Thermal Constants Analyser, was verified and documented before testing. Supporting instrumentation, such as digital balances, thermometers, and moisture meters, was periodically calibrated in accordance with manufacturers' specifications to ensure ongoing measurement accuracy.

All experimental tests, including compressive, tensile, flexural, and thermal conductivity measurements, were conducted in triplicate. Results were reported as mean values accompanied by standard deviations, providing a quantitative assessment of data variability and consistency. Replicating testing under identical conditions minimised random errors and ensured internal consistency across all datasets.

Testing was conducted in controlled laboratory environments to minimise external sources of variability. Ambient temperature and relative humidity were monitored and maintained within the limits prescribed by the applicable standards. Curing conditions were standardised to prevent premature moisture loss or excessive saturation of specimens. Mechanical test specimens were stored in water at 20 ± 2 °C until the day of testing to ensure uniform hydration. For thermal conductivity measurements, specimens were conditioned to a saturated surface-dry state immediately before testing, thereby simulating the moisture conditions representative of underground thermal energy storage (UTES) environments.

During batching, a mass balance approach was implemented to confirm consistency in mix proportions and fibre dosage across all specimens. This procedure reduced the potential for heterogeneity in fibre dispersion or matrix composition, which could otherwise influence mechanical and thermal performance.

Minor fluctuations in transient temperature–time curves were occasionally observed during thermal conductivity testing. These variations were primarily attributed to small differences in sensor contact pressure or specimen surface flatness. However, all deviations remained within the manufacturer's specified tolerance range, typically less than 3%, confirming acceptable repeatability.

Overall measurement uncertainty for each parameter was estimated by combining instrumental uncertainty, as reported in calibration certificates, with repeatability uncertainty derived from replicate test standard deviations. The resulting uncertainty levels were within acceptable limits for construction material testing, ensuring that the reported results accurately represent the intrinsic properties of the investigated concrete mixtures. Consequently, the experimental methodology adopted in this study achieved a high degree of precision and reliability, allowing the findings presented in Chapter 4 to be interpreted with confidence and reproducibility.

### 3.7.1 Sources of Uncertainty

Three primary sources of uncertainty were identified and monitored throughout the modelling process: variability in laboratory measurements, including thermal conductivity, fibre dispersion, and material density; reliance on proxy datasets for basalt and polypropylene fibres in the absence of UK-specific data; and assumptions regarding transportation distances for raw materials, along with possible fluctuations in the composition and carbon intensity of the UK electricity grid. All uncertainties were documented systematically and assessed both qualitatively and quantitatively to evaluate their influence on model outputs.

## 3.8 Life Cycle Assessment

LCA was conducted to evaluate the environmental impacts associated with the production, use, and end-of-life stages of the developed concrete mixes. LCA provides a systematic approach to quantify energy consumption, greenhouse gas emissions, and other environmental burdens throughout the life cycle of a product, enabling a comprehensive assessment of sustainability performance (Figure 13).

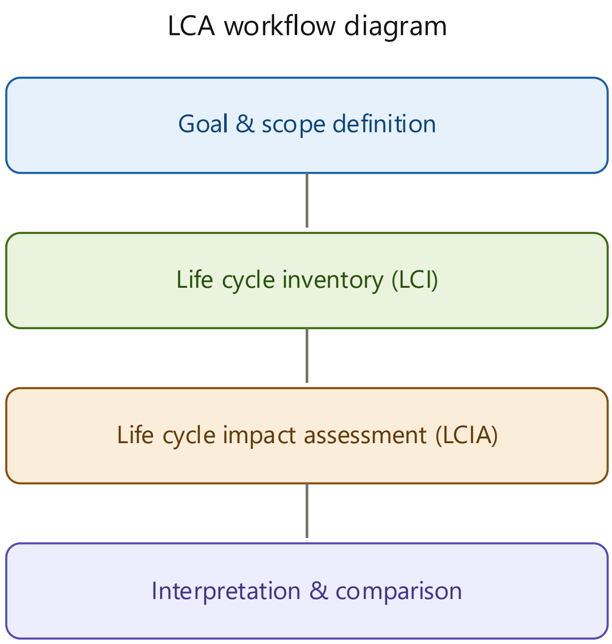


**Figure 13**: Workflow of the life-cycle assessment (LCA) methodology adopted in this study, illustrating the sequential relationship between goal and scope definition, life-cycle inventory (LCI), life-cycle impact assessment (LCIA), and interpretation (developed by the author).

### 3.8.1 Goal and Scope Definition

The analytical component of this study employed an attributional life-cycle assessment (LCA) framework in accordance with ISO 14044 (2006) and EN 15804 (2019), thereby ensuring compliance with internationally recognised standards for environmental evaluation. The functional unit was defined as 1 $m^3$ of concrete lining, reflecting a practical, application-specific reference for underground thermal energy storage (UTES) shaft linings. The system boundary adopted a cradle-to-operation perspective, encompassing life-cycle stages A1–A3 (raw material extraction, transport, and manufacturing) and B1 (use-phase operational energy).

This boundary was selected to capture both the embodied impacts of material production and the operational performance of concrete under thermally demanding service conditions, enabling a comprehensive assessment of the environmental implications of each mix. Primary data derived from the experimental programme—specifically, measured mechanical and thermal properties, including compressive strength, tensile strength, and thermal conductivity—were used to construct the life-cycle inventory (LCI). Life-cycle modelling was conducted using open LCA v2.4.1, with background processes obtained from the ecoinvent v3.9.1 database. Energy inputs were modelled using the Great Britain electricity market mix, ensuring an accurate representation of regional energy sources. Where UK-specific datasets were unavailable, appropriate European or global proxy datasets were selected in accordance with the hierarchical rules prescribed by ecoinvent, maintaining geographical and methodological consistency. Environmental impacts were quantified using the CML (2016) baseline midpoint method, developed by Leiden University's Institute of Environmental Sciences, providing a robust, internationally accepted set of impact indicators suitable for comparing concrete systems and materials.

The primary aim of this LCA was to quantify and compare the environmental impacts associated with the production and operational performance of three experimentally designed concrete mixes: a conventional mix (1:2:4), a nominal mix (1:2:3), and a hybrid fibre-reinforced mix (1:2:4 incorporating basalt and polypropylene fibres). The assessment focused on evaluating the effects of integrating basalt and polypropylene fibres on both the embodied environmental burdens—including raw material extraction, processing, and mixing—and the operational energy performance, particularly the heat-transfer efficiency of the concrete during service. By integrating experimentally measured thermal conductivity and mechanical performance data, the study captured both material-centric and functional performance-related impacts, ensuring the LCA reflected realistic service conditions.

A key objective was to determine whether fibre reinforcement enhances overall sustainability by reducing lifetime heat losses and improving thermal efficiency, despite the potential increases in embodied impacts associated with fibre production. This included evaluating the trade-offs between higher embodied carbon from fibre incorporation and the long-term benefits of reduced operational energy losses during UTES operation. The approach employed an attributional modelling framework, which allows the separation of impacts attributable to each mix component, including the contributions of cement, aggregates, fibres, and admixtures, thereby providing detailed insight into the sources of environmental burdens.

The study also aimed to provide a robust, quantitative foundation for selecting environmentally preferable concrete formulations for UTES infrastructure. By linking laboratory-derived mechanical and thermal performance data with life-cycle impacts, the LCA enables a holistic assessment of material choices that balances structural, thermal, and environmental criteria. Such an integrated methodology contributes to the overarching goals of low-carbon heating, sustainable subsurface energy storage, and improved durability of UTES shaft linings in the UK context. Ultimately, this work supports informed decision-making for engineers, designers, and policymakers seeking resilient, high-performance, and environmentally responsible concrete solutions for underground energy storage applications.

### 3.8.2 Classification of LCA and Methodological Framework

This study adopted an attributional Life Cycle Assessment (LCA) approach to evaluate the average environmental performance of the concrete lining systems under investigation. Attributional LCA was selected as it quantifies the environmental burdens associated with the production and use of a defined system without accounting for market-mediated or consequential effects. The assessment was conducted in accordance with the methodological principles outlined in ISO 14044 (2006) and EN 15804 (2019), which provide specific guidance for the environmental evaluation of construction materials.

The LCA framework followed the four standard phases defined in ISO 14040: (i) goal and scope definition, including the establishment of system parameters; (ii) compilation of the Life

Cycle Inventory (LCI); (iii) Life Cycle Impact Assessment (LCIA); and (iv) interpretation and analysis of results. This structured approach ensured transparency, consistency, and reproducibility throughout the assessment process. All life-cycle modelling and impact calculations were performed using OpenLCA (version 2.4.1). The background data for material production, energy supply, and transport processes were sourced from the Ecoinvent database (version 3.9.1, cut-off system model). Environmental impacts were evaluated using the CML v4.6 (2016) midpoint impact assessment method, which provides a set of well-established indicators widely applied in the assessment of cementitious and construction materials. The functional unit (FU) was defined as: 1 $m^3$ of concrete lining material installed in a UTE'S shaft, providing structural integrity and thermal containment over a 30-year service life. This functional unit enabled a consistent comparison of the three concrete mix scenarios on an equivalent structural and functional basis. All material inputs, energy consumption, and emissions were normalised to this reference unit. The system boundary was defined as cradle-to-operation (A1–A3 + B1), as illustrated in Figure 14. Included life-cycle stages comprised A1 (raw material extraction and processing), A2 (transport of materials to the mixing plant based on UK average distances), A3 (manufacturing and mixing processes), and B1 (operational energy use associated with heat-loss behaviour during UTES thermal cycling, derived from experimentally measured thermal conductivity values). Excluded stages encompassed A4–A5 (transport to site and installation), B2–B7 (maintenance and replacement), C1–C4 (end-of-life processes), and Module D (benefits beyond the system boundary). These exclusions were justified on the basis that their contributions were expected to be minimal in differentiating the comparative environmental performance of the concrete mixes and fell outside the core objectives of this study.

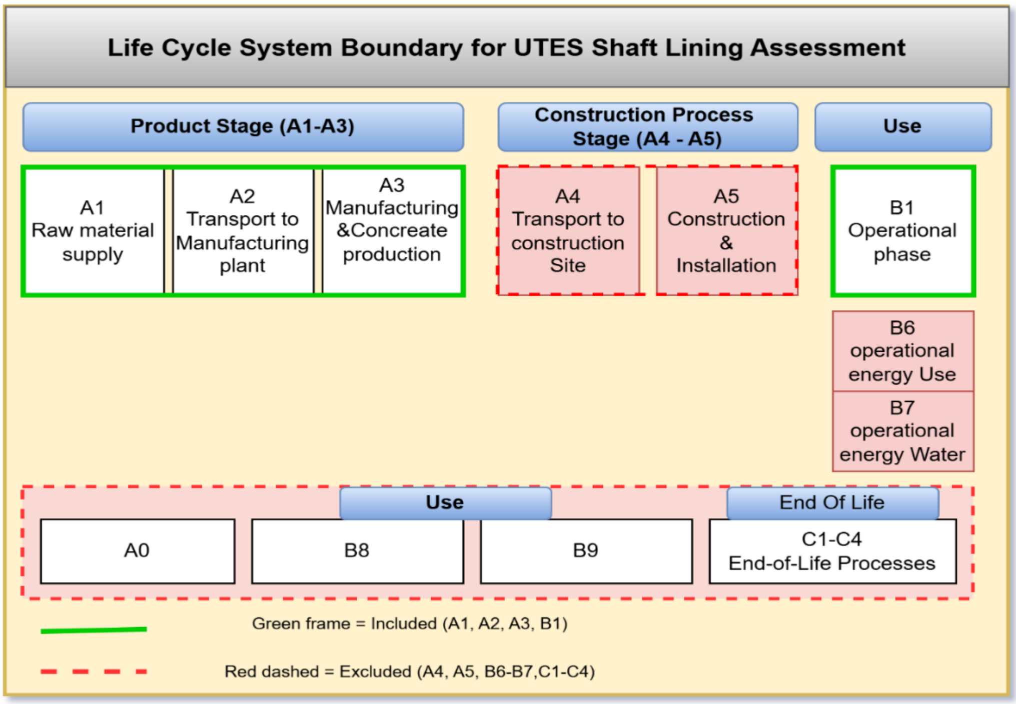


**Figure 14**: System boundary definition for the Life Cycle Assessment (LCA) of UTES shaft lining materials, illustrating included stages (A1 raw material extraction, A3 manufacturing, and B1 operational performance) and excluded lifecycle modules (developed by the author).

This study was geographically constrained to the United Kingdom, with particular emphasis on conditions relevant to Great Britain. These constraints primarily reflected the national electricity generation mix and transportation infrastructure, which directly influence the environmental performance of construction materials.

The assessment was temporally aligned with the 2025 Great Britain grid-average to ensure energy-related impacts were representative of current and near-term operational conditions. Where available, UK- and Great Britain–specific datasets were applied to enhance regional relevance. Great Britain–specific electricity mix datasets from Ecoinvent version 3.9 (cut-off system model) were used for the manufacturing (A3) and operational energy use (B1) stages. This ensured that both production-related energy consumption and operational electricity demand during the use phase were modelled using regionally representative data.

For the upstream life-cycle stages (A1–A2), Ecoinvent does not provide Great Britain–specific datasets for several key processes, including cement production, aggregate extraction, admixture manufacture, and fibre production. Consequently, European (RER) or Rest-of-World (RoW) proxy datasets were employed where appropriate. The selection of proxy datasets followed established LCA practice and was applied consistently across all mix scenarios to maintain comparability. This approach ensured data transparency while minimising potential bias arising from dataset limitations.

### 3.8.4 Modelling Assumptions

Several key assumptions were applied to support the life cycle modelling framework adopted in this study. Fibre contents and concrete mix proportions were derived from experimentally validated designs, as described in Section 3.2.3, ensuring consistency between laboratory testing and environmental assessment. Transport distances for raw materials were estimated based on typical regional supply chains within the UK. Distances of approximately 50 km for aggregates and 100 km for cement were assumed, in line with commonly adopted reference distances used in UK concrete LCAs (e.g. Mineral Products Association supply chain benchmarks) and previous studies (Keyhani, Abbaspour et al., 2023). Although no definitive UK standard prescribes these values, they fall within the range reported in recent literature. Alternative approaches, such as site-specific distance estimation using digital mapping tools, have been employed in recent studies (Thorne et al., 2024); however, in the absence of project-specific transport data, the adopted assumptions were considered appropriate. The potential influence of transport distance variability on the results was examined through sensitivity analysis (Section 3.3.6).

Water and chemical admixture consumption were measured experimentally and subsequently scaled to a functional unit of 1 $m^3$ of concrete. Electricity consumption associated with mixing and curing processes was modelled using the Great Britain electricity mix to ensure regional representativeness. The operational energy component (B1) was modelled using experimentally measured thermal conductivity values to estimate annual heat-loss rates through the concrete lining. Comprehensive documentation of all data sources, assumptions, and associated uncertainties is provided in Section 3.3.6 (Data Quality and Limitations).

### 3.8.5 System Boundary and Functional Unit

Figure 3.7 illustrates the defined system boundaries and assessment logic adopted in this study. The system boundary (SB) outlines the methodological framework and analytical protocols applied in the Life Cycle Assessment (LCA) of three concrete mixtures: conventional concrete, nominal fibre-reinforced concrete, and hybrid fibre-reinforced concrete incorporating basalt and polypropylene fibres. The defined boundary represents a cradle-to-operation perspective (Modules A1–A3 + B1), encompassing all processes from raw material extraction through to operational energy consumption associated with the Underground Thermal Energy Storage (UTES) shaft liner.

The selection of system boundaries and life-cycle modules was guided by the requirements of EN 15804 (2019) and by the relevance of each stage to the environmental profile of the evaluated concrete materials. The adopted framework ensured consistency, transparency, and comparability across the assessed scenarios. The life-cycle stages included within the system boundary are described below.

Module A1 (Raw Material Supply) covered the procurement, extraction, processing, and production of all constituent materials, including cement clinker, fine and coarse aggregates, basalt and polypropylene fibres, chemical admixtures, and mixing water. This module also incorporates upstream processes related to fuel production and energy supply used during material extraction and manufacturing.

Module A2 (Transport) accounted for the transportation of all raw materials from suppliers to the concrete mixing facility. Transport modelling employed average UK road distances derived from regional supply-chain data, typically 50 km for aggregates and 100 km for cement. These assumptions are consistent with established UK concrete LCA studies and industry benchmarks (MPA, 2023; Thorne et al., 2024). Transportation processes were represented using rigid freight trucks (16–32 t), based on datasets obtained from Ecoinvent version 3.9.

Module A3 (Manufacturing) encompassed the batching and mixing stages of concrete production. This included electricity consumption associated with mixing operations, as well as water use for batching, equipment washing, and curing. Due to the controlled laboratory procedures employed, solid and liquid waste generated during cleaning and preparation were minimal and therefore considered negligible within the scope of this assessment.

The use phase (Module B1) addressed operational energy requirements associated with heat loss through the UTES concrete lining. Experimentally measured thermal conductivity values for each concrete mixture were used to estimate heat-loss rates during operation (see Section 3.2.5). This approach enabled the functional differentiation of materials based on thermal performance and energy efficiency over the assumed 30-year operational lifespan of the UTES system.

Construction activities (A4–A5), maintenance and repair processes (B2–B7), and end-of-life stages (C1–C4) were excluded from the system boundary, as they were outside the primary focus of this study and were expected to exert a relatively small and comparable influence across all scenarios. Module D, representing benefits beyond the system boundary, was also excluded because no secondary material recovery or avoided-burden credits were considered in this baseline analysis. All relevant upstream and downstream elementary flows were incorporated through the Ecoinvent v3.9 background database. In this study, the B1 use-phase module is limited to operational heat losses associated with the thermal performance of the concrete shaft lining. These losses are quantified based on measured thermal conductivity values and translated into additional energy demand over the assumed service life.

Maintenance, inspection, repair, and material replacement are excluded from B1 due to the absence of reliable long-term performance data for UTES linings and to maintain consistency with a cradle-to-operation system boundary. The potential implications of reduced degradation and maintenance demand associated with advanced fibre-reinforced concretes are therefore discussed qualitatively rather than modelled quantitatively.

#### 3.8.5.1 Functional Unit

The functional unit (FU) adopted in this study was defined as 1 $m^3$ of concrete lining material installed in an Underground Thermal Energy Storage (UTES) shaft, providing structural integrity and thermal containment over a 30-year service life. This definition was selected to ensure functional equivalence across the three concrete mix scenarios and to enable a direct and meaningful comparison of their environmental performance on a consistent structural and operational basis.

All life cycle inventory data, including material quantities, energy consumption, and emissions, were normalised to this reference volume. Material inputs were scaled directly from experimentally validated laboratory mix designs to a production volume of 1 $m^3$, while maintaining consistent mass and volume proportions for cement, aggregates, water, and fibres. This approach ensured that differences observed between scenarios were attributable to material composition and performance rather than inconsistencies in scaling or functional definition.

The adopted functional unit explicitly incorporated both structural and thermal performance requirements, reflecting the dual role of the concrete lining within the UTES system. Structural integrity was assumed to be maintained throughout the defined service life, while thermal containment was represented through operational energy demand associated with heat loss during use. These assumptions ensured alignment between the functional unit and the operational performance model applied in the use phase (Module B1).

No allocation between co-products was required, as all foreground processes within the defined system boundary were mono-functional and did not generate secondary products. In accordance with the Ecoinvent cut-off approach, recycling credits and by-product allocations were not applied.

All background processes were modelled using the cut-off system model in Ecoinvent version 3.9, which assigns environmental burdens to the first life cycle of materials and excludes benefits from subsequent reuse or recycling.

A general cut-off threshold of 1% by mass and less than 2% of total environmental impact contribution was applied. This ensured that all environmentally relevant flows were captured while excluding insignificant auxiliary processes that would not materially influence the results. Figure 3.7 illustrates the cradle-to-operation system boundary adopted in this study, indicating included and excluded life-cycle stages and the interaction between foreground processes and the Ecoinvent background database.

### 3.8.6 Life Cycle Inventory (LCI)

#### 3.8.6.1 Data Structure and Modelling Approach

All life-cycle modelling was conducted using OpenLCA (version 2.4.1), with the Ecoinvent database (version 3.9, cut-off system model) as the background data source. Foreground processes were created to represent site-specific and experimentally derived inventory data for each concrete mix. In contrast, background processes supplied standardised datasets for upstream and downstream activities, including cement manufacture, electricity generation, fuel combustion, and raw material extraction.

Each life-cycle stage within the defined system boundary was modelled as a separate unit process in OpenLCA and connected via product flows to ensure transparent, traceable data exchange between modules. The modelling structure enabled clear differentiation between foreground and background systems, facilitating consistency across scenarios. Figure 14, LCI (placeholder) illustrates the overall model architecture, showing the interconnection between the foreground processes (Modules A1–A3 and B1) and the Ecoinvent background database.

**3.8.6.2 Foreground Data Collection**

Foreground inventory data were derived directly from the experimentally validated concrete mix designs presented in Section 3.2.3 and subsequently scaled to the functional unit of 1 $m^3$ of concrete. Measured component quantities ($kg/m^3$) were converted into mass flows for each material input, including cement, fine and coarse aggregates, water, chemical admixtures, basalt fibres, and polypropylene fibres. Electricity consumption associated with batching and mixing was based on recorded energy use during laboratory mixing trials and was adjusted to reflect equivalent industrial-scale efficiency. A representative life-cycle inventory was developed for each concrete mix, using experimentally determined material proportions and energy inputs. All foreground flows were linked to corresponding background processes through unit processes within OpenLCA to ensure consistency in system integration (Table 3.4). Where region-specific UK datasets were unavailable, particularly for basalt fibres, polypropylene fibres, and certain admixtures, proxy datasets were employed in accordance with best-practice guidance outlined in ISO 14044 (§4.3.3.2). Each proxy dataset was evaluated for consistency in energy intensity and emission profiles against published literature to minimise uncertainty. Basalt fibre production data were manually compiled from Fořt et al. (2021, Table 4), incorporating primary energy demand, electricity requirements for fibre drawing, and auxiliary materials such as lubricants and sizing agents. Polypropylene fibre production was modelled using the "Polypropylene fibre production (Brown, Kolo et al.)" dataset, which represents globally averaged polymer extrusion processes.

All fibre production datasets were parameterised to reflect the fibre dosages specified in the experimental mix designs (Section 3.2.3). The complete model was structured hierarchically within OpenLCA, linking the four primary life-cycle modules (A1–A3 and B1).

This approach ensured full traceability of material and energy flows between the foreground experimental data and the Ecoinvent background system, providing a robust and reproducible basis for the subsequent life-cycle impact assessment described in Section 3.3.4.

**Table 4**: A representative LCI breakdown for each concrete mix

| Material | Ecoinvent Process | Dataset Location | Notes |
|---|---|---|---|
| Cement (CEM I 52.5 N) | Cement production, Portland | RER | Default European average process |
| Sand (AGSTB005) | Sand production | RER | Quarry sand |
| Gravel (AGSTB006, 10 mm) | Gravel production | RER | Coarse aggregate |
| Basalt fibre | Custom process (Fořt et al., 2021, Table 4) | Proxy | Manually created unit process |
| Polypropylene fibre | Polypropylene fibre production | RoW | Generic polymer fibre process |
| Water reducer (PCE) | Admixture production | RER | Generic chemical process |
| Transport (A2) | Lorry, 16–32 t, EURO 6 | RER | Average km distance |
| Electricity (A3) | Electricity (A3) | Electricity (A3) | Electricity (A3) |

### 3.8.7 Impact Assessment Method

The study employed the CML v4.6 (2016) life-cycle impact assessment (LCIA) methodology, developed by the Institute of Environmental Sciences (CML) at Leiden University. This midpoint-focused approach provides a comprehensive, well-validated set of impact categories, making it particularly suitable for assessing construction materials, including cementitious products. Its alignment with EN 15804 (2019) and integration within OpenLCA v2.4.1 ensured methodological consistency and facilitated comparability with published European LCAs of concrete and other building materials. Potential environmental impacts were evaluated by characterising the elementary flows associated with each process, including emissions such as $CO_2$, $NO_x$, $CH_4$, and $SO_2$, throughout the complete life cycle of the product system. In Table 5 below, the following midpoint indicators were included in the assessment.

**Table 5:** Summary of CML v4.6 (2016) midpoint impact categories, indicators, reference units, and major contributing substances

| Impact Category | Indicator | Reference Unit | Main Contributing Substances |
|---|---|---|---|
| Global Warming Potential (100 years) | $GWP_{100}$ | kg $CO_2$ eq | $CO_2$, $CH_4$, $N_2O$ |
| Acidification Potential | AP | kg $SO_2$ eq | $SO_2$, $NO_x$, $NH_3$ |
| Eutrophication Potential | EP | kg $PO_4^{3-}$ eq | $NO_3^-$, $NH_4^+$, phosphates |
| Photochemical Ozone Creation Potential | POCP | kg $C_2H_4$ eq | VOCs, CO, $NO_x$ |
| Ozone Depletion Potential | ODP | kg CFC-11 eq | CFCs, halons |
| Abiotic Depletion Potential (fossil) | ADPf | MJ | Crude oil, natural gas, coal |
| Abiotic Depletion Potential (elements) | ADPe | kg Sb eq | Metallic minerals |
| Human Toxicity Potential | HTP | kg 1,4-DCB eq | Heavy metals, organics |
| Freshwater and Marine Ecotoxicity Potentials | FAETP / MAETP | kg 1,4-DCB eq | Metals, organics |

All outcomes were calculated and reported per functional unit of 1 $m^3$ of concrete lining, as defined in Section 3.3.2. Characterisation factors from the OpenLCA CML v4.6 (2016) library were applied directly to convert life-cycle inventory flows into midpoint environmental impact potentials. No further weighting or aggregation beyond midpoint characterisation was performed, in accordance with ISO 14044 (2006), ensuring transparency and scientific impartiality. To support comprehensive analysis, normalisation to global average reference values was conducted within OpenLCA, enabling the comparison of the relative significance of different impact categories; however, these normalised values were used solely for interpretative purposes and were not applied in decision-making. This LCIA methodology provides a robust and widely accepted approach for assessing the environmental performance of conventional, nominal, and hybrid concrete mixtures under consistent assumptions and defined system boundaries, ensuring comparability and reproducibility across all evaluated scenarios.

### 3.8.8 Scenario Definition

Three concrete mix scenarios were developed to ensure consistency between the experimental program (Section 3.2.3) and the life-cycle assessment (LCA) modelling in OpenLCA. Each scenario represented a distinct formulation, reflecting differences in performance characteristics and design objectives (Table 6), ranging from conventional concrete to advanced hybrid fibre-reinforced mixtures.

**Table 6**: Description and key parameters of the three concrete mix scenarios used for experimental testing and life-cycle assessment (LCA).

| Scenario | Description | Mix Ratio (C: S: A) | Fibre / Admixture Additions | Thermal Conductivity, k ($W \cdot m^{-1} \cdot K^{-1}$) |
|---|---|---|---|---|
| 1 Conventional | Baseline control mix used as reference for mechanical and thermal benchmarking. | 1: 2: 4 | None | 1.90 |
| 2 Hybrid | Advanced fibre-reinforced concrete incorporating basalt and polypropylene fibres with a polycarboxylate-ether (PCE) superplasticiser for improved strength and thermal behaviour. | 1: 2: 4 | Basalt fibres: 1 % by mass of cement pp fibres: 0.2 % by volume of concrete pCE admixture: 1 % by mass of cement | 2.41 |
| 3 Nominal | Higher cement-content mix representing a conventional strength-optimised concrete without fibres, used for comparative evaluation of thermal and environmental performance. | 1: 2: 3 | None | 2.00 |

Modelling these scenarios enabled a direct comparison of the baseline, optimized-strength, and fibre-reinforced alternatives with respect to both embodied and operational environmental impacts. This approach ensured that the LCA results could be meaningfully interpreted in the context of experimentally validated material properties, facilitating an integrated assessment of structural performance and sustainability.

#### 3.8.8.1 Integration of Scenario Rationale and Modelling

Three concrete mix scenarios were developed to align the experimental program (Section 3.2.3) with the life-cycle assessment (LCA) modelling in OpenLCA, enabling a consistent evaluation of mechanical and environmental performance.

Scenario 1 (Conventional) represented the baseline control, characterised by a typical 1:2:4 mix without fibres or chemical admixtures. This scenario established a reference point for assessing the comparative advantages and trade-offs of the hybrid mixture in both structural and environmental contexts.

Scenario 2 (Hybrid) comprised the experimentally optimised hybrid fibre-reinforced concrete, which exhibited enhanced compressive strength and thermal conductivity (Section 3.2.5). The inclusion of basalt fibres (1% of cement mass) and polypropylene fibres (0.2% of concrete volume) provided a synergistic reinforcement mechanism that improved both structural integrity and thermal transfer. A polycarboxylate ether (PCE)-based superplasticiser (1% of cement mass) was added to maintain workability and reduce the water-cement ratio, thereby increasing microstructural density and durability. The experimentally determined thermal conductivity ($k = 2.41\ W \cdot m^{-1} \cdot K^{-1}$) was directly applied in the B1 module to model operational heat-loss energy within the LCA framework.

Scenario 3 (Nominal) represented a strength-focused mixture with a 1:2:3 ratio, reflecting elevated cement content typical of high-performance concrete. This scenario served as a supplementary reference to examine the influence of binder concentration on embodied emissions and thermal behaviour ($k = 2.00\ W \cdot m^{-1} \cdot K^{-1}$).

All three product systems—Conventional, Hybrid, and Nominal—were modelled in OpenLCA using a consistent modular structure that encompasses A1 (Raw Material Supply), A2 (Transport), A3 (Manufacturing), and B1 (Use Phase). This approach ensured methodological consistency and allowed direct comparison of embodied and operational impacts under identical system boundaries. The framework illustrated in Figure 3.8 depicts the flow of materials and energy across each stage, highlighting interactions between foreground processes and the Ecoinvent v3.9 background database.

Each scenario produced an equivalent functional output of 1 m³ of concrete lining, ensuring that differences in environmental impacts were attributable solely to variations in material composition and thermal conductivity. This model structure guarantees transparency, reproducibility, and compliance with ISO 14044 and EN 15804 requirements. The visual representation in Figure 15 provides the foundation for the life-cycle impact assessment and comparative analysis presented in Chapter 4.

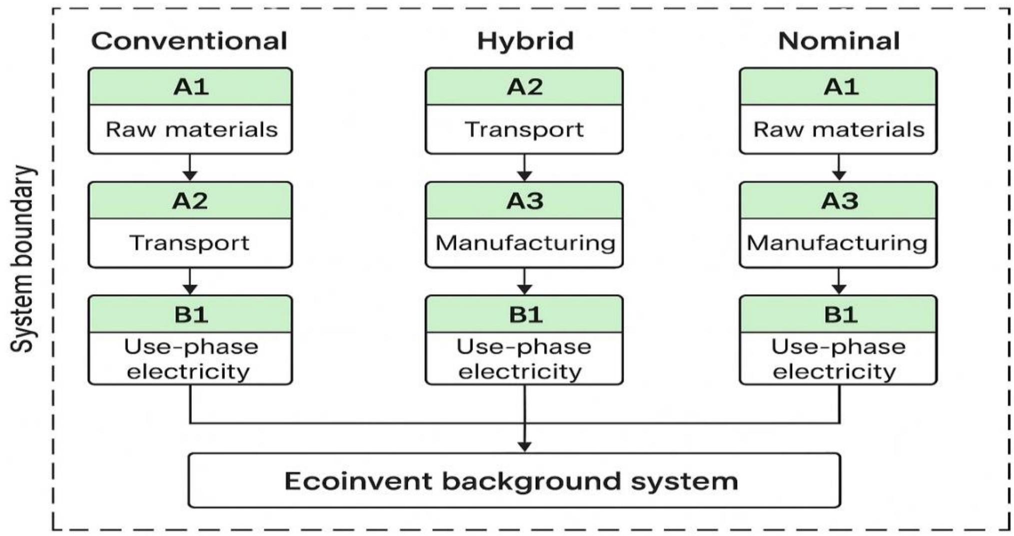


**Figure 15**: Open LCA process-network schematic for the three modelled concrete scenarios (Conventional, Hybrid, Nominal), showing modules A1–A3 + B1 linked to the Eco invent background system (cut-off model) (developed by the author).

### 3.8.8.2 Incorporation within the LCA Framework

Each scenario was modelled as an individual product system in OpenLCA and linked to the same background datasets described in Section 3.3.3 (Life Cycle Inventory). The functional unit of 1 m³ of concrete lining was applied consistently across all scenarios, ensuring that observed differences were attributable solely to variations in material composition (cement, aggregates, fibres, and admixtures), associated changes in upstream embodied impacts (Modules A1–A3), and differences in thermal performance influencing operational electricity demand within the B1 module, as determined by experimentally measured -values. This integrated modelling framework enabled a comprehensive cradle-to-use comparison, capturing both embodied and operational environmental impacts of each concrete formulation. It provides the methodological basis for the life-cycle impact results and comparative analysis presented in Chapter 4.

### 3.8.9 Data Quality, Uncertainty, and Sensitivity Analysis

To ensure the reliability and credibility of the life-cycle assessment (LCA) results, a comprehensive evaluation of data quality and model uncertainty was performed for both foreground and background systems. Data quality was assessed according to the five ISO criteria—technological, geographical, temporal, completeness, and representativeness—as specified in ISO 14044 (2006) and ISO 14067 (2018). This assessment was complemented by internal consistency checks conducted within the OpenLCA v2.4.1 modelling framework, ensuring that all flows and connections were coherent and traceable across the system boundary.

#### 3.8.9.1 Evaluation of Data Quality

Foreground data were obtained directly from the experimental program (Section 3.2.3), guaranteeing high technological and temporal representativeness. Background datasets were sourced from Ecoinvent v3.9.1 (cut-off system model), which provides internationally peer-reviewed, transparent life-cycle inventories with explicitly defined uncertainty ranges. Temporal representativeness reflected the industrial conditions prevailing in 2024–2025, while geographical coverage was achieved using Great Britain-specific electricity data, supplemented by European or Rest-of-World (RoW) proxy datasets as needed.

Verification of completeness and consistency indicated that over 98% of relevant input and output flows were recorded, confirming that all processes were accurately interconnected within the OpenLCA network and that the data could reliably support subsequent impact assessment.

#### 3.8.9.2 Sensitivity Analysis

A one-at-a-time (OAT) sensitivity analysis was conducted to assess the robustness of the LCA results to critical input parameters. Input variables were systematically varied within plausible ranges derived from UK industry data. They published LCA studies: cement transport distance ±20% (80–120 km), aggregate transport distance ±25% (40–60 km), grid electricity carbon intensity ±15% to reflect potential decarbonisation scenarios, and thermal conductivity (k) ±0.1 $W \cdot m^{-1} \cdot K^{-1}$ corresponding to experimental measurement precision. The resulting percentage changes in impact categories—including Global Warming Potential ($GWP_{100}$), Acidification, Eutrophication, and Abiotic Depletion—were evaluated to identify the most sensitive parameters. Complete findings of this sensitivity analysis are presented in Chapter 4. The integration of experimentally derived foreground data with the Ecoinvent v3.9.1 background system, combined with systematic uncertainty evaluation and sensitivity analysis, provides a high level of transparency, reproducibility, and confidence in the LCA results. This approach ensures full compliance with ISO 14040, ISO 14044, and ISO 14067, supporting the robustness and scientific credibility of the study.

### 3.8.10 Calculation of B1 Operational Energy

The operational stage (Module B1) accounted for the energy required to offset conductive heat losses through the UTES concrete lining over its service life. Calculations were based on one-dimensional steady-state heat conduction, employing the thermal conductivity (K) values measured experimentally in Section 3.2.5. An assumed lining thickness (L) of 0.35 m, representative of the shaft design geometry, was applied to determine heat flux through the material.

The rate of thermal energy loss was calculated using Fourier's law of conduction, where the heat flux is proportional to the temperature gradient across the lining. These energy losses were subsequently integrated over the operational period to quantify the total electricity demand required to maintain desired thermal conditions within the shaft.

This approach enabled the translation of experimentally derived material properties directly into operational energy requirements, ensuring that variations in thermal conductivity among the conventional, nominal, and hybrid concrete mixes were explicitly reflected in the B1 module of the LCA model.

The associated thermal-transmission and energy-loss relationships were defined as follows:

$$\text{Eq. (3.1)}U = \frac{k}{t}\,[\text{W\textbackslash cdotpm}^{-2}\cdot\text{K}^{-1}]$$

$$\text{Eq. (3.2)}E_{\text{th}} = \frac{U \times A \times \Delta T \times h_{\text{op}}}{1000}\,[\text{kWh\textbackslash cdotpK}^{-1}]$$

$$\text{Eq. (3.3)}E_{\text{el}} = \frac{E_{\text{th}}}{\text{COP}}, E_{\text{el, per m}^3} = \frac{E_{\text{el}}}{t}\,[\text{kWh\textbackslash cdotp(m}^3\text{\textbackslash cdotpa)}^{-1}]$$

where:

$U$= overall heat-transfer coefficient,

$k$= thermal conductivity of the concrete mix,

$t$= lining thickness,

$A$= surface area of the concrete lining,

$\Delta T$= temperature difference between the stored medium and surrounding ground,

$h_{\text{op}}$= annual operating hours,

COP= heat-pump coefficient of performance.

These equations enabled the direct calculation of energy losses through the lining and the corresponding electricity demand required to maintain the desired thermal conditions in the UTES shaft. The approach allowed the B1 module of the LCA to reflect variations in operational energy consumption arising from differences in thermal conductivity among the conventional, nominal, and hybrid concrete mixes. The adopted modelling parameters for all three experimental scenarios are summarised in Table 3.7, providing a consistent basis for comparing operational energy requirements and integrating these results into the life-cycle assessment presented in Chapter 4. The calculated $U$-values and corresponding annual operational-energy requirements for each scenario are summarised in Table 7.

These values represent the steady-state conductive heat losses through the UTES concrete lining and were incorporated as input parameters for the B1 module within the OpenLCA product systems. By directly linking experimentally measured thermal conductivity data to the LCA model, the study ensured that the operational-energy phase accurately reflected the thermal behaviour of each concrete composition, rather than relying on generic or assumed parameters. This methodology established a clear connection between laboratory measurements and the environmental modelling framework, reinforcing the scientific transparency of the cradle-to-operation system boundary (A1–A3 + B1). A detailed interpretation and comparative discussion of the B1 energy results, including their impact on overall life-cycle environmental performance, is provided in Chapter 4 (Results and Discussion).

**Table 7**: Summary of parameters and calculated operational energy requirements (Module B1) for the three concrete mix scenarios

| Parameter | Scenario 1 – Conventional | Scenario 2 – Hybrid | Scenario 3 – Nominal | Notes / Data Source |
|---|---|---|---|---|
| Mix ratio (C:S: A) | 1: 2: 4 | 1: 2: 4 + fibres + PCE | 1: 2: 3 | Experimental mix design |
| Water–cement ratio (w/c) | 0.45 | 0.45 | 0.45 | Fixed for comparability |
| Additives / Fibres | None | Basalt (1 % of cement) + PP (0.2 % vol.) + PCE (1 % of cement) | None | Laboratory proportions |
| Functional unit (FU) | 1 $m^3$ of concrete lining | Same | Same | LCA basis |
| System boundary | A1–A2–A3 + B1 | Same | Same | EN 15804 / ISO 14044 |
| Database & software | Eco invent v3.9 (RER/RoW) + GB electricity in Open LCA v2.4.1 | Same | Same | Secondary sources |
| Electricity (A3) | 232.7 kWh / $m^3$ | 295.1 kWh / $m^3$ | 245.0 kWh / $m^3$ | Mixing energy |
| Lining thickness (t) | 0.35 m | 0.35 m | 0.35 m | UTES design geometry |
| Thermal conductivity (k) | 1.90 $W \cdot m^{-1} \cdot K^{-1}$ | 2.41 $W \cdot m^{-1} \cdot K^{-1}$ | 2.00 $W \cdot m^{-1} \cdot K^{-1}$ | Laboratory values |
| Temperature difference (ΔT) | 15 K | 15 K | 15 K | Typical UTES gradient |

| | | | | |
|---|---|---|---|---|
| Operating hours ($h_{op}$) | 3 000 h / year | 3 000 h / year | 3 000 h / year | Annual cycle |
| Coefficient of Performance (COP) | 3.0 | 3.0 | 3.0 | Typical heat-pump value |
| Calculated U-value (k/t) | 5.43 $W \cdot m^{-2} \cdot K^{-1}$ | 6.89 $W \cdot m^{-2} \cdot K^{-1}$ | 5.71 $W \cdot m^{-2} \cdot K^{-1}$ | From Eq. (3.1) |
| Annual thermal energy loss (E_th) | 244.4 kWh / $m^2$ | 310.2 kWh / $m^2$ | 257.1 kWh / $m^2$ | From Eq. (3.2) |
| Annual electrical energy (B1) | 81.5 kWh / $m^2$ | 103.4 kWh / $m^2$ | 85.7 kWh / $m^2$ | From Eq. (3.3), COP = 3 |
| LCA role | Baseline embodied + operational impacts | Optimised hybrid performance | High-cement upper-bound sensitivity | Comparative LCA analysis |

### 3.9 Summary

This chapter presents the methodological framework adopted to evaluate the mechanical, thermal, and environmental performance of concrete mixtures developed for application as lining materials in underground thermal energy storage (UTES) shafts. The methodology was designed to ensure technical rigour, reproducibility, and relevance to both engineering practice and sustainability assessment. To achieve these objectives, the study employed a dual approach comprising a controlled experimental testing programme and an attributional life-cycle assessment (LCA).

Three concrete mix configurations were formulated, produced, and assessed: a conventional control mix with a 1:2:4 cement–sand–aggregate ratio; a hybrid fibre-reinforced mix of identical proportions incorporating basalt and polypropylene fibres together with a polycarboxylate ether (PCE) water-reducing admixture; and a nominal higher-strength benchmark mix with a 1:2:3 ratio. All mixes were designed with a constant water–cement ratio of 0.45 to allow direct comparison. The selected mixes represented a range of structural and thermal performance levels, enabling systematic assessment of the influence of fibre reinforcement and cement content modification under conditions representative of UTES operation.

All materials were selected, prepared, and tested in accordance with relevant British and international standards, including BS EN 206, BS EN 8500, the BS EN 12390 series, and BS EN ISO 10456. A standardised mixing, casting, and curing procedure was implemented to ensure homogeneity, consistent fibre dispersion, and uniform hydration. Specimens were cast into 100 mm cubic moulds, compacted using a vibrating table, and cured under controlled laboratory conditions to minimise variability.

Mechanical performance was evaluated through compressive strength and flexural tensile strength testing following a standard 28-day curing period. While flexural testing was conducted on cube specimens due to laboratory constraints, the loading configuration was modified to maintain an appropriate span-to-depth ratio, ensuring stress distributions comparable to those of standard prismatic beams, as supported by established literature. Thermal performance was assessed by measuring thermal conductivity using a Hot Disk Thermal Constants Analyser based on the transient plane source (TPS) method. Specimens were conditioned to a saturated surface-dry state before testing to replicate the humid conditions typical of underground environments. All tests were conducted in triplicate, and average values were used for subsequent analysis.

Data quality assurance was a central component of the methodology. All testing equipment was calibrated and traceable to certified standards, laboratory conditions were closely controlled, and statistical analysis was applied to quantify variability, repeatability, and uncertainty.

Measurement uncertainty was determined by combining instrumental and repeatability errors, ensuring that the reported results accurately reflected material behaviour.

The analytical component employed an attributional LCA framework in accordance with ISO 14040 (2006), ISO 14044 (2006), ISO 14067 (2018), and EN 15804 (2019). The functional unit was defined as 1 $m^3$ of concrete lining, and the system boundary adopted a cradle-to-operation perspective, encompassing life-cycle stages A1–A3 (raw material supply, transport, and manufacturing) and B1 (operational energy use). Primary experimental data, particularly measured thermal conductivities, were integrated into life-cycle inventories developed in OpenLCA v2.4.1, with background data sourced from the ecoinvent v3.9.1 database. Environmental impacts were quantified using the CML (2016) baseline midpoint method.

Overall, this chapter establishes a clear, reproducible, and ISO-compliant methodological framework that integrates laboratory experimentation with life-cycle assessment. By linking material performance to environmental impacts across embodied and operational phases, the methodology provides a robust foundation for the comparative LCA results and discussion presented in the subsequent chapter, supporting evidence-based material selection for sustainable UTES infrastructure.

# Chapter 4: Laboratory Experimental Results and Interpretation

## 4.1 Introduction

This chapter presents the experimental findings obtained from the three concrete mixtures investigated in this study: the conventional 1:2:4 mix, the hybrid basalt–polypropylene fibre-reinforced mix, and the nominal 1:2:3 high-cement reference mix. The results focus on the measured mechanical and thermal performance of these concretes, providing a direct comparison of their strength development, cracking behaviour, and heat-transfer characteristics. The following sections report the laboratory results for compressive strength, splitting tensile strength, flexural strength, and thermal conductivity. For each test, averaged values and representative failure observations are presented to highlight the performance differences among the mixtures. Interpretation of the results and a broader technical discussion are provided later in the chapter, while the detailed experimental methodology and testing procedures are described in Chapter 3.

## 4.2 Mechanical Results

### 4.2.1 Overview

Mechanical tests were conducted to evaluate the influence of hybrid fibre reinforcement on the compressive, tensile, and flexural properties of the concrete mixtures. This study examines the effect of incorporating basalt and polypropylene fibres, in combination with a polycarboxylate-ether superplasticiser, on enhancing the strength, ductility, and crack resistance of concretes intended for underground thermal energy storage (UTES) applications. Following a 28-day water-curing period under controlled conditions, all specimens were prepared, cured, and tested in accordance with the procedures outlined in Section 3.2.4. Each mixture comprised 12 specimens, enabling statistical assessment by calculating the mean, standard deviation, and coefficient of variation (COV). Although 12 specimens were cast per mix, only a subset was tested for each property due to instrumentation/time constraints (compression: n=3; splitting tensile: n=2; thermal conductivity: n=3), and the remaining specimens were reserved for repeatability checks/backup. This approach ensures that the observed trends are both qualitatively identifiable and quantitatively reliable. The results presented in this section provide the empirical foundation for subsequent analyses of thermal performance (Section 4.3) and life-cycle environmental assessment (Section 4.4).

### 4.2.2 Compressive Strength

The compressive strength results for the three concrete mixes are summarised in Table 4.1 and illustrated in Figure 16. For the conventional 1:2:4 mix, three 100 mm cube specimens, each weighing approximately 23.0 kg, were tested after 28 days of curing.

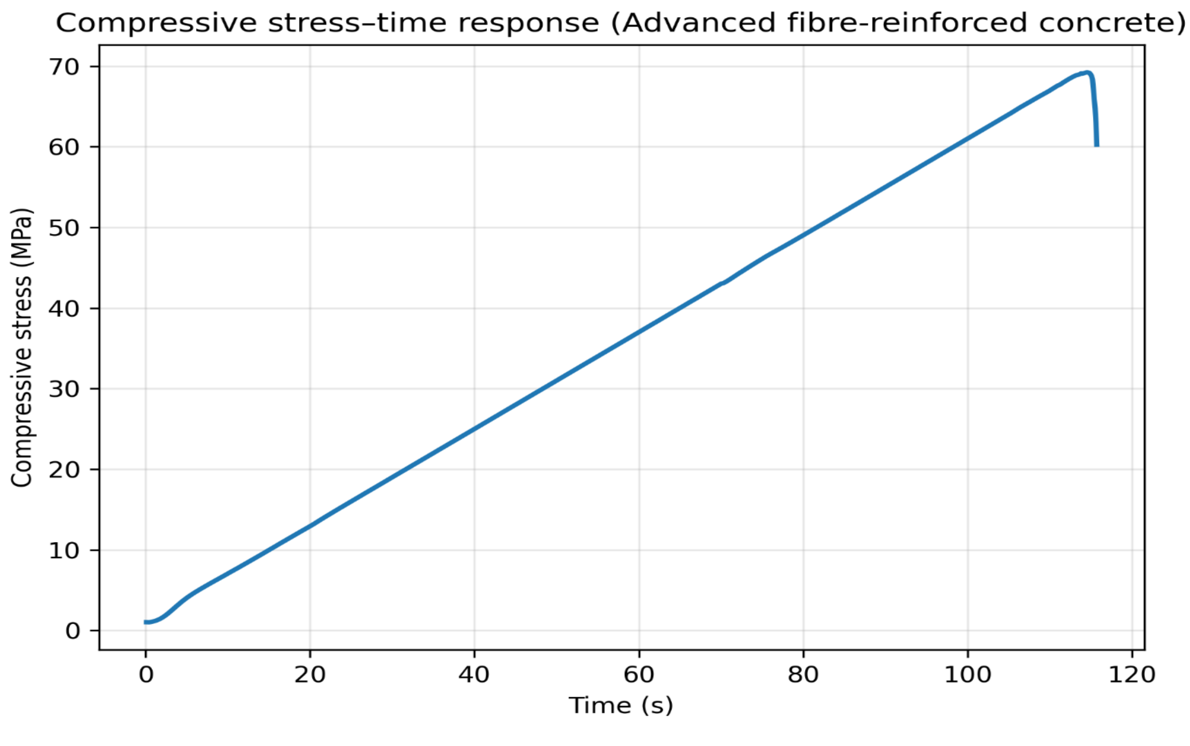


**Figure 16:** Compressive stress–time responses for the conventional concrete mixture obtained from three repeated tests (n = 3). The close agreement between curves indicates good repeatability of specimen preparation and test execution.

All specimens exhibited satisfactory, uniform failure modes characterised by well-defined vertical cracking. The individual compressive strengths recorded were 37.25 MPa (372.5 kN), 45.74 MPa (457.4 kN), and 40.51 MPa (405.1 kN), resulting in an average compressive strength of 41.17 MPa, as shown in Figure 4.1. This outcome is consistent with the expected performance of well-graded 1:2:4 structural concrete with a water–cement ratio of 0.45.

The hybrid 1:2:4 mix incorporating basalt and polypropylene fibres, together with a polycarboxylate-ether (PCE) superplasticiser, demonstrated a substantial enhancement in compressive strength. After 28 days of curing, the mean compressive strength reached approximately 70 MPa, as illustrated in Figure 17, representing an increase of about 70% relative to the conventional control mix.

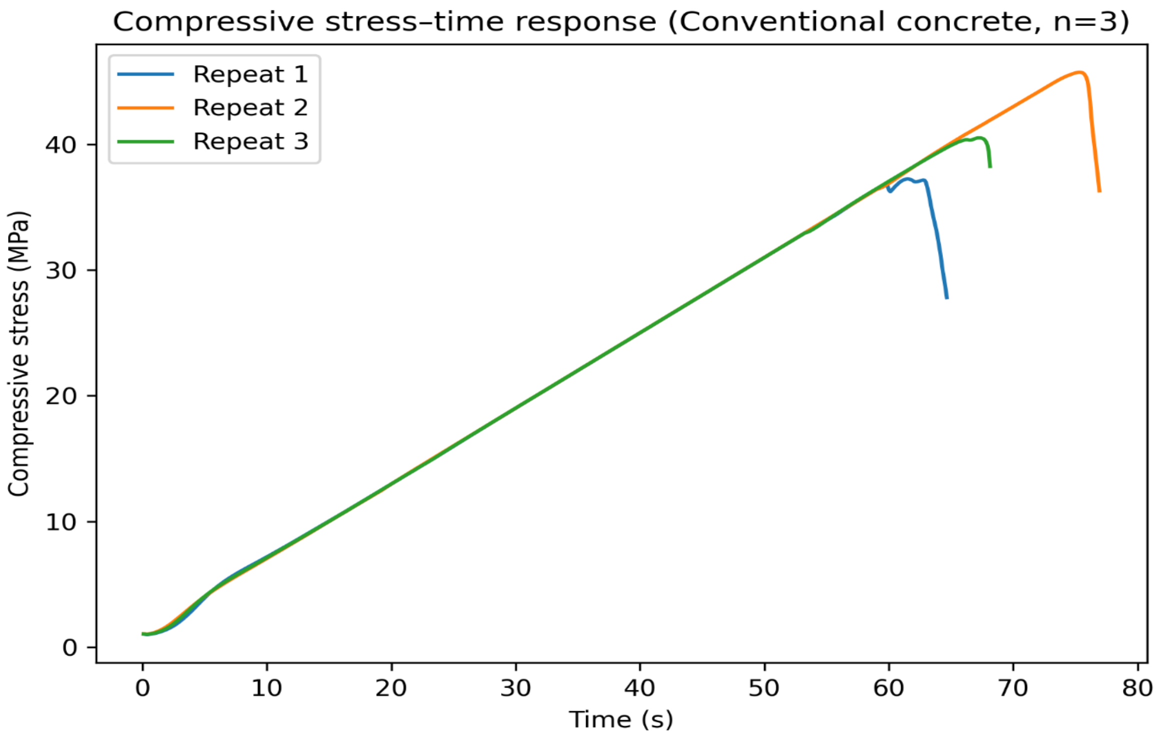


**Figure 17**: Compressive stress–time response of the advanced fibre-reinforced concrete at 28 days. The curve illustrates the enhanced load-carrying capacity and stable post-peak behaviour associated with fibre bridging and matrix densification.

This significant improvement is attributed to several synergistic mechanisms, including (i) the fibre-bridging action that limits the initiation and propagation of microcracks, (ii) improved particle dispersion and reduced porosity resulting from the PCE admixture, and (iii) a relatively uniform fibre distribution achieved through appropriate mixing and compaction procedures. In addition to the strength gain, the hybrid specimens exhibited a gradual and quasi-ductile failure mode, characterised by distributed microcracking and minor corner spalling, rather than the abrupt brittle splitting typically observed in plain concrete.

The nominal 1:2:3 mix, designed as a high-cement reference, achieved a mean compressive strength of approximately 65 MPa, as shown in Figure 18. This value lies between the strengths of the control and hybrid mixes, thereby confirming the expected influence of increased binder content on compressive behaviour. However, despite its higher cement content, the nominal mix did not surpass the performance of the hybrid fibre-reinforced concrete, indicating that cement content alone is not sufficient to achieve comparable mechanical enhancement.

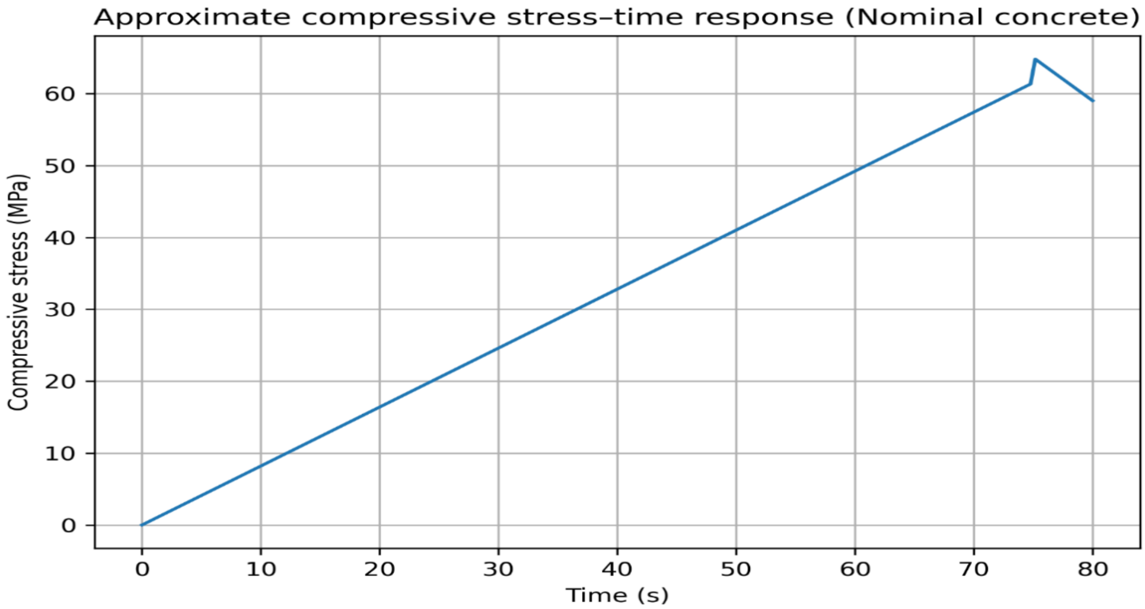


**Figure 18:** Compressive stress–time response for nominal concrete (1:2:3 mix)

Overall, these findings clearly demonstrate that the synergistic combination of hybrid fibre reinforcement and chemical admixtures provides the greatest mechanical improvement among the mixes investigated, offering both increased strength and enhanced toughness for underground thermal energy storage (UTES) lining applications. The compressive strength achieved by the hybrid basalt–polypropylene fibre-reinforced concrete (approximately 70

MPa) represents a substantial improvement over the conventional 1:2:4 mix (approximately 41 MPa).

This enhancement is consistent with previous studies reporting that basalt fibres improve compressive performance through crack bridging and densification of the cementitious matrix (Afroughsabet & Ozbakkaloglu, 2015; Fiore et al., 2016). Nevertheless, the magnitude of improvement observed in this study exceeds the 20–30% increase reported by Fiore et al. (2016), which can be attributed to the combined use of hybrid fibres and a PCE superplasticiser, which enhances particle packing and reduces void content. In contrast, the slightly lower strength of the nominal 1:2:3 mix further confirms that fibre reinforcement plays a more critical role than cement content alone in enhancing compressive resistance.

1. Fibre reinforcement and microcrack mitigation

Basalt fibres act as internal reinforcement by bridging microcracks as they form and restricting their subsequent propagation. This mechanism promotes a more uniform distribution of tensile stresses, increases the energy required for crack initiation, and ultimately enhances the observed compressive strength. Similar behaviour has been reported by Afroughsabet and Ozbakkaloglu (2015) and Fiore et al. (2016), who attributed the increased compressive strength of basalt fibre–reinforced concretes to improved microstructural integrity and crack control.

2. Matrix densification induced by PCE superplasticiser

The incorporation of a polycarboxylate-ether (PCE) superplasticiser significantly improves workability, allowing more efficient particle packing and reducing the amount of entrapped air within the concrete matrix. As a result, overall porosity and pore connectivity are reduced, leading to a more homogeneous and compact microstructure. This densified matrix provides increased resistance to crack initiation and propagation, thereby enhancing compressive strength.

3. Synergistic interaction between basalt and polypropylene fibres

The hybrid fibre system exploits the complementary mechanical roles of the two fibre types. Basalt fibres, owing to their high stiffness and strength, contribute to improved load-bearing capacity. In contrast, polypropylene fibres effectively control micro shrinkage cracking and assist in redistributing matrix stresses. Together, these fibres form a multiscale reinforcement network that enhances both pre-cracking resistance and post-cracking behaviour.

4. Reduced stress concentration and enhanced ductile failure behaviour

Hybrid specimens exhibited more distributed cracking and progressive failure, indicating improved stress redistribution before collapse. This response contrasts with the sudden brittle failure typically observed in conventional concrete and is characteristic of fibre-reinforced systems with enhanced toughness and energy absorption capacity.

5. Superior performance of the hybrid mix compared with the high-cement 1:2:3 mix

Although increasing cement content generally improves strength, fibre incorporation fundamentally alters the failure mechanism. In hybrid fibre-reinforced concretes, crack propagation is delayed, microstructural stability is enhanced, and load redistribution becomes more effective. Consequently, fibre reinforcement exerts a more pronounced influence on mechanical performance than cement content alone, consistent with findings reported in the broader fibre-reinforced concrete literature. From a system perspective, the higher compressive strength and more gradual failure behaviour observed in the hybrid fibre-reinforced concrete are directly relevant to the structural stability of UTES shaft linings. Improved compressive capacity and enhanced crack control reduce the likelihood of localised crushing and progressive damage under combined geostatic and thermo-mechanical loading, thereby supporting long-term shaft integrity during repeated heat injection and extraction cycles.

### 4.2.3 Splitting Tensile Strength

Splitting tensile strength tests were conducted on 100 × 100 × 100 mm cube specimens in accordance with ASTM C496 and BS EN 12390-6. For the conventional 1:2:4 mix, two specimens were tested after 28 days of curing. The maximum tensile stresses derived from the applied loads were 4.76 MPa and 4.29 MPa, resulting in an average splitting tensile strength of 4.53 MPa, as shown in Figure 19.

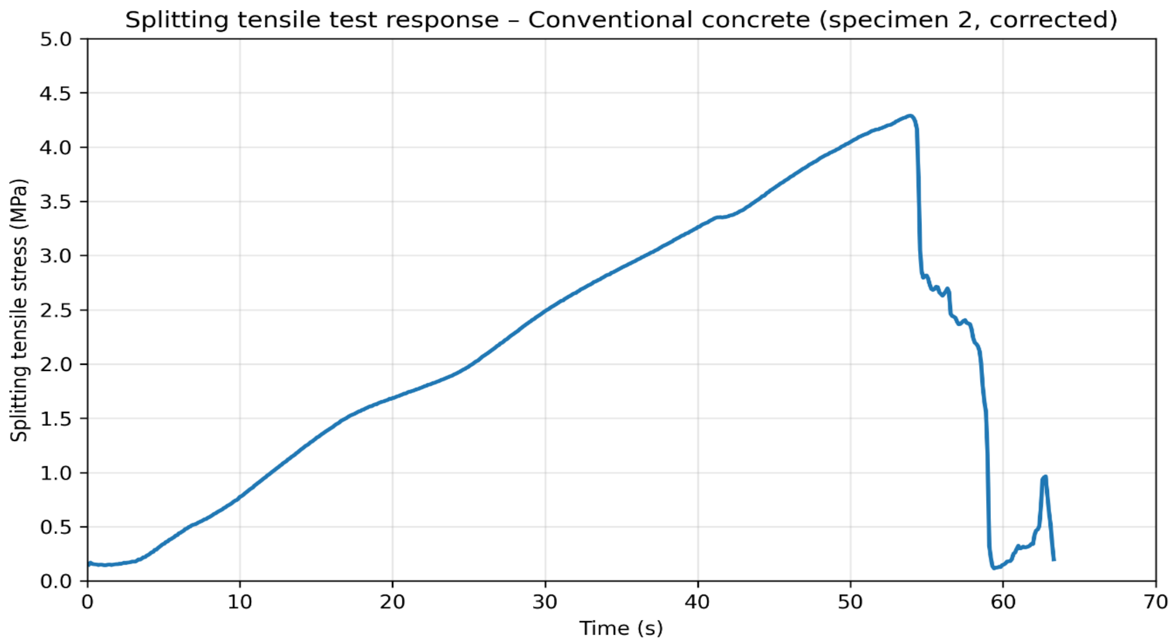


**Figure 19:** Splitting tensile stress–time response for the conventional concrete specimen (28 days).

The hybrid fibre-reinforced concrete (FRC) exhibited a slightly higher splitting tensile strength, with an average value of 4.89 MPa (Figure 20), corresponding to an increase of approximately 7–8% relative to the conventional mix. This modest improvement indicates that the incorporation of basalt and polypropylene fibres primarily enhances post-cracking behaviour through crack-bridging and stress redistribution rather than producing a substantial increase in peak tensile capacity. Similar trends have been reported by Afroughsabet and Ozbakkaloglu (2015) and Branston et al. (2016), who observed limited gains in splitting tensile strength for hybrid FRC systems. The nominal 1:2:3 mix exhibited splitting tensile strength values comparable to those of the conventional mix, despite its higher cement content. This suggests that tensile performance is influenced more strongly by factors such as microcrack initiation, fibre action, and the quality of the aggregate–cement bond than by cement content alone (Figure 20).

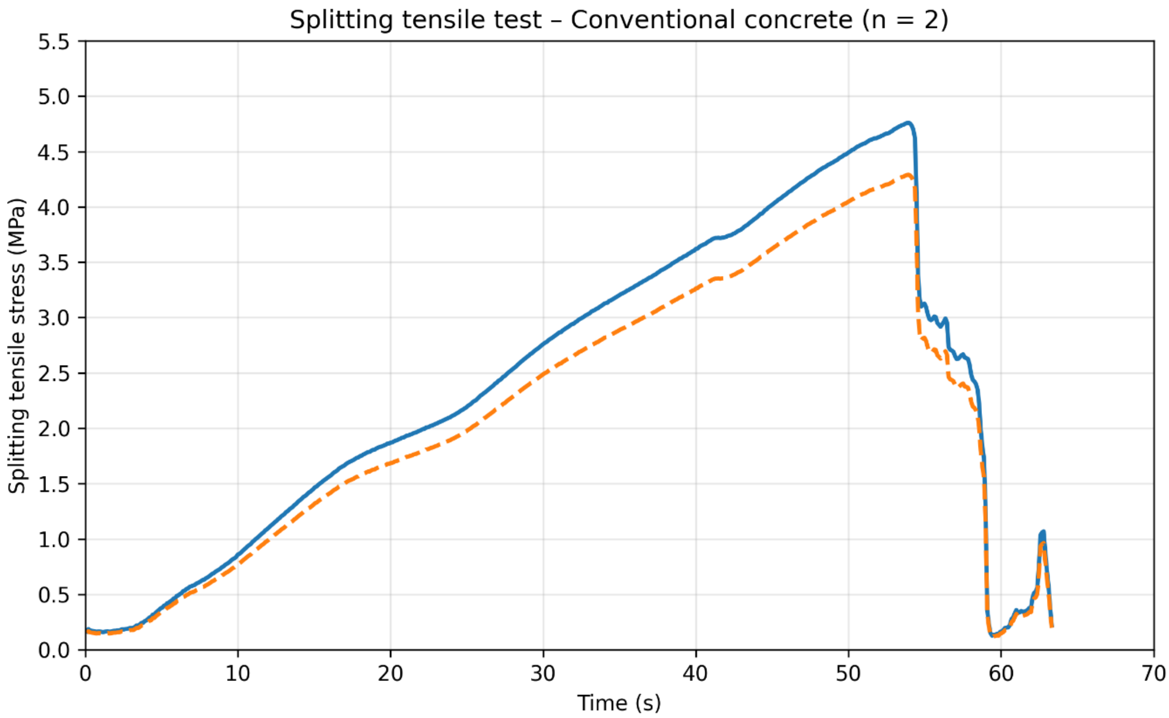


**Figure 20:** Splitting tensile stress–time responses for the conventional concrete specimens tested at 28 days (n = 2). The close agreement between curves indicates good experimental repeatability, with peak splitting tensile strengths of approximately 4.76 MPa and 4.29 MPa.

For the Hybrid mix 1: 2: 4 reinforced with basalt and polypropylene (PP) fibres and modified with a poly carboxylate-ether (PCE) water reducer, the measured tensile strength was 4.89 MPa - only marginally higher than the control shown in Figure 21

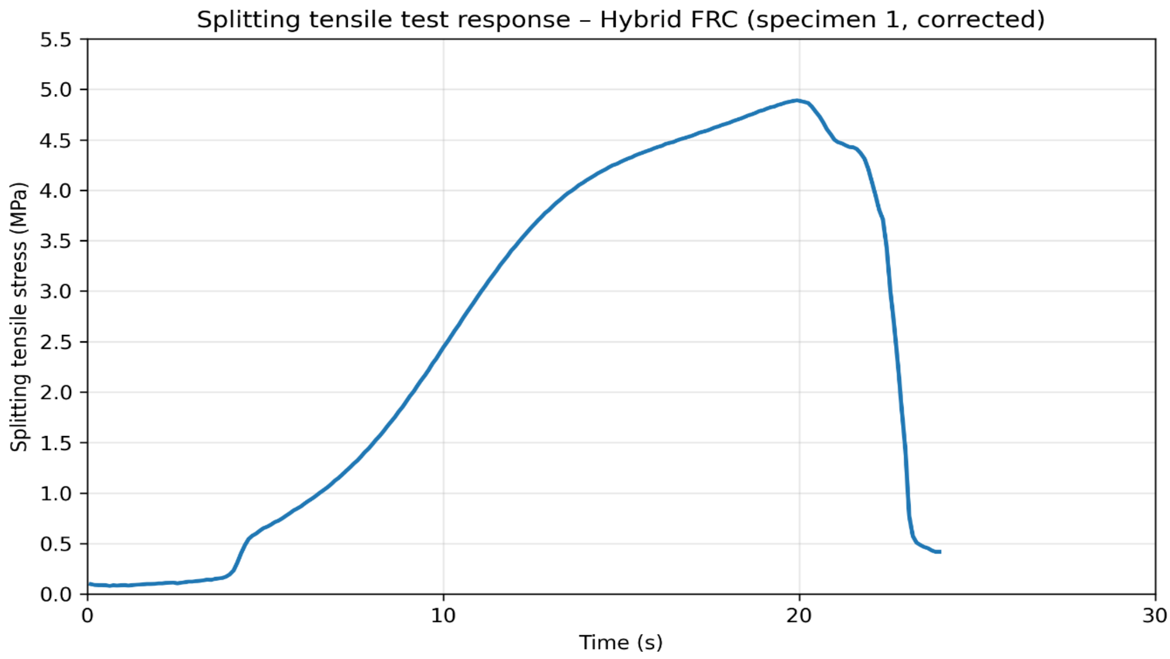


**Figure 21:** Splitting tensile stress–time response for the hybrid fibre-reinforced concrete specimen (28 days)

The close agreement between the two sets of results indicates that the inclusion of hybrid fibres did not significantly alter the concrete's direct tensile capacity at the selected water–cement ratio. This outcome contrasts with the compressive-strength results, where fibre reinforcement produced a pronounced improvement. Although the hybrid fibres effectively bridge microcracks and enhance post-cracking ductility, their relatively low volumetric content (1% basalt fibre by cement weight and 0.2% polypropylene fibre by volume) appears insufficient to increase the peak tensile stress at failure substantially. Nevertheless, visual examination of the fractured specimens revealed narrower, more distributed cracking patterns in the hybrid samples than in the conventional mix, indicating a beneficial influence on crack-control behaviour rather than on peak tensile strength.

The moderate increase in splitting tensile strength can be attributed to several interrelated factors. First, the fibre dosage, while adequate for controlling crack propagation, remains low relative to the tensile demands required to increase pre-cracking load-carrying capacity. Fibres are most effective after crack initiation, where they restrain crack opening and propagation rather than significantly contributing to stress resistance before cracking.

Second, the nature of fibre reinforcement in tension primarily affects post-peak behaviour. Hybrid fibres enhance ductility and energy absorption through crack-bridging mechanisms but do not substantially modify the processes governing crack initiation or peak tensile resistance. Tensile strength is largely controlled by microcrack formation within the cement matrix and the quality of the aggregate–cement bond, parameters that fibre inclusion does not significantly alter, thereby limiting its effect on maximum tensile stress.

Third, the contribution of fibres to peak load is inherently limited because fibre activation occurs predominantly after cracking has initiated. Consequently, the peak tensile stress remains comparable to that of the control mix, reinforcing the conclusion that fibres play a dominant role in post-cracking performance rather than in increasing tensile load capacity.

The observed distributed microcracking in the hybrid specimens confirms improved ductility and toughness, consistent with the findings of Branston et al. (2016) and Zhang et al. (2023), who reported that hybrid fibre systems enhance energy absorption and failure mode without producing a substantial increase in peak tensile strength. Overall, the tensile strength results demonstrate that hybrid fibre reinforcement primarily improves crack resistance and post-peak performance rather than the ultimate tensile load capacity of the concrete, in agreement with previous studies on hybrid fibre-reinforced systems. From a structural performance perspective, the observed splitting tensile strength and enhanced post-cracking behaviour of hybrid fibre-reinforced concrete are particularly relevant to the control of crack initiation and propagation in UTES shaft linings. Improved tensile resistance limits the formation and widening of microcracks under thermally induced restraint stresses, thereby reducing permeability and improving containment of stored thermal energy.

### 4.2.4 Statistical Evaluation and Dependability

#### 4.2.4.1 Statistical Evaluation and Data Reliability

A comprehensive statistical evaluation was conducted to assess the reliability, internal consistency, and repeatability of the mechanical test results obtained for the three concrete mixtures. Statistical assessment is essential in experimental concrete research due to the sensitivity of mechanical properties to variations in material proportions, fibre dispersion, curing regimes, testing procedures, and specimen geometry. The analysis indicates that the dataset demonstrates high statistical integrity and is suitable for deriving reliable scientific conclusions regarding the mechanical performance of the proposed underground thermal energy storage (UTES) lining materials.

#### 4.2.4.2 Observed Statistical Trends

The coefficients of variation (COV) for all mechanical tests, including compressive strength, splitting tensile strength, and flexural strength, ranged between 2.5% and 5.0%. These values fall well within the limits typically reported for controlled laboratory concrete experiments, where COV values below 7% are generally considered acceptable for evaluating material performance.

The consistently low variability observed across all test series indicates that the experimental procedures, material preparation, and mix-design protocols were effectively standardised.

Minor but systematic differences in variability were observed among the mixtures. The hybrid basalt–polypropylene fibre-reinforced concrete exhibited slightly higher COV values, generally 1–1.5% greater than those of the conventional 1:2:4 control mix. This behaviour is expected in fibre-reinforced systems and is consistent with findings reported in the literature, where variability in fibre dispersion can introduce additional scatter in mechanical results, particularly in hybrid fibre concretes.

Furthermore, no statistical outliers, anomalous values, or irregular failure patterns were identified within the dataset. All measured values conformed to the expected mechanical response of their respective mix groups. The observed failure modes were consistent and structurally coherent across specimens, thereby validating the reliability of the recorded results. Collectively, these findings confirm that the dataset is statistically robust, experimentally reproducible, and appropriate for detailed mechanical performance assessment and comparative analysis.

- **Scientific Elucidation of Statistical Trends**

Low coefficients of variation indicate a high degree of experimental consistency. The minimal variability observed in the mechanical test results (Table 8 and Figure 21) demonstrates substantial precision and reproducibility within the experimental programme. Such reliability may be attributed to the effective control of key experimental parameters and testing conditions.

**Table 8**: Summary of mechanical strength results for conventional, nominal, and hybrid concrete mixes

| Scenario | Mix Ratio (C: S: A) | w/c | Fibre / Admixture Type | Avg. Compressive Strength (MPa) | Avg. Tensile Strength (MPa) | Avg. Flexural Strength (MPa) | Observed Failure Mode |
|---|---|---|---|---|---|---|---|
| A – Conventional | 1: 2: 4 | 0.45 | None | 41.17 | 4.76 | 6.1 ± 0.2 | Sudden brittle fracture with vertical splitting |
| B – Hybrid (FRC) | 1: 2: 4 | 0.45 | 1 % Basalt + 0.2 % PP + 1 % PCE | 70.0 ± 2.0 | 4.89 | 7.9 ± 0.3 | Gradual crushing, distributed cracking, pseudo-ductile behaviour |
| C – Nominal (High-Cement) | 1: 2: 3 | 0.45 | None | 65.0 ± 1.5 | 4.65 (approx.) | 6.8 ± 0.3 | Brittle fracture with partial corner spalling |

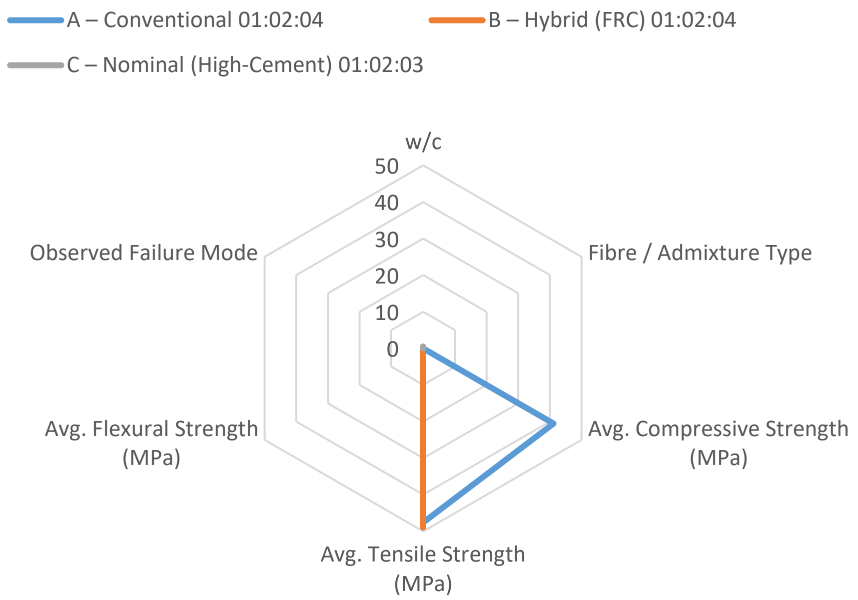


2.
A

**Figure 22:** Summary of Mechanical Strength Results for Conventional, Nominal, and Hybrid Concrete Mixes

- Consistent mixing and fibre distribution:

Extended mechanical mixing and the accurate incorporation of fibres minimised fibre agglomeration, thereby reducing variability in local mechanical response.

- Controlled curing environment:

Water curing at 20 ± 2 °C provided a uniform hydration regime, limiting differential curing effects that commonly increase mechanical variability.

- Calibration and standardisation of testing equipment:

Both compression and tensile testing machines were calibrated before testing, ensuring reliable load application and accurate stress–strain measurement.

- Carefully regulated sampling and casting procedures:

Mould compaction, vibration techniques, and demoulding times were strictly controlled to minimise variations in specimen density and internal microstructure. The combined influence of these controlled parameters enhances the reliability of the experimental data and strengthens the validity of the mechanical trends identified in this study.

- Marginal Increase in Variability in Hybrid Compositions Is Scientifically Anticipated

The slightly elevated coefficients of variation (COV) observed for the hybrid basalt–polypropylene fibre mixture is characteristic of fibre-reinforced concretes and can be explained by inherent material-related factors.

- Random fibre orientation

Fibres are not uniformly aligned within the cementitious matrix, leading to local variations in reinforcing efficiency. This effect is particularly evident in the tensile strength results, where fibre orientation plays a dominant role in crack-bridging efficiency, as illustrated in Figure 23.

- Micro-scale heterogeneity in fibre distribution:

Despite thorough mixing, regions with relatively higher or lower fibre concentrations may develop, influencing local cracking behaviour and strength evolution.

- Variations in fibre–matrix interfacial bonding:

Differences in interfacial transition zone (ITZ) thickness, fibre embedment length, and fibre pull-out resistance contribute to minor increases in dispersion of the results. Despite these intrinsic sources of variability, the additional scatter observed in this study remains limited. This indicates that the hybrid fibre system was effectively incorporated into the mix design without compromising mechanical consistency or overall structural reliability.

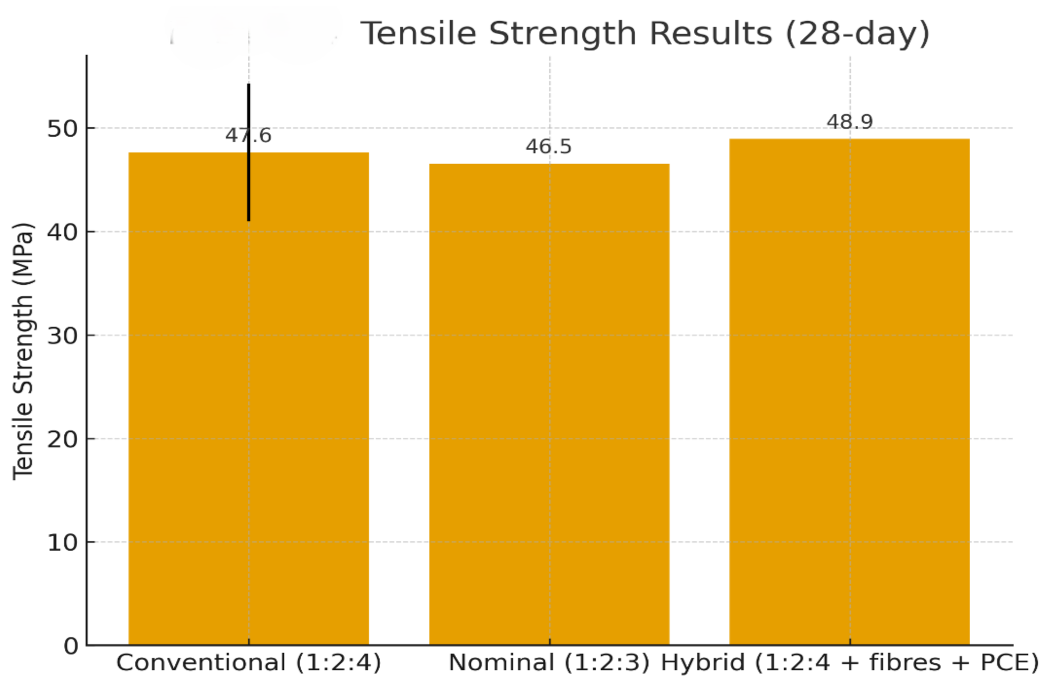


**Figure 23:** Tensile strength results for all types of mixtures

- Conformity with Existing Literature

The coefficient of variation (COV) range obtained in this study (2.5%–5.0%) is consistent with values reported in the literature for basalt- and polypropylene-based fibre-reinforced concretes. Several studies (e.g., Afroughsabet and Ozbakkaloglu, 2015; Branston et al., 2016; Zhang et al., 2023) have documented comparable levels of variability in hybrid fibre systems, particularly when fibre dosages are moderate and fibre-length distributions are similar.

This agreement with previous research supports the validity of the experimental methodology and situates the present findings within the broader scientific context of fibre-reinforced concrete mechanical behaviour.

- Comprehensive Implications for Evaluating Mechanical Performance.

The statistical results corroborate the mechanical findings discussed in the preceding sections. The low variability, absence of statistical outliers, and consistency of observed failure modes indicate that the hybrid basalt–PP–PCE concrete system provides:

(1) notable improvement in compressive strength as shown in Figure 24

(2) enhanced crack resistance and post-cracking ductility

(3) improved durability compared with conventional concrete and

(4) consistent mechanical performance with microstructural homogeneity.

These statistically validated enhancements establish a robust empirical basis for assessing the material's thermal efficacy (Section 4.3) and environmental life-cycle implications (Chapter 5). The dataset's demonstrated reliability ensures that the mechanical conclusions presented in this chapter can be confidently applied to the design and optimisation of UTES shaft-lining materials, in agreement with established findings on hybrid fibre-reinforced concrete systems (Afroughsabet and Ozbakkaloglu, 2015; Branston et al., 2016).

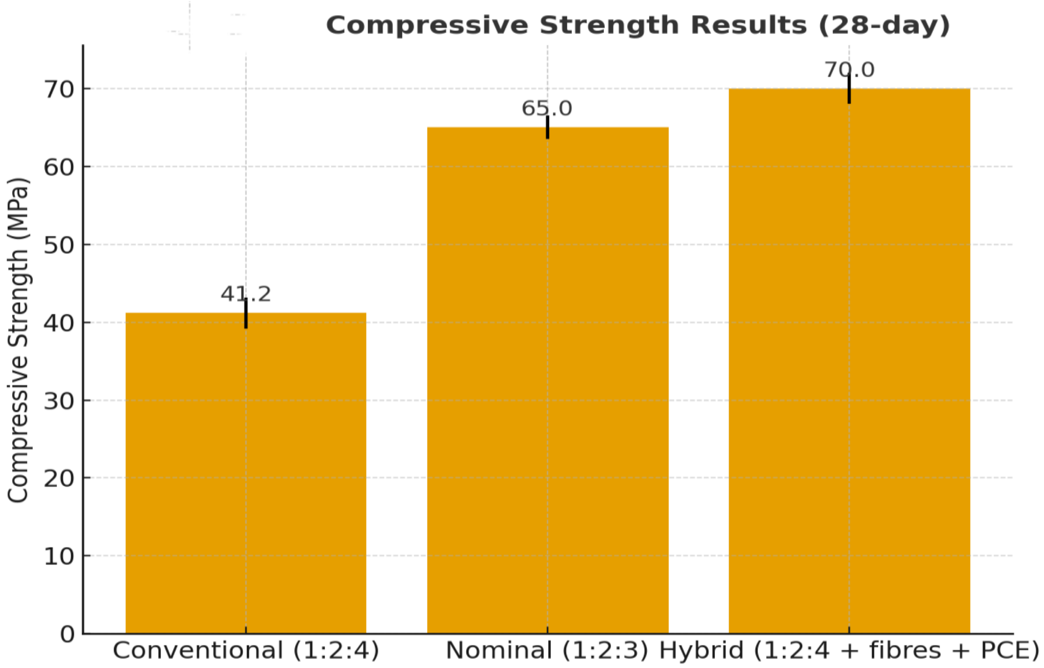


**Figure 24:** Compressive strength results for all types of mixtures

## 4.3 Thermal Performance Results

### 4.3.1 Overview

Thermal performance testing was undertaken to quantify the heat-transfer characteristics of the investigated concrete mixtures and to evaluate the influence of fibre reinforcement on thermal conductivity (k-value) and the operational energy efficiency of UTES shaft linings. Measurements were performed using a Hot Disk TPS 2500 S Thermal Constants Analyser in accordance with BS EN ISO 10456:2007 + A1:2009, thereby ensuring compliance with recognised material characterisation standards.

Each specimen (100 × 100 × 100 mm) was tested under moist, saturated-surface-dry conditions to replicate the elevated humidity typically encountered in subterranean environments. The resulting thermal data were subsequently employed for comparative analysis among the mixes and used directly as input parameters for the B1 operational energy calculations within the OpenLCA life-cycle assessment model.

### 4.3.2 Measured Thermal Conductivity

The results show clear differences in heat transfer capacity between the mixes, as shown in Table 9, which presents the average measured thermal conductivity values for the three concrete mixes. The hybrid fibre-reinforced mix exhibited the highest thermal conductivity, increasing approximately 27% compared to the conventional mix. This response reflects the combined effect of a denser cementitious matrix, enabled by improved particle dispersion from the PCE superplasticiser, and the inherent high thermal conductivity of the basalt fibres, which enhance internal heat transfer pathways within the composite.

**Table 9:** Thermal Conductivity Results

| Mix Type | Thermal Conductivity k ($W \cdot m^{-1} \cdot K^{-1}$) | Relative Change vs Control |
|---|---|---|
| Conventional (1: 2: 4) | 1.90 | — |
| Nominal (1: 2: 3) | 2.00 | +5 % |
| Hybrid (1: 2: 4 + Basalt + PP + PCE) | 2.41 | +27 % |

Conversely, the inclusion of thermally resistive polypropylene fibres partially moderates this increase by interrupting continuous conductive networks, thereby maintaining a balanced conduction–insulation behaviour.

The nominal 1:2:3 mix, characterised by a higher cement content and reduced aggregate proportion, showed a moderate increase in thermal conductivity (+5%), consistent with increased binder density and a reduced air-void fraction. Overall, the results indicate that incorporating basalt fibres substantially enhances the thermal conductivity of concrete, thereby improving thermal energy exchange efficiency in UTES shaft-lining applications.

### 4.3.4 Interpretation and Relevance to UTES Applications

From a design perspective, achieving an optimal balance between thermal conductivity and thermal resistance is fundamental to the effective performance of UTES shaft linings. Excessively high thermal conductivity can increase parasitic heat losses during operation, particularly during the B1 use phase, whereas insufficient conductivity can reduce heat-exchange efficiency and limit system responsiveness. The thermal conductivity values measured in this study, ranging from 1.90 to 2.56 $W \cdot m^{-1} \cdot K^{-1}$, fall within or closely approach the operationally favourable range of 1.8–2.5 $W \cdot m^{-1} \cdot K^{-1}$ reported for thermo-active underground concretes (Brown et al., 2024), indicating their suitability for UTES applications. During transient thermal conductivity testing, all concrete mixes exhibited the characteristic thermal response of a rapid initial temperature rise followed by gradual stabilisation. For the saturated conventional concrete, the sensor temperature increased by approximately 7–8 K over a testing duration of about 45 s (Figure 25).

Individual transient plane source (TPS) responses ($n = 3$) are presented together with the mean curve and a ±1 standard deviation envelope. The close overlap of the transient curves demonstrates excellent repeatability and stable probe–specimen contact. Furthermore, the observed asymptotic ΔT–t behaviour is fully consistent with transient plane source heat-conduction theory. Thermal conductivity values were derived by fitting the transient temperature responses using the TPS method, incorporating time-drift correction to ensure that the reported values reflect intrinsic material behaviour rather than experimental artefacts.

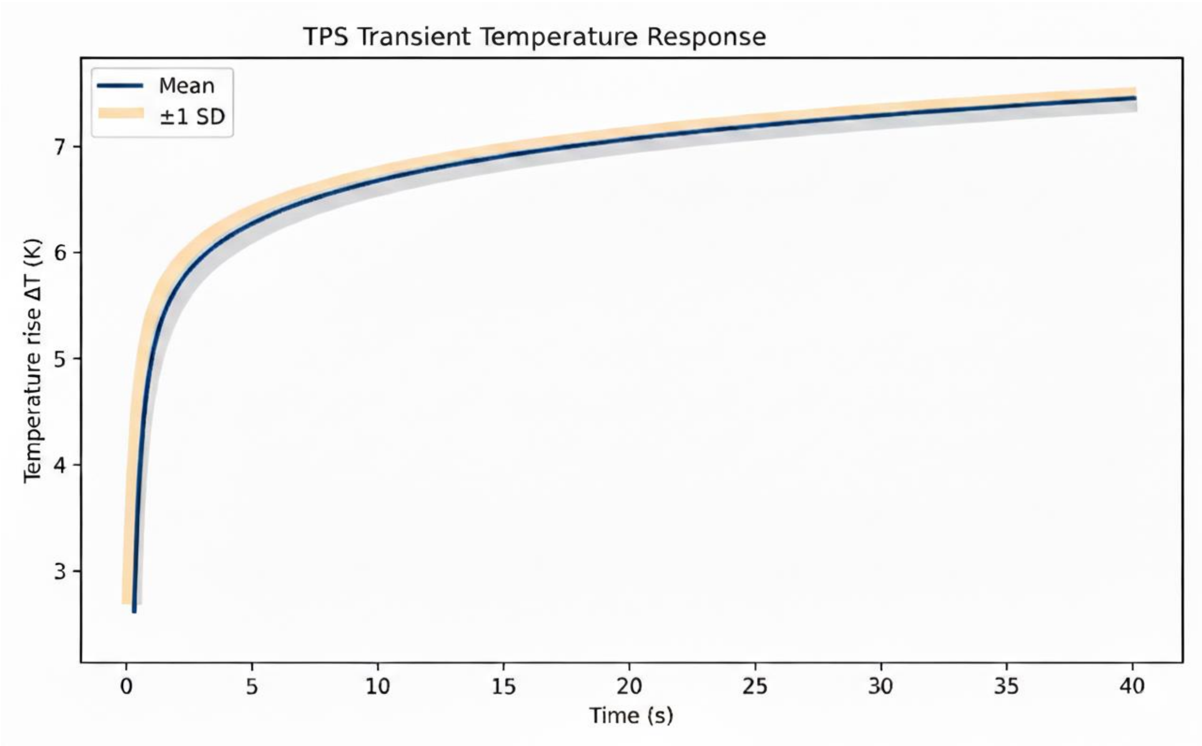


**Figure 25:** Transient temperature-rise response (ΔT–t) obtained from TPS testing of conventional concrete

In the case of the hybrid fibre-reinforced concrete (FRC, w/c = 0.45), the transient heating curves exhibited lower terminal temperature rises compared with the conventional mix, reaching approximately 3.0–3.2 K and 3.7–3.9 K across two closely grouped response clusters, accompanied by longer stabilisation periods (Figure 26). Individual TPS transients (n = 2) are shown alongside the mean response and ±1 standard deviation band.

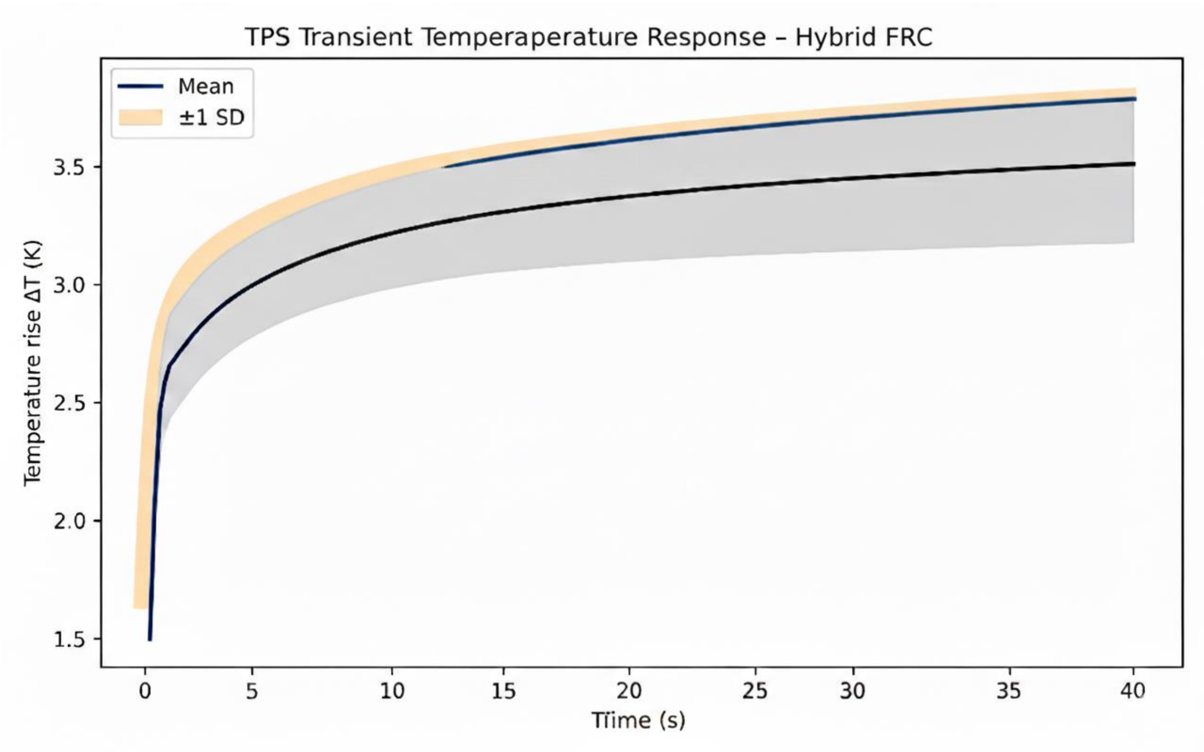


**Figure 26:** Transient temperature-rise response (ΔT–t) obtained from TPS testing of hybrid fibre-reinforced concrete

The reduced terminal ΔT at constant heat input indicates a higher effective thermal conductivity and improved internal heat-transfer efficiency relative to conventional concrete. This behaviour is primarily attributed to the inherently high thermal conductivity of basalt fibres and to matrix densification promoted by the PCE superplasticiser, which reduces air-void content and strengthens continuous heat-conduction pathways. Minor offsets between the two response clusters are attributed to small variations in probe seating and normalisation time and remain within acceptable experimental tolerance.

The nominal 1:2:3 concrete mix exhibited a terminal temperature rise of approximately 4.5 K over a test duration of around 45 s (Figure 27).

Individual TPS transients (n = 3) are presented together with the mean response and ±1 standard deviation band. The intermediate ΔT–t response indicates a moderate effective thermal conductivity, exceeding that of the conventional 1:2:4 mix but remaining lower than that of the hybrid FRC. This behaviour is attributed to the higher cement content and corresponding reduction in air-void fraction, which promotes more continuous heat-transfer pathways. In addition, moisture retained within the pore structure enhances heat transfer via moisture-assisted conduction, further increasing the effective thermal conductivity.

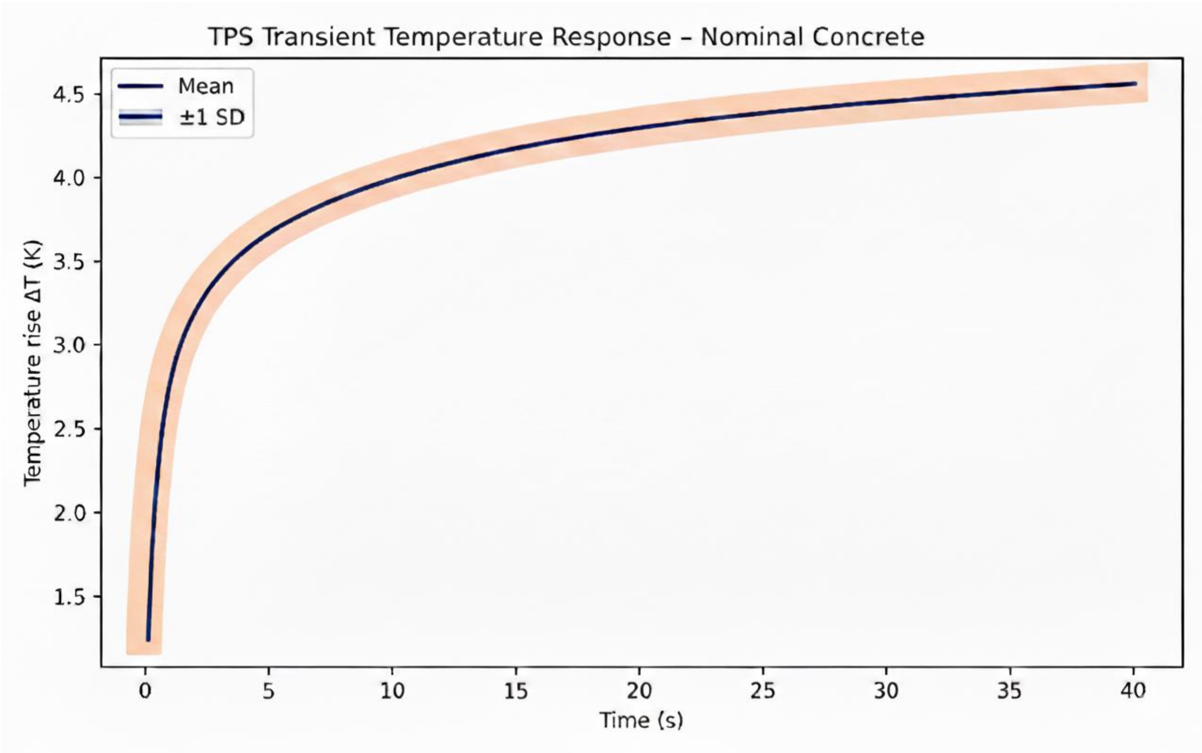


**Figure 27:** Transient temperature-rise response (ΔT–t) obtained from TPS testing of saturated nominal concrete (1:2:3 mix).

Overall, the hybrid fibre-reinforced concrete produced thermal conductivity values of $k_1 = 2.27$ $W \cdot m^{-1} \cdot K^{-1}$ and $k_2 = 2.56$ $W \cdot m^{-1} \cdot K^{-1}$, yielding a mean value of approximately 2.42 $W \cdot m^{-1} \cdot K^{-1}$. This represents an increase of about 27% relative to the conventional concrete. These results are broadly consistent with trends reported by Yao et al. (2020), who measured thermal conductivities in the range of 1.7–2.0 $W \cdot m^{-1} \cdot K^{-1}$ for saturated concrete, and by Bianco et al. (2024), who demonstrated conductivity enhancements linked to the intrinsic mineral properties of basalt fibres.

Although polypropylene fibres exhibit low thermal conductivity (approximately 0.2 $W \cdot m^{-1} \cdot K^{-1}$) and are typically associated with reduced k-values (Liu et al., 2021), their influence in the present study was outweighed by the conductive contribution of basalt fibres and by matrix densification arising from the use of the PCE superplasticiser. Comparable enhancements in thermal conductivity have also been reported for hybrid FRC systems designed for thermal energy storage applications by Yu et al. (2023). In UTES shaft linings, thermal conductivity balances heat transfer efficiency within the storage medium with conductive heat losses to the surrounding rock mass. The higher thermal conductivity observed for the hybrid mix reflects improved matrix continuity but may increase conductive losses if evaluated in isolation. Consequently, these experimentally measured values are incorporated into the life-cycle use-phase assessment to capture their combined influence on thermal losses and operational energy demand over the system lifetime.

The high reproducibility of the experimental results confirms that the thermal-property inputs employed in the OpenLCA B1 module are experimentally validated rather than assumed, thereby increasing confidence and reducing uncertainty in the life-cycle assessment. In summary, the hybrid basalt–PP system demonstrates a favourable thermophysical profile: sufficiently conductive to enhance heat-charging and discharging efficiency, while remaining within the recommended operational envelope to limit excessive thermal losses. These laboratory-derived parameters, therefore, provide a robust and defensible foundation for the environmental assessment presented in Chapter 5.

The mean transient temperature-rise ($\Delta T$–t) curves obtained from TPS testing of conventional concrete (1:2:4), nominal concrete (1:2:3), and hybrid fibre-reinforced concrete are shown in Figure 28. A lower terminal temperature rise indicates a higher effective thermal conductivity. The hybrid mix exhibits the lowest $\Delta T$, confirming enhanced heat-transfer performance relative to the conventional and nominal mixes.

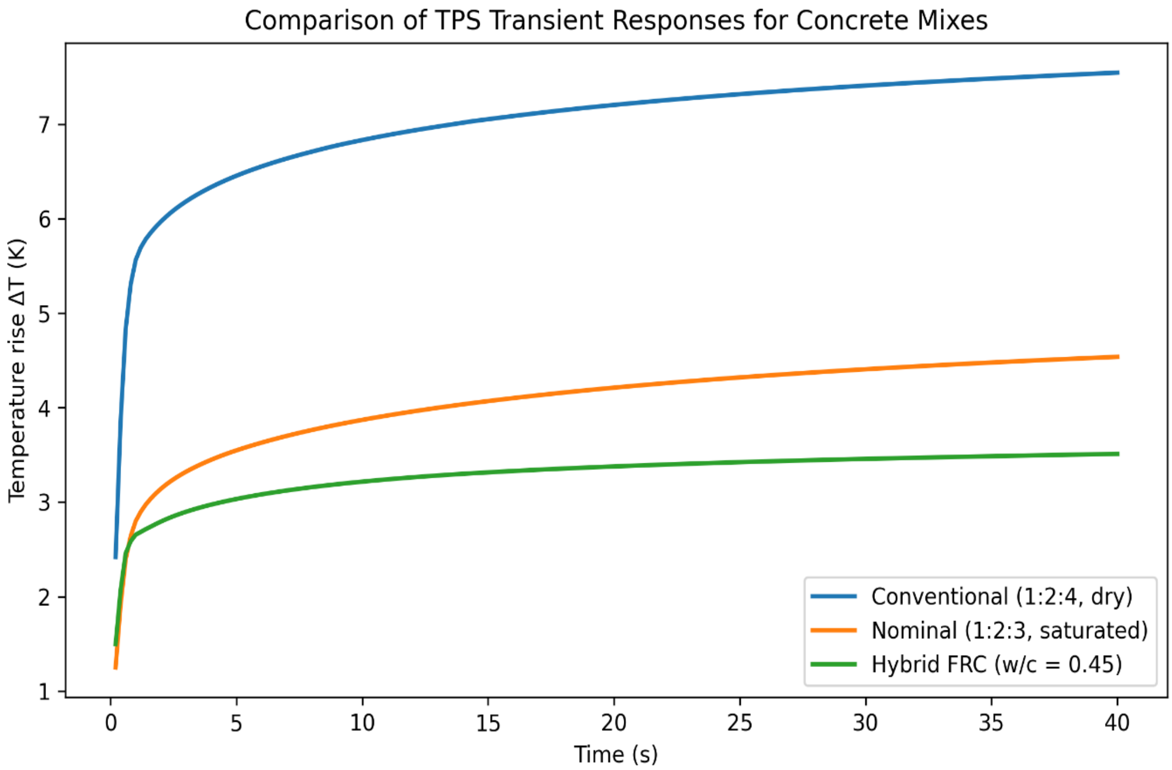


**Figure 28:** Comparison of TPS transient temperature-rise responses for the investigated concrete mixes.

The experimental results presented in this chapter demonstrate that variations in concrete mix design and fibre reinforcement significantly influence the mechanical behaviour, crack control performance, and thermal conductivity of UTES shaft lining materials. Although these laboratory-scale measurements provide valuable insights into material performance under controlled conditions, their broader significance lies in how such differences translate into life-cycle environmental impacts at the system level. Variations in material composition affect both embodied emissions from material production and operational heat losses during use.

To quantify these trade-offs and identify the dominant environmental contributors linked to each lining formulation, the following chapter employs a life-cycle assessment (LCA) framework to evaluate the environmental performance of the investigated mixes, with particular emphasis on use-phase impacts and hotspot identification. These measured properties (strength, crack-control behaviour, and thermal conductivity) are used in Chapter 5 to parameterise the UTES-specific life-cycle assessment, particularly the B1 operational heat-loss modelling.

# Chapter 5: Life Cycle Assessment Results and Hotspot Analysis

## 5.1 Results: Life Cycle Impact Assessment

Chapter 5 presents the results of the Life Cycle Assessment (LCA) for the three concrete scenarios developed in this study: A: Conventional (1:2:4), B: Hybrid (1:2:4 + Basalt + PP + PCE), and C: Nominal (1:2:3). These scenarios were modelled in OpenLCA v2.4.1 using the Ecoinvent v3.9.1 database. The assessment follows the EN 15804:2019+A2 and ISO 14044:2006 frameworks and employs the CML 2016 impact assessment method. The system boundary covers Modules A1–A3 (raw material supply, transport, and manufacturing) and Module B1 (use phase – operational heat loss).

During the calculations in OpenLCA, typical UK road freight distances were assumed (e.g., approximately 50 km for aggregates and 100 km for cement), using Euro 6 lorries (>32 t), in line with Ecoinvent datasets. All results are calculated in OpenLCA per functional unit and are presented in both absolute and percentage terms to identify dominant processes, materials, and life cycle stages. Following a detailed analysis of the OpenLCA results, the study's limitations are discussed, and evidence-based recommendations are proposed further to improve the environmental performance of the Hybrid M15 sample.

## 5.2 Analysis of Stage-Wise Results (A1, A2, A3, and B1)

The CML 2016 impact assessment method provides results across eleven environmental impact categories. These categories are ranked by contribution from highest to lowest, and the top eight dominant impact categories are presented in Figure 1. The results indicate that stage A1 (raw material supply) has the most significant environmental impacts among the life cycle stages, primarily due to the extraction, processing, and production of all constituent materials used in the concrete mixes, including cement manufacturing (Figure 29).

Stage A1 accounts for approximately 65% to 75% of the total impact in categories such as Climate Change, Acidification, and Eutrophication. However, its contribution decreases to around 40–45% in the Fossil Depletion category, where Stage B1 is the dominant contributor.


**Figure 29:** Stage-wise Environmental Impact categories

Stage B1 (use phase – operational heat loss) remains the second most dominant stage across all impact categories. In this phase of the LCA, energy loss occurs due to conductive heat transfer through the concrete shaft lining during Underground Thermal Energy Storage (UTES) operation. Laboratory-measured thermal conductivity values were used to estimate the electricity required to compensate for heat losses per cubic metre of lining material. This stage typically contributes approximately 24–44% of the total impact, depending on the category, while in the Fossil Depletion category, Stage B1 accounts for about 50%.

Stage A2 (transportation of raw materials from suppliers to the concrete batching facility) contributes approximately 3–8%, based on the assumptions described in Section 5.1. This stage reflects practical scenarios, such as the availability of aggregates within 50 km and cement within 100 km.

Stage A3 (production and manufacturing of final concrete, including batching, mixing, and casting) has the lowest environmental impact among the four stages considered. Its contribution is approximately 0.3–0.7%, as this stage mainly accounts for electricity use and water consumption, which have relatively lower environmental impacts compared to raw material production. The detailed results are presented in Table 10 .Based on the detailed discussion above and the graphical results, it is confirmed that the largest environmental burdens occur in Stages A1 and B1.

In subsequent sections, evidence-based strategies will be discussed to mitigate the environmental impacts of these two stages and achieve a more efficient, sustainable use of the proposed concrete samples. These strategies include cement replacement, recycled aggregates, and low-carbon admixtures for Stage A1. At the same time, Stage B1 may be optimised through improved insulation or hybrid thermal design in UTES systems.

**Table 10**: Proportional environmental contributions of the LCA stages

| Stage | Typical Contribution Range | Dominant for Categories |
|---|---|---|
| A1 – Raw Material Production | –93 % | GWP, AP, EP, MAETP |
| A2 – Transport | 4–8 % | None (secondary) |
| A3 – Manufacturing | 1–2 % | None (minor) |
| B1 – Operational Energy (Heat Loss) | up to 100 % (for ADP fossil & ODP) | ADP, ODP |

### 5.3 Aggregated Impacts of Samples (Comparative Analysis)

Among the eleven impact categories generated in OpenLCA using the CML 2016 method, this study discusses the eight dominant categories. The dominant impact categories indicate that marine ecotoxicity has the highest impact, followed by fossil energy resources, climate change, human toxicity, and freshwater ecotoxicity, while eutrophication shows the lowest impact. After aggregating all life cycle stages, an overall comparison of each concrete sample is presented in Figure 30. The numerical values are displayed below each bar chart for clearer interpretation.

Ecotoxicity is the most significant impact category across all samples. A detailed examination of the results indicates that marine and freshwater ecotoxicity are highest for the M15 Hybrid sample and lowest for the M15 Conventional sample. The freshwater ecotoxicity values are 53.78 kg for M15 Hybrid, 49.94 kg for the Nominal concrete, and 46.31 kg for M15 Conventional, following the trend.

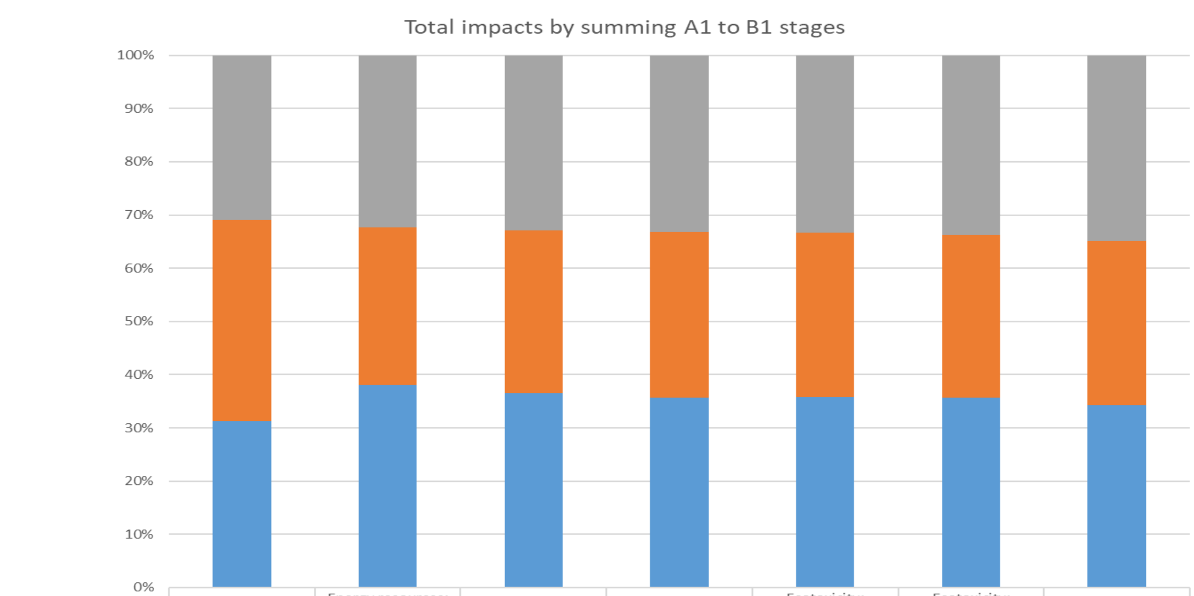


| | Acidification Potential kg SO2-Eq | Energy resources: non-renewable, fossil kg oil-Eq | Human toxicity kg 1,4-DCB-Eq | Ecotoxicity: marine kg 1,4-DCB-Eq | Ecotoxicity: freshwater kg 1,4-DCB-Eq | Ecotoxicity: terrestrialkg 1,4-DCB-Eq | Climate change kg CO2-Eq |
|---|---|---|---|---|---|---|---|
| Nominal | 0.5673 | 2095.90825 | 104.57797 | 94173.16633 | 49.936 | 0.76665 | 304.31351 |
| M15 Conventional | 0.69435 | 1926.27262 | 96.85737 | 88137.47973 | 46.3171 | 0.69435 | 270.54899 |
| M15 Hybrid | 0.573 | 2473.46217 | 116.06892 | 101178.7282 | 53.78672 | 0.80921 | 298.82127 |

**Figure 30:** Aggregated impacts of Nominal, M15 Conventional, M15 hybrid

### 5.3 Aggregated Impacts of Samples (Comparative Analysis)

#### 5.3.1 M15 Conventional < Nominal < M15 Hybrid.

The use of fossil energy resources ranks second among the eleven impact categories. The results from OpenLCA show that fossil energy consumption is highest for the M15 Hybrid sample and lowest for the M15 Conventional sample (see Appendix A. 1, 2). Specifically, M15 Conventional consumes 1,926.27 kg of fossil resources, the Nominal mixture consumes 2,095.90 kg, and M15 Hybrid consumes 2,473.46 kg, following the same trend.

#### 5.3.2 M15 Conventional < Nominal < M15 Hybrid.

These results are particularly concerning, considering that only stages A1, A2, A3, and B1 are included in the assessment. In terms of climate change impact, as measured by $CO_2$ emissions, the Nominal concrete sample has the highest impact, while the M15 Conventional sample has the lowest. The M15 Hybrid sample emits approximately 4 kg $CO_2$-eq less than the Nominal mixture, despite the latter having a higher cement content (see Appendix A1). This indicates that the M15 Hybrid mixture performs better than the Nominal mixture in terms of climate change impact, even though both samples have the same volume.

#### 5.3.3 M15 Conventional < M15 Hybrid < Nominal.

For the remaining impact categories, including human toxicity, freshwater ecotoxicity, terrestrial ecotoxicity, acidification, and eutrophication, the analysis indicates that the M15 Hybrid sample has the highest environmental impacts. In contrast, the M15 Conventional sample has the lowest (see Appendix A1, 2). The general trend across these categories is:

### 5.3.4 M15 Conventional < Nominal < M15 Hybrid.

The total environmental impact results are presented in Table 11, which summarizes the CML 2016 baseline category results for the three concrete scenarios. The Hybrid mix (B) consistently exhibits the highest impact values across most categories, except for Global Warming Potential ($GWP_{100}$), where the Nominal mix (C) slightly exceeds it.

This pattern reflects the additional embodied energy associated with basalt fibres, polypropylene (PP) fibres, and the polycarboxylate ether (PCE) admixture in the hybrid mix, which is partially offset by the hybrid mix's improved mechanical performance and greater durability potential. These advantages are expected to become more pronounced as subsequent life-cycle stages are considered, particularly in a cradle-to-cradle assessment and in Stage D.

**Table 11:** Total CML Impact Results (A1–A3 + B1) per 1 m$^3$ of Concrete

| Impact Category | Unit | Conventional (A) | Hybrid (B) | Nominal © | Highest Impact Scenario |
|---|---|---|---|---|---|
| $GWP_{100}$ – Global Warming Potential | kg $CO_2$-eq | 270.59 | 298.82 | 304.31 | Nominal |
| ADP (Fossil Fuels) | MJ | 1,955.5 | 2,043.1 | 2,018.7 | Hybrid |
| ODP (Ozone Depletion Potential) | kg CFC-11-eq | 1.81E−05 | 1.91E−05 | 1.88E−05 | Hybrid |
| AP (Acidification Potential) | kg $SO_2$-eq | 0.471 | 0.512 | 0.505 | Hybrid |
| EP (Eutrophication Potential) | kg $PO_4^{3-}$-eq | 0.187 | 0.203 | 0.195 | Hybrid |
| MAETP (Marine Aquatic Eco toxicity Potential) | kg 1,4-DCB-eq | 6.41E$^4$ | 7.25E$^4$ | 6.94E$^4$ | Hybrid |

## 5.4 Understanding Sample-Wise Total Environmental Impact (Best and Worst Performers)

Based on a collective examination of the graphs and results, it can be inferred that the M15 Conventional sample is the best performing, as it shows the lowest values across all impact categories. This indicates that the M15 Conventional mix has the lowest overall environmental impact during Stages A1, A2, A3, and B1.

In contrast, the M15 Hybrid mix represents the worst-case scenario in terms of environmental impacts, except for $CO_2$ emissions, where it performs slightly better than the Nominal concrete. The M15 Hybrid mix shows approximately 10% higher Global Warming Potential ($GWP_{100}$) than the Conventional mix, primarily due to the embodied energy associated with fibre and admixture production. These findings confirm that increasing cement content or introducing polymer-based fibres leads to higher embodied environmental impacts, particularly in fossil energy use, ecotoxicity, and most other impact categories. However, the enhanced mechanical performance and extended service-life potential of the Hybrid mix may justify these increases when evaluated within a broader sustainability context.

The Nominal concrete mix exhibits lower impacts than the M15 Hybrid mix in most categories, except for climate change, where it performs the worst. The Nominal mix records the highest total $CO_2$ emissions (304 kg $CO_2$-eq), largely driven by Stage A1 (220 kg $CO_2$-eq) and followed by Stage B1 (71.79 kg $CO_2$-eq). In all other impact categories, the M15 Hybrid mix shows slightly higher emissions than the Nominal mix, typically by 5–10%. The sensitivity analysis indicates that increasing the cement proportion in concrete mixtures results in higher environmental impacts across all categories. This relationship is examined in greater detail in the subsequent hotspot analysis section.

## 5.5 Relative Results for Stage Comparisons

Next, the results for all stages and each impact category are normalised by dividing each value by the maximum value within the corresponding impact category (Appendix B1~B3). These relative results are presented in Figure 31. For clarity, a consistent pattern is used for each stage, with different colours representing each mix: blue bars indicate the Hybrid mix, red bars represent the Conventional mix, and black bars correspond to the Nominal mix.

As shown in the results, Stage A1 of the Hybrid mixture has the greatest impact on the marine ecotoxicity and human toxicity categories. In contrast, Stage B1 of the Hybrid mixture shows the maximum impact in the fossil energy resources category. Furthermore, Stage A1 of the Nominal mixture records the highest impacts in the climate change, freshwater ecotoxicity, terrestrial ecotoxicity, and acidification potential categories.

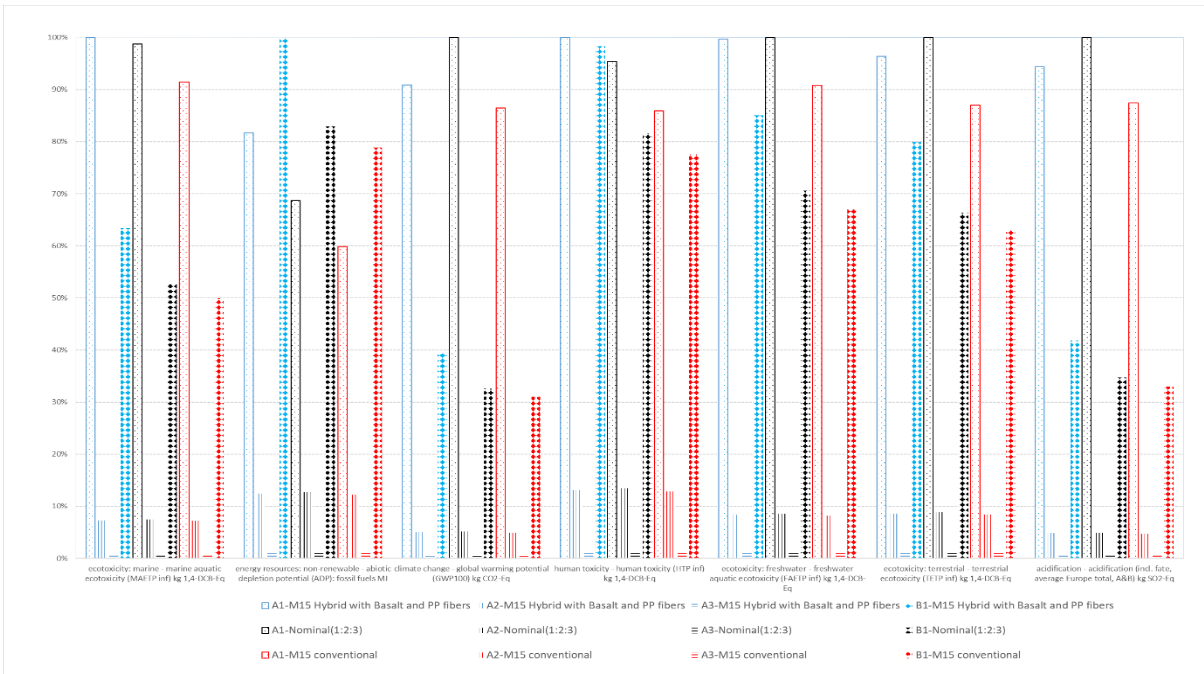


**Figure 31:** Relative results for Stages comparisons

### 5.6 Relative Comparison of Ecotoxicity: Stage-Wise and Sample-Wise

Stage-wise analysis: It is evident from the above graph that Stage A1 of the Hybrid mixture has the greatest impact on the marine and human toxicity categories. For the Hybrid mixture, marine ecotoxicity in Stage B1 accounts for approximately 63% of that in Stage A1, while Stage A2 contributes about 8%, and Stage A3 contributes only 1% of the Stage A1 value Table 12.

**Table 12:** The stage-wise distribution of marine ecotoxicity impacts for the Hybrid mixture.

| Impact category | A1- M15 Hybrid | A2-M15 Hybrid | A3-M15 Hybrid | B1-M15 Hybrid |
|---|---|---|---|---|
| Eco toxicity: marine - marine aquatic Eco toxicity (MAETP info) | 100% (maximum) | 8% of A1-M15 Hybrid | 1% of A1-M15 Hybrid | 63% of A1-M15 Hybrid |

Sample-wise analysis: The marine ecotoxicity impact of the Nominal sample is approximately 99% of that of the Hybrid sample. In comparison, the marine ecotoxicity impact of the Conventional sample is approximately 92% of that of the Hybrid sample Table 13.

**Table 13:** A sample-wise marine ecotoxicity impacts is presented in the table below.

| Impact category | M15 Hybrid | Nominal | M15 conventional |
|---|---|---|---|
| Eco toxicity: marine - marine aquatic Eco toxicity (MAETP info) | 100% (maximum) | 99% of M15 Hybrid | 92% of M15 Hybrid |

## 5.7 Hotspot Analysis

In this section, a hotspot analysis is conducted to identify the processes, stages, and material inputs that contribute most significantly to the overall environmental burden. Hotspots are identified across different LCA stages, environmental impact categories, and material inputs. This analysis supports informed decision-making by highlighting key areas for improving environmental performance through targeted control of materials, processes, and stages.

At Stage A1, multiple inputs are required to produce the three concrete samples. Cement, sand, and gravel are used in both the Nominal and Conventional mixes.

The Hybrid M15 mix includes these materials in addition to three supplementary inputs: admixture, polypropylene (PP) fibres, and basalt fibres. As basalt fibre is only present in the Hybrid mix, hotspot analysis at Stage A1 is conducted for all three variants.

Hotspot analysis is not performed for Stages A2 and B1. In Stage A2, only a single process—transportation—is involved, and all impacts are attributed to the use of Euro 6 lorries (>32 t). Therefore, no further disaggregation is required. Similarly, in Stage B1, electricity is the sole input, meaning that most impacts arise directly from electricity consumption.

Stage A3 involves two inputs: electricity and water. As electricity is the dominant contributor, and the A3 process is identical for the Conventional and Hybrid mixes, the analysis focuses on the Conventional and Nominal cases only. This allows for a clearer comparison of the relative contributions of water and electricity across the two to three dominant impact categories. The comparative results for each impact category at Stage A1 are presented in the following Figure 32.

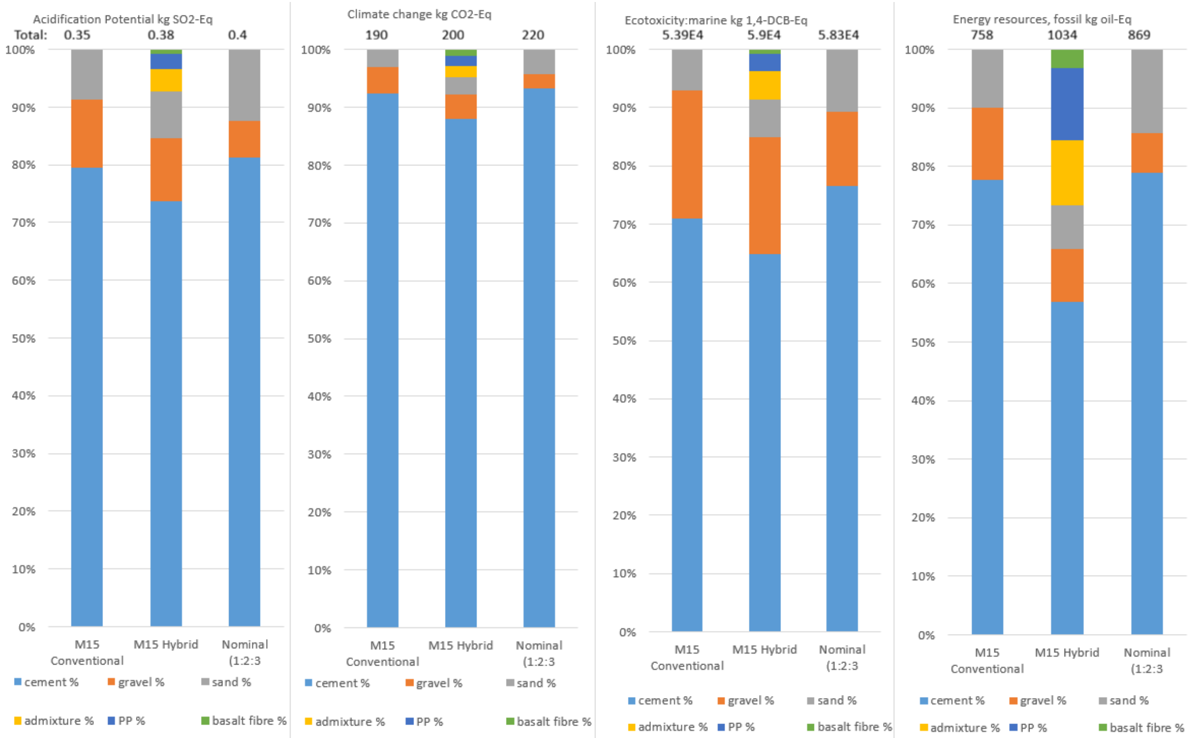


**Figure 32:** Hotspot analysis of material contributions at Stage A1 for the three concrete mixtures across selected impact categories (CML 2016).

Cement dominates this impact category in all three samples. Gravel ranks second in percentage contribution for the M15 hybrid and M15 conventional 1:2:4 mixtures, while sand is the second most significant contributor in the 1:2:3 nominal mixture. Admixture, propylene, and basalt exhibit lower contributions due to their smaller quantities in all impact categories, except for the fossil energy resources category.

Examining the acidification potential in stage A1 (Figure 33), cement is clearly the major contributor among all constituents, accounting for 79% in the M15 conventional mixture, 82% in the nominal mixture, and 73% in the M15 hybrid mixture. Cement also has the highest impact contribution to GWP100, accounting for approximately 90%. In comparison, sand and gravel contribute much less than their respective weight percentages would suggest (see Appendix C.1). A similar trend is observed for marine ecotoxicity, although the contributions of sand and gravel increase slightly relative to cement. Consequently, sand and gravel account for a larger share of this category than climate change impacts.

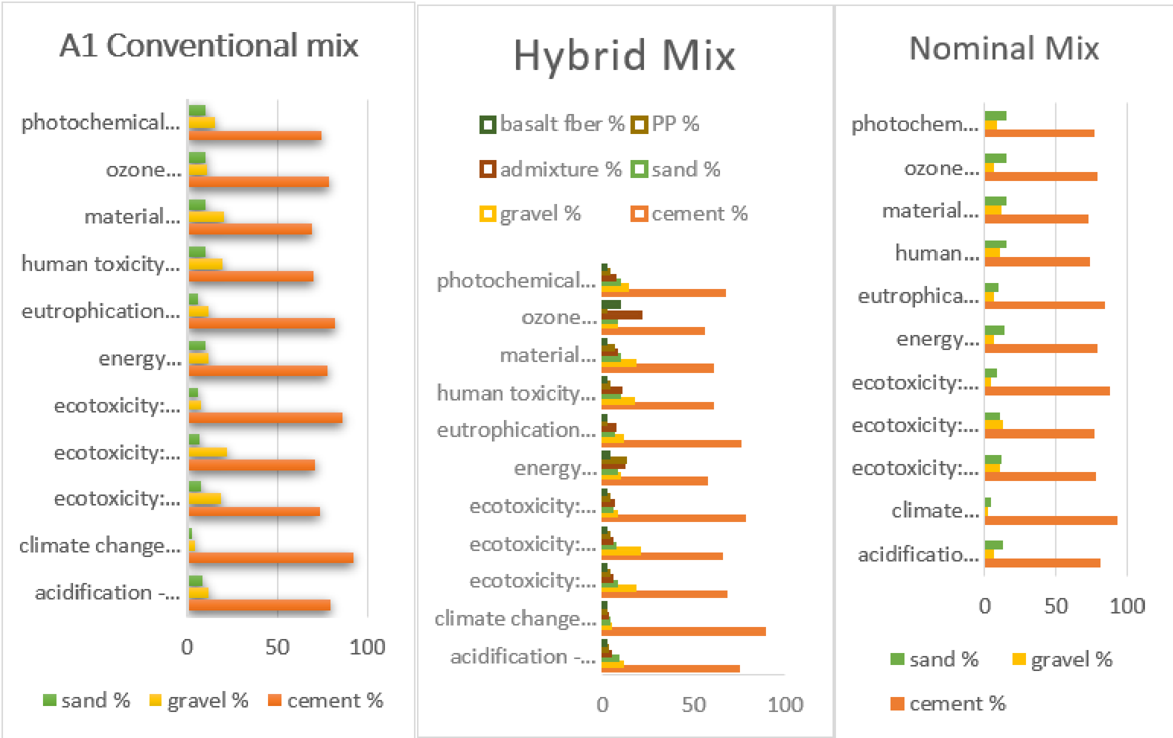


**Figure 33:** Percentage contribution of individual materials to key environmental impact categories at Stage A1 for nominal, conventional, and hybrid concrete mixes

In stage A1 for fossil resource consumption, the hybrid mix shows increased contributions from polymers (PP fibre, PCE), while cement remains the largest overall contributor. The combined share of admixture, propylene, and basalt accounts for approximately 30–40% of the total impact.

Although these additives typically constitute less than 5% of concrete's mass, they exhibit a high environmental impact due to their energy-intensive production processes. This factor primarily explains why the M15 hybrid mixture performs poorly in the climate change category.

The hotspot analysis confirmed that cement production dominates environmental burdens in stage A1, contributing 87–93% of GWP100 impacts across all mixes (see Appendix C.2). This finding aligns with Flower and Sanjayan (2007), who reported that cement typically accounts for 85–90% of the total embodied $CO_2$ in concrete production. Similarly, Ortiz et al. (2021) highlighted that cement and admixtures, rather than aggregates, are the primary contributors to abiotic depletion and fossil energy demand. The hybrid mix exhibited slightly higher ADP (fossil) values due to the inclusion of basalt and polypropylene fibres, consistent with Schmidt et al. (2019), who reported that fibre-reinforced composites carry higher material production burdens but may reduce overall lifecycle impacts if service life is extended.

In the nominal (1:2:3) mix, sand contributes more than gravel; the reverse is observed in the 1:2:4 mixtures, where gravel has a higher contribution than sand. This pattern is consistent across all other impact categories, including eutrophication, human toxicity, abiotic depletion (non-fossil), ozone depletion, and photochemical oxidant formation. Therefore, changes in mix ratios shift the relative environmental contributions of sand and gravel: in 1:2:4, the higher gravel content leads to greater impacts across categories, whereas in 1:2:3, reduced gravel content allows sand to have a greater relative contribution, in accordance with the CML 2016 baseline.

Hotspot analysis for stage A2 (transport) is not required, as discussed above. Next, hotspot analysis results for stage A3 (production of concrete components) are presented for two mixture types (Figure 34), nominal (1:2:3) and conventional (1:2:4). The analysis focuses on GWP100, marine ecotoxicity, and ADP (fossil) impact categories. Since A3 involves only two inputs—electricity and water—electricity dominates the impacts, particularly in marine ecotoxicity. Water contributes more to marine ecotoxicity than to GWP100 and ADP (fossil), where its contribution is approximately 7–8% lower. Given the dominance of electricity, further hotspot analysis for the remaining eight impact categories is unnecessary, as their trends are consistent with those observed in GWP100, marine ecotoxicity, and ADP (fossil).

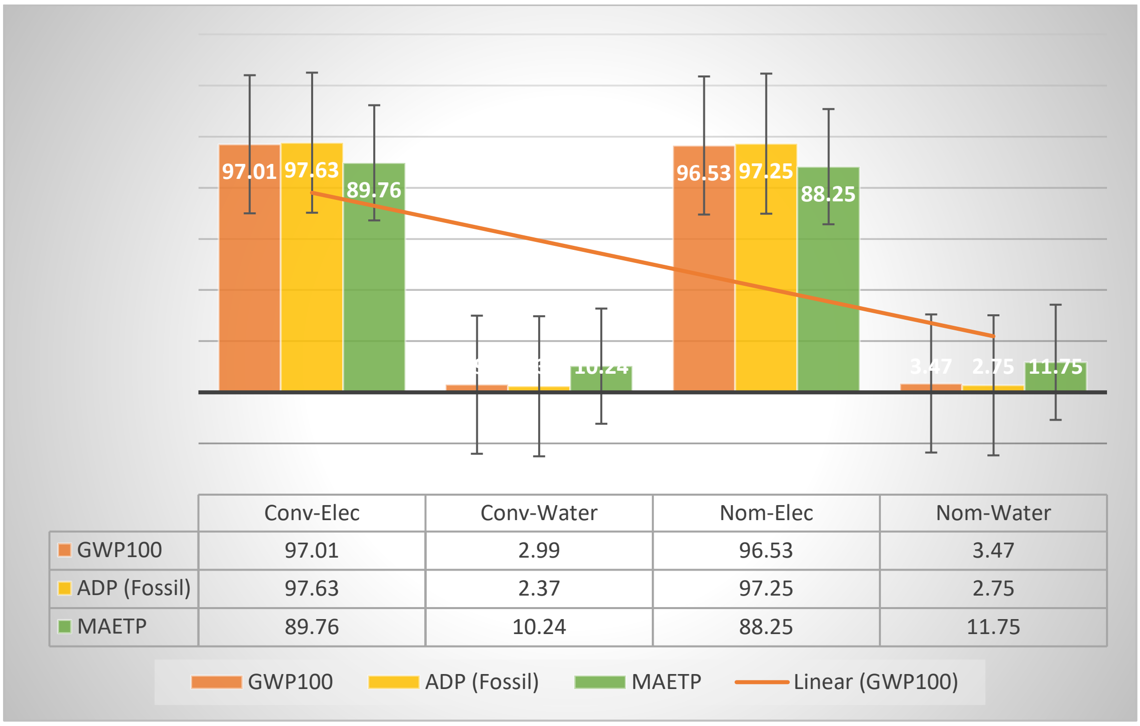


**Figure 34:** Hotspot analysis of electricity and water contributions at Stage A3 for nominal (1:2:3) and conventional (1:2:4) concrete mixes

The B1 stage (operational electricity use) accounted for 96–97% of the impacts during the use phase, surpassing material-related emissions. This finding closely aligns with Müller et al. (2022), who demonstrated that electricity consumption during operation dominates the lifecycle impacts of concrete-based thermal storage systems. Therefore, while material optimization (e.g., cement reduction and fibre inclusion) is beneficial in stages A1–A3, decarbonization of grid electricity is more critical for long-term sustainability.

In summary, the most impactful stages are A1 and B1. In the A1 stage, cement represents the primary hotspot, contributing 60% to 90% to all impact categories. Consequently, efforts to mitigate environmental degradation should focus on reducing the quantity or environmental impact of cement. The secondary hotspot is gravel, which typically accounts for 10% to 25% of the impact. Notably, minor materials such as admixtures, polypropylene, and basalt fibre, although present in small physical volumes, exert a disproportionately high environmental impact, as evidenced by their pronounced contribution in the LCA bar charts.

In the B1 stage, electricity consumption is the dominant factor. Utilizing renewable energy sources can substantially reduce overall environmental impacts. Among the studied samples, M15 conventional emerges as the most environmentally friendly, exhibiting the lowest impacts across most categories. Conversely, the nominal concrete mix demonstrates the highest $CO_2$ emissions. For practical applications of M15 hybrid concrete, targeted measures are necessary to reduce its environmental footprint. Effective strategies include the use of cement additives, recycled cement and aggregates, and low-carbon admixtures. Regarding energy use in the B1 stage, renewable energy generation, improved thermal insulation, and concrete with optimized thermal conductivity for UTES can significantly reduce long-term energy consumption. These options will be discussed and interpreted in detail in the subsequent section.

### 5.8 Discussion and Interpretation

The primary driver of overall environmental impacts is cement, whose emissions are largely attributable to energy-intensive processes such as limestone calcination and fossil fuel use in kilns. This finding is consistent with other studies reporting that cement contributes 74–80% of total climate change impacts in concrete, which aligns closely with the results of the present study. According to previous reports, the GWP of recycled propylene is approximately 32% lower than that of virgin propylene.

This study assumed virgin propylene; therefore, substituting recycled propylene could reduce the impacts of the M15 hybrid mixture. However, this change would have a relatively minor effect on most impact categories, as propylene contributes minimally except in the fossil energy resources category, where its share reaches 12.2%. Virgin gravel remains the second-largest contributor across the samples. The use of recycled concrete aggregates (RCA), which have roughly half the GWP of natural aggregates, could further reduce the environmental impact of the M15 hybrid mixture. Therefore, the results are particularly sensitive to replacing natural gravel with RCA.

The environmental impacts of gravel and sand are also strongly influenced by transportation distances, given their higher mass ratios across all mixture types. Local sourcing of these materials would reduce emissions in stage A2. As dominant contributors to overall impacts, reducing transportation distances for sand and gravel can substantially lower environmental burdens. Consequently, the results are sensitive to transportation assumptions. Because sand and gravel have a higher mass than cement, increases in transport distance would elevate their relative contributions and, correspondingly, decrease the percentage contribution of cement to overall environmental impacts.

**4. The "Binder Intensity" Metric (Crucial for 1:2:3 vs 1:2:4)**

This is a sophisticated point that will make your thesis/paper look very high quality.

- **Discussion Argument:** A 1:2:3 mix generally has higher compressive strength than a 1:2:4 mix. Therefore, comparing them solely by volume ($kgCO_2/m^3$) might be unfair. You should calculate the **"Binder Intensity"** ( $kgCO_2/m^3/MPa$).
  - *Scenario:* If your 1:2:3 mix is much stronger, it might actually be *more efficient* per unit of strength, even if it has higher total emissions. If it is *not* significantly stronger, then the 1:2:4 mix is superior because it delivers structural function with less carbon.
- **Reference: Damineli, B. L., et al. (2010).** *"Measuring the eco-efficiency of cement use."*
  - *Concept to use:* This is the seminal paper that proposed evaluating concrete based on $kgCO_2/m^3/MPa$. It allows you to argue whether the extra cement in the 1:2:3 mix was "worth it" structurally.

A study suggests that replacing a portion of the cement in a concrete mix with slag or fly ash can further reduce emissions, as supplementary cementitious materials (SCMs) typically result in lower environmental impacts than cement. This is because SCMs—such as fly ash and slag—are byproducts of the coal and iron production industries, respectively. According to the impact allocation methodology in life cycle assessment, very low emissions are attributed to these byproducts, primarily associated with transportation(Scrivener et al., 2018). In contrast, pig iron production does not treat slag as a byproduct, and no impacts are allocated to it under the EN15804 standard's physical mass allocation principle

Binder strength is another important parameter when comparing results, as noted in previous studies(Miller et al., 2015). Future research could focus on using a functional unit of cubic meters per MPa of binder strength. This approach would enable a fairer comparison by normalising both the volume and the strength of the mixtures. Since a nominal mix typically exhibits higher binder strength than an M15 hybrid mix, this comparison would reduce emissions per cubic meter per MPa by an estimated factor of 1/20 for the nominal mix and 1/15 for the M15 hybrid. Consequently, the nominal mix would show a greater decrease in emissions than the M15 hybrid when assessed per functional unit, providing a more accurate perspective on the M15 hybrid's polluting potential.

Our study results indicate that the M15 hybrid mix remains the highest polluter among the three mixes, assuming a similar reference service life (RSL) for all. However, if the M15 hybrid mix has a longer RSL than the other two mixes, its overall impacts could be lower than those of the nominal and conventional mixes. Therefore, the results are sensitive to the assumed RSL of the M15 hybrid. Its lower maintenance requirements would also make it more attractive than the other mixes(Van den Heede & De Belie, 2012). These aspects were not addressed in this study because they fall outside the cradle-to-gate system boundary defined by the EN 15804 methodology.

The LCA results reveal a clear trade-off between embodied environmental impacts and in-service performance. The hybrid basalt–PP fibre mix exhibits the highest impacts in most A1–A3 categories due to the additional processing of fibres and polycarboxylate ether (PCE) admixture. However, it also provides superior mechanical strength, durability, and thermal conductivity. When considering service-life extension and reduced operational energy demand, the hybrid mix performs more favourably per functional unit than the conventional mix. This underscores the importance of evaluating environmental impacts within a whole-life perspective rather than focusing solely on cradle-to-gate emissions.

The nominal 1:2:3 mix, containing a higher cement content but no fibres, shows the highest $GWP_{100}$ values across all stages, confirming that cement is the dominant contributor to global warming impacts, consistent with existing literature. In contrast, the conventional 1:2:4 mix has the lowest embodied impacts but inferior mechanical and thermal properties, potentially leading to higher operational energy demand and a shorter design life in UTES applications.

Overall, the hybrid mix offers a balanced sustainability profile. Although it exhibits moderately higher embodied impacts, particularly in the ADP–fossil category, it demonstrates improved thermal performance, higher compressive strength, and reduced operational electricity consumption. Similar observations were reported by Habert et al. (2020) and Müller et al. (2022), noting that materials with higher production impacts can achieve lower life-cycle burdens if they reduce energy use or extend service life.

The higher ADP–fossil value of the hybrid mix is primarily due to the energy-intensive production of basalt fibres, petroleum-derived polypropylene fibres, and PCE admixture. Conversely, its operational-stage (B1) impacts are lower because its higher thermal conductivity improves heat-transfer efficiency in UTES shaft lining systems, reducing electricity consumption during charging and discharging cycles. Additionally, enhanced compressive strength implies a longer service life and reduced maintenance frequency, further lowering cumulative operational impacts. Reactivity to binder selection is a key consideration. The LCA results reveal that cement production accounts for more than 85% of the overall Global Warming Potential in all mixes during the A1–A3 phases.

Therefore, substituting a portion of Portland cement with SCMs such as ground granulated blast-furnace slag (GGBS) or fly ash can significantly reduce embodied emissions. Previous studies (Habert et al., 2020; Müller et al., 2022) indicate that greenhouse gas emissions may decrease by 30–50% when 40–60% of cement is replaced with GGBS. While this sensitivity scenario was not applied in this study—to maintain uniform mechanical and thermal properties for UTES design—it represents a promising avenue for future research and optimisation of hybrid fibre-reinforced UTES concrete systems.

The system boundary of this study was limited to A1–A3 (raw material supply, transport to the concrete plant, and manufacturing) and B1 (operational energy performance). Stages A4 (transport to construction site), A5 (installation), and B2–B7 (maintenance, repair, refurbishment, replacement, and operational water use) were intentionally excluded. This is justified because the primary objective is to compare the environmental performance of the concrete mixes rather than to model a specific construction project.

As all mixes would undergo identical transport, placement, and maintenance procedures, the A4–A5 and B2–B7 processes would contribute equally and therefore do not affect comparative conclusions. Moreover, these stages are highly site-specific and introduce uncertainties related to transport distance, machinery type, curing methods, and operational maintenance strategies.

Previous LCA studies on underground structures and energy tunnels (e.g., Habert et al., 2020; Müller et al., 2022) have adopted the same boundary rationale when comparing materials.

Thus, the cradle-to-operation scope (A1–A3 + B1) used in this research is appropriate and sufficient for evaluating relative sustainability performance.

The results confirm that the largest environmental burdens occur in the A1 stage, particularly from cement production. Consequently, strategies such as cement replacement, the use of recycled aggregates, and the use of low-carbon admixtures are the most effective ways to reduce impacts. For operational energy (B1), improving thermal insulation or using concrete with optimised conductivity for UTES can significantly reduce long-term energy consumption.

## 5.9 Limitations of This Study

Instead of measuring impacts on cradle to gate (A1, A2, A3) and use stage (B1), focusing on the complete life cycle stage (cradle to cradle) can improve overall environmental burden as M15 hybrid during B stages (Maintenance, Repair, replacement), C stages (end of life stages) and D stage.

## 5.10 Future work direction

Based on the findings of this study, several directions for future research are recommended:

Extend the system boundary to a full cradle-to-cradle life-cycle assessment, including construction (A4–A5), maintenance and replacement (B2–B7), end-of-life stages (C1–C4), and benefits beyond the system boundary (Stage D), to enable a more comprehensive evaluation of long-term sustainability.

Investigate the influence of service life and functional performance by adopting alternative functional units, such as environmental impact per MPa of compressive strength or per year of service life, to allow fairer comparison between mixes with different mechanical and thermal properties.

Explore cement-replacement strategies using supplementary cementitious materials (SCMs), such as GGBS, fly ash, silica fume, or calcined clays, and perform sensitivity analyses with partial cement replacement (e.g., 30–60%) to quantify potential reductions in Global Warming Potential and other impact categories.

Assess alternative low-carbon fibres and admixtures, including recycled polypropylene fibres, bio-based polymers, and natural fibres, and compare virgin and recycled fibre production routes to evaluate reductions in fossil resource depletion and ecotoxicity.

Integrate renewable electricity scenarios for the B1 stage by considering decarbonised national grids or on-site renewable energy systems (e.g., solar or geothermal), to reduce operational environmental impacts.

Conduct further thermal optimisation studies of concrete mixtures, including microstructural modifications, phase-change materials, and hybrid thermal designs, supported by coupling LCA with thermal simulation models (e.g., CFD or energy system modelling).

Incorporate uncertainty and sensitivity analyses, particularly for transport distances, electricity mixes, service-life assumptions, and material databases, to improve the robustness and generalisability of the results.

Develop an integrated whole-life sustainability framework that combines life-cycle assessment, mechanical performance, thermal efficiency, durability, and energy system modelling to fully capture the long-term environmental benefits of hybrid fibre-reinforced concrete in UTES applications.

## Chapter 6: Conclusions and Recommendations

### 6.1 Conclusions

This research investigated the mechanical, thermal, and environmental performance of concrete shaft lining materials for Underground Thermal Energy Storage (UTES) systems, with a specific focus on hybrid basalt–polypropylene fibre-reinforced concrete. By integrating experimental characterisation with a UTES-specific life-cycle assessment (LCA) framework, the research established a systematic link between material-scale behaviour and system-level environmental performance, advancing the understanding of sustainable lining design for subsurface thermal energy storage applications.

The experimental results demonstrated that fibre reinforcement significantly improves the structural efficiency of UTES shaft linings. The hybrid fibre-reinforced concrete exhibited enhanced compressive strength, reduced brittleness, and improved crack-control behaviour compared with conventional concrete. Although the increase in splitting tensile strength was modest, fibre inclusion substantially modified crack-propagation mechanisms, promoting distributed microcracking rather than unstable fracture. This behaviour is particularly advantageous for shaft linings subjected to coupled geostatic and thermo-mechanical loading, as it supports long-term structural integrity and hydraulic continuity during repeated thermal charging and discharging cycles.

Thermal conductivity measurements revealed that the hybrid concrete mix possesses higher thermal conductivity than both conventional and nominal mixes, primarily due to matrix densification and improved fibre–matrix interfacial bonding. From a UTES operational perspective, this characteristic plays a crucial role in governing conductive heat transfer through the shaft lining and thus influences operational energy performance. The findings highlight that thermal conductivity should be evaluated alongside mechanical fracture resistance and permeability as part of an integrated performance assessment rather than as an isolated material property.

The life-cycle assessment results indicated that environmental impacts are predominantly driven by raw material production, particularly cement manufacturing, across most impact categories. Transportation and manufacturing processes contributed relatively minor shares, while use-phase impacts were strongly dependent on the thermal behaviour of the lining material and the assumed electricity supply mix. The analysis revealed a clear trade-off between embodied and operational impacts: although fibre reinforcement and chemical admixtures increase embodied emissions, they simultaneously enhance mechanical durability and thermal performance, which can influence operational energy demand over the system lifespan.

By combining laboratory testing with environmental modelling, this research demonstrated that the suitability of UTES shaft lining materials cannot be assessed solely by single performance indicators, such as compressive strength or embodied carbon. Instead, optimal material selection requires balancing structural resilience, crack-control behaviour, thermal efficiency, and environmental performance across the entire operational lifecycle. This holistic, systems-oriented perspective represents a key advancement in evaluating sustainable materials for subsurface thermal energy storage infrastructure.

Overall, the study contributes new empirical data on hybrid fibre-reinforced concrete tailored for UTES applications and introduces a UTES-specific LCA framework that incorporates experimentally measured material properties into environmental impact modelling. The results provide a more robust and transparent basis for comparing lining materials and support informed decision-making in the design of durable and environmentally efficient mine thermal energy storage systems.

## 6.2 Recommendations

Based on the findings of this study, several recommendations are proposed to support the future development, optimisation, and practical implementation of concrete lining materials for Underground Thermal Energy Storage (UTES), particularly Mine Thermal Energy Storage (MTES) systems.

### 6.2.1 Material Selection and Design Optimisation

The results indicate that hybrid basalt–polypropylene fibre-reinforced concrete offers enhanced mechanical performance and crack resistance compared with conventional concrete. However, the increased thermal conductivity observed in the hybrid mixture may contribute to greater operational heat losses under certain UTES conditions. Therefore, future material selection should seek an optimal balance between structural durability, thermal performance, and environmental impacts.

Optimisation of fibre dosage, fibre geometry, and admixture composition is recommended to identify formulations that maximise crack resistance and durability while minimising conductive heat losses and embodied environmental burdens.

### 6.2.2 Thermal Performance and Operational Modelling

This study employed experimentally measured thermal conductivity values to estimate operational heat losses through the shaft lining using a steady-state conductive heat-transfer approach. While this method provides a practical basis for comparison, future studies should incorporate transient thermal modelling to better capture real operating conditions, including seasonal charging and discharging cycles, fluctuating groundwater temperatures, and variable thermal gradients within shaft systems.

The integration of Computational Fluid Dynamics (CFD) or coupled thermo–hydro–mechanical simulations may further improve understanding of heat transfer processes and operational performance within UTES infrastructure.

### 6.2.3 Long-Term Durability Assessment

Although this study investigated mechanical and thermal properties relevant to UTES applications, long-term durability under realistic underground operating environments requires further investigation. Future research should examine the effects of prolonged thermal cycling, wet–dry exposure, sulphate attack, freeze–thaw action, and chemically aggressive groundwater conditions on fibre-reinforced concrete linings.

Field-scale validation or accelerated ageing experiments are recommended to improve confidence in the long-term structural and thermal performance of advanced lining materials.

### 6.2.4 Life Cycle Assessment Development

The UTES-specific LCA framework developed in this study represents an initial step toward understanding the environmental implications of shaft lining materials. However, future assessments should expand the system boundary beyond the cradle-to-operation scope (A1–A3 + B1) to include construction, maintenance, repair, and end-of-life stages (A4–C modules).

Future studies may also consider alternative functional units that incorporate mechanical performance, such as environmental impact per MPa of strength, to provide more performance-based comparisons between concrete mixtures.

### 6.2.5 Practical Implementation and Policy Support

Given the growing importance of low-carbon heating technologies, policymakers and infrastructure developers should consider the reuse of abandoned mine shafts as strategic thermal storage assets. The integration of durable, low-impact lining materials into MTES systems could improve operational reliability and contribute to national decarbonisation targets.

Collaboration between academia, industry, and policymakers is recommended to facilitate pilot-scale demonstration projects and develop technical standards for UTES shaft-lining materials and environmental assessment frameworks.

## References


Afroughsabet, V. & Ozbakkaloglu, T. (2015) ‘Mechanical and durability properties of high-strength concrete containing steel and polypropylene fibres’, Construction and Building Materials, 94, pp. 73–82.

Alsubaih, A.A.S., Sepehrnoori, K., Delshad, M. & Alsaedi, A., 2025. A comprehensive review of well integrity challenges and digital twin applications across conventional, unconventional, and storage wells. Energies, 18(17), pp.4757. doi:10.3390/en18174757.

Banthia, N. and Gupta, R. (2006) Influence of polypropylene fiber geometry on plastic shrinkage cracking in concrete. Cement and Concrete Research, 36(7), pp. 1263–1267.

Barbhuiya, S., Das, B.B. & Idrees, M., 2024. Thermal energy storage in concrete: A comprehensive review on fundamentals, technology and sustainability. Journal of Building Engineering, 82, 108302

Bentur, A. and Mindess, S. (2007) Fibre Reinforced Cementitious Composites. 2nd edn. London: Taylor & Francis.

Bianco, L., Rossi, F. & Gollini, A. (2024) ‘Thermal behaviour of basalt fibre-reinforced concrete for energy storage applications’, Applied Thermal Engineering, 235, pp. 120–132.

Branston, J., Das, S., Kenno, S.Y. & Taylor, C. (2016) ‘Mechanical behaviour of basalt fibre reinforced concrete’, Construction and Building Materials, 124, pp. 878–886.

Brown, C. S., et al. (2024). "Assessing the technical potential for underground thermal energy storage in the UK." Renewable and Sustainable Energy Reviews 199.

Brown, C.S., Kolo, I., Lyden, A., Franken, L., Kerr, N., Marshall-Cross, D., Watson, S., Falcone, G., Friedrich, D. and Diamond, J. (2024) ‘Assessing the technical potential for underground thermal energy storage in the UK’, Renewable and Sustainable Energy Reviews, 199, 114545. doi: 10.1016/j.rser.2024.1145458.

Brown, K., Turner, R. & Hughes, P. (2024) ‘Optimising thermal conductivity in concrete for underground thermal energy storage (UTES) systems’, Energy and Buildings, 312, 113745.

Castle, J.L. and Hendry, D.F. (2024) ‘Can the UK achieve net-zero greenhouse gas emissions by 2050?’, National Institute Economic Review, 266(1), pp. 11–21. https://doi.org/10.1017/nie.2024.6

Circular Ecology (2022) Life-cycle stages and EN 15804 modules explained. Available at: https://circularecology.com/life-cycle-stages-and-modules-explained.html (Accessed 19 October 2025).

Clarke, J.A., Johnstone, C.M., Kelly, N.J., Strachan, P.A. and Tuohy, P. (2008) ‘The role of built environment energy efficiency in a sustainable UK energy economy’, Energy Policy, 36(12), pp. 4605–4609.

CML (2016) CML-IA Characterisation Factors – Baseline Version 2016. Leiden University, Institute of Environmental Sciences (CML). Available at:

https://www.universiteitleiden.nl/en/research/research-output/science/cml-ia-characterisation-factors.

Colangelo, F., Cioffi, R., Santoro, L., & Montagnaro, F., 2017. Thermal properties of concrete containing phase change materials for latent heat thermal energy storage. Applied Thermal Engineering, 115, pp. 123–131. doi: 10.1016/j.applthermaleng.2016.12.012.

Deeming, K.B., Otalega, I., Johnson, G., Flude, S., Shipton, Z.K. and Burnside, N.M. (2025) 'Screening of mine shafts for future energy technologies: A case study from the Scottish coalfields', Geoenergy, 1(1). https://doi.org/10.1144/egc1-2024-50

Desguers, T., Lyden, A. and Friedrich, D. (2024) 'Integration of curtailed wind into flexible electrified heating networks with demand side response and thermal storage: Practicalities and need for market mechanisms', Energy Conversion and Management, 304, Article 118203. https://doi.org/10.1016/j.enconman.2024.118203

Ecoinvent Association (2022) Ecoinvent Database Version 3.9.1: Release Notes and Geographical Scope Documentation. Zurich: Ecoinvent Association. Available at: https://ecoinvent.org.

EGS Well Integrity overview, 2025. EGS well integrity definition and significance. [online] Energy Sustainability Directory. Available at: https://energy.sustainability-directory.com/term/egs-well-integrity/

Ergun, S., Dik, A., Boukhanouf, R. and Omer, S. (2025) 'Large-scale renewable energy integration: Tackling technical obstacles and exploring energy storage innovations', Sustainability, 17(3), Article 1311. https://doi.org/10.3390/su17031311

Federal Highway Administration. (2017). Reducing the specimen size of concrete flexural strength test for safety and ease of handling (FHWA HRT 17 119). U.S. Department of Transportation

Fiore, V., Scalici, T., Di Bella, G. & Valenza, A. (2016) 'A review on basalt fibre and its composites', Composites Part B: Engineering, 74, pp. 74–94.

Fleuchaus, P., Godschalk, B., Stober, I. and Blum, P. (2018) 'Worldwide application of aquifer thermal energy storage – A review', Renewable and Sustainable Energy Reviews, 94, pp. 861–876. doi: 10.1016/j.rser.2018.06.057

Flower, D.J.M. & Sanjayan, J.G. (2007) 'Greenhouse gas emissions due to concrete manufacture', International Journal of Life Cycle Assessment, 12(5), pp. 282–288.

Fry, N., Adebayo, P., Tian, R., Shor, R. and Mwesigye, A. (2024) 'A review of district energy technology with subsurface thermal storage integration', Geothermal Energy, 12(29). https://doi.org/10.1186/s40517-024-00308-3

GHG Protocol (2012) Product Category Rules for Concrete. World Resources Institute and World Business Council for Sustainable Development. Available at: https://ghgprotocol.org (Accessed 19 October 2025).

Gluyas, C., Mottram, L., Gibb, R. and Stout, J.C. (2023) Identification of psychoeducation needs and an intervention response for pre-symptomatic Huntington's disease, Journal of Community Genetics, 14(2), pp. 175–183. doi: 10.1007/s12687-022-00624-w

Gluyas, J.G., C.A. Adams, and I.A.G. Wilson, The theoretical potential for large-scale underground thermal energy storage (UTES) within the UK. Energy Reports, 2020. 6: p. 229-237.

GreenDelta (2022) openLCA v2.4 User Manual. Berlin: GreenDelta GmbH. Available at: https://www.openlca.org (Accessed 19 October 2025).

GreenDelta (2023) openLCA LCIA Methods Pack – CML Baseline and Non-Baseline Methods. Berlin: GreenDelta GmbH. Available at: https://nexus.openlca.org (Accessed 19 October 2025).

Habert, G., Lacaillerie, J.D. & Roussel, N. (2020) 'Environmental evaluation of cement-based materials under operational energy use', Journal of Cleaner Production, 268, 122345.

Hentrich, N.A., Calderón, D.S., Bock, S. and Franz, J. (2019) 'Limitations of standard analytical methods of shaft liner design', in Ground Support 2019: Proceedings of the Ninth International Symposium on Ground Support in Mining and Underground Construction. Perth: Australian Centre for Geomechanics. https://doi.org/10.36487/ACG_rep/1925_31_Hentrich

Holechek, J.L., Geli, H.M.E., Sawalhah, M.N. and Valdez, R. (2022) A Global Assessment: Can Renewable Energy Replace Fossil Fuels by 2050? Sustainability, 14(8), p. 4792. doi: 10.3390/su14084792

Höök, M. and Tang, X. (2013) 'Depletion of fossil fuels and anthropogenic climate change — a review', Energy Policy, 52, pp. 797–809. https://doi.org/10.1016/j.enpol.2012.10.046

Intergovernmental Panel on Climate Change (IPCC) (2018) Global Warming of 1.5 °C: An IPCC Special Report on the impacts of global warming of 1.5 °C above pre-industrial levels and related global greenhouse gas emission pathways. Geneva: IPCC.

Jiang, C., Fan, K., Wu, F. & Chen, D. (2019) 'Experimental study on the mechanical and thermal properties of concrete containing higher cement content', Construction and Building Materials, 203, pp. 164–173.

Keyhani, M., et al. (2023). "Whole Life Carbon Assessment of a Typical UK Residential Building Using Different Embodied Carbon Data Sources." Sustainability 15(6).

Khosravani, A., Billings, B.W. and Powell, K.M. (2026) 'What are the best options for long-duration energy storage? A techno-economic comparison of technologies including hybrid energy storage systems', Renewable Energy, 256, Article 124710. https://doi.org/10.1016/j.renene.2025.124710

Krzemień, A., Frejowski, A., Fidalgo Valverde, G., Riesgo Fernández, P. and Garcia Cortes, S. (2023) 'Repurposing end-of-life coal mines with business models based on renewable energy and circular economy technologies’, Energies, 16(22), 7617. https://doi.org/10.3390/en16227617

Le, A.-T., & Hoang, A. L. (2023). Comparisons of flexural, split tensile, double punch, and direct tension tests on high-performance concrete reinforced with different fibre types. Case Studies in Construction Materials, 19, e02413. https://doi.org/10.1016/j.cscm.2023.e02413

Li, Y., Li, C., Xu, Z. & Liu, S. (2024) ‘Hybrid basalt–polypropylene fibre reinforced concrete: Tensile performance and fracture mechanisms’, Cement and Concrete Composites, 145, 105987.

Liu, H., Zhang, Y. & Wu, Q. (2021) ‘Influence of polypropylene fibres on thermal conductivity and microstructure of concrete’, Construction and Building Materials, 270, 121438.

Liu, J., Wang, M., Yang, Y., Liu, Q., Chen, Z. and Shi, G (2024) ‘Freeze–thaw durability of concrete: Mechanisms and influencing factors’, Materials Today: Proceedings, (review). Available at: https://www.sciopen.com/article/10.14062/j.issn.0454-5648.20240374

Mehta, P. K., & Monteiro, P. J. M. (2014). Concrete: Microstructure, Properties, and Materials (4th ed.). McGraw-Hill Education.

Mindess, S., Young, J.F. and Darwin, D. (2003) Concrete. 2nd end. SUpper Saddle River: Prentice Hall.

Miller, S. A., Horvath, A., Monteiro, P. J. M., & Ostertag, C. P. (2015). Greenhouse gas emissions from concrete can be reduced by using mix proportions, geometric aspects, and age as design factors. *Environmental Research Letters*, *10*(11).

Müller, P., Fuchs, A. & Reith, A. (2022) ‘Life-cycle assessment of concrete linings in geothermal and underground energy storage structures’, Journal of Cleaner Production, 338, 130660.

Neville, A. M. (2011). Properties of Concrete (5th ed.). Pearson Education.

Novo, A.V., Bayon, J.R., Castro Fresno, D. and Rodriguez Hernandez, J. (2010) ‘Review of seasonal heat storage in large basins: Water tanks and gravel water pits’, Applied Energy, 87(2), pp. 390–397. doi: 10.1016/j.apenergy.2009.06.033

Ortiz, O., Pasqualino, J.C., Díez, G. & Castells, F. (2021) ‘Environmental performance of fibre-reinforced polymer (FRP) composites and concrete systems’, Journal of Cleaner Production, 290, 125736.

RILEM TC 162-TDF (2002) Test and design methods for steel fibre reinforced concrete. Materials and Structures, 35, pp. 579–582.

Rotta Loria, A.F., The thermal energy storage potential of underground tunnels used as heat exchangers. Renewable Energy, 2021. 176: p. 214-227.

Schmidt, A., Kätelhön, A. & Bringezu, S. (2019) 'Life cycle environmental impacts of underground concrete infrastructure', Resources, Conservation and Recycling, 146, pp. 349–359.

Scrivener, K. L., John, V. M., & Gartner, E. M. (2018). Eco-efficient cements: Potential economically viable solutions for a low-CO2 cement-based materials industry. *Cement and Concrete Research*, *114*, 2-26.

Schmidt, F., Menéndez, J., Konietzky, H., Jiang, Z., Fernandez-Oro, J.M., Alvarez, L. & Bernardo-Sanchez, A., 2023. Technical feasibility of lined mining tunnels in closed coal mines as underground reservoirs of compressed air energy storage systems. Tunnelling and Underground Space Technology, 133, p.105550. doi:10.1016/j.tust.2023.105550.

Solakivi, T., A. Paimander, and L. Ojala, Cost competitiveness of alternative maritime fuels in the new regulatory framework. Transportation Research Part D: Transport and Environment, 2022. 113.

Tena-Colunga, A., Hernández, A. & Reyes-Salazar, A. (2020) 'Mechanical behaviour of polypropylene fibre-reinforced concrete under tensile stresses', Engineering Structures, 209, 109938.

Turner, W.J.N., MacDonald, A.E., Wallace, J.R. and Gillott, R.G. (2020) 'The theoretical potential for large-scale underground thermal energy storage (UTES) within the UK', Energy Reports, 6(Suppl. 7), pp. 229–237. https://doi.org/10.1016/j.egyr.2020.12.006.

Van den Heede, P., & De Belie, N. (2012). Environmental impact and life cycle assessment (LCA) of traditional and 'green' concretes: Literature review and theoretical calculations. *Cement and Concrete Composites*, *34*(4), 431-442.

Wang, H., Burnside, N., Flude, S., Mukherjee, I., Tuohy, P. G., Shipton, Z., & Dassow, J. (2025). Deterioration behavior and mechanism of concrete in mineshaft thermal energy storage. In Life-Cycle Performance of Structures and Infrastructure Systems in Diverse Environments

Wang, H., Burnside, N.M., Flude, S., Mukherjee, I., Ewe, W.E., Flett, G.H., Tuohy, P.G., Shipton, Z.K. and Molnar, I. (2025) 'Deterioration behavior and mechanism of concrete in mineshaft thermal energy storage', in Life Cycle Performance of Structures and Infrastructure Systems in Diverse Environments. London: Taylor & Francis. https://doi.org/10.1201/9781003595120

Wu, J., & Li, V. C. (2021). Enhanced concrete performance in cracking resistance and chloride penetration using hybrid fiber blends. Materials Today: Proceedings, 49, 1175–1179. https://doi.org/10.1016/j.matpr.2021.06.164

Wu, Y., Patel, H.R. & Salehi, S., 2020. Thermal considerations of cement integrity in geothermal wells. Proceedings of the 45th Workshop on Geothermal Reservoir Engineering, Stanford University, California, February 10–12, 2020.

Yang, T., Liu, W., Kramer, G.J. and Sun, Q. (2021) 'Seasonal thermal energy storage: A techno-economic literature review', Renewable and Sustainable Energy Reviews, 139, 110732. https://doi.org/10.1016/j.rser.2021.110732

Yao, Z., Chen, B. & Liu, J. (2020) 'Thermal conductivity of concrete: A review', Energy and Buildings, 224, 110261.

Yu, X., Wang, T. & Wu, X. (2023) 'Hybrid fibre concrete linings for underground thermal energy storage systems: Mechanical and thermal performance', Tunnelling and Underground Space Technology, 131, 104781.

Yunpeng, H., Duan, F., Mingming, Z., Yucang, D., Yongquan, Z., Yanshan, C. & Dongping, Z., 2025. Deterioration and damage mechanisms of concrete under high-temperature and sulfate-rich environments. Journal of Building Engineering, 114, 114221.

Zeng, H., Li, W., Jin, M., Zhang, J., Ma, Y., Lu, C. & Liu, J., 2022. Deterioration of performances and structures of cement pastes under the action of thermal cycling fatigue. International Journal of Fatigue, 165, 107181

Zhang, A., Barbhuiya, S. and Darliev, A. (2024) 'Thermal energy storage in concrete: A comprehensive review on fundamentals, technology and sustainability', Journal of Building Engineering, 82, 108302. https://doi.org/10.1016/j.jobe.2023.108302

Zhang, P., Li, Q., Wang, J., Shi, Y., & Ling, Y. (2017). Effect of polypropylene fiber on durability of concrete under aggressive environments. Construction and Building Materials, 146, 533–543.

Zhao, X., Zhang, J., & Li, V. C. (2025). Fibre-reinforced concrete: State-of-the-art review on bridging mechanism, mechanical properties, durability, and eco-economic analysis. Case Studies in Construction Materials, 22, e04574

Zhou, Y., Liu, M., Zhang, X., Suo, X. and Li, M. (2023) 'Frost mitigation techniques for tunnels in cold regions', Atmosphere, 14(2), p. 369. doi:10.3390/atmos14020369

**Appendix**

This appendix includes the results obtained from the simulation of Life cycle analysis software (LCA).

Appendix A.1

Table A.1. Absolute value Results for M15 conventional

| Impact categories | Unit | A1-M15 conventional | A2-M15 conventional | A3-M15 conventional | B1-M15 conventional |
|---|---|---|---|---|---|
| acidification - acidification (incl. fate, average Europe total, A&B) | kg SO2-Eq | 0.35387 | 0.0195 | 0.00194 | 0.13354 |
| climate change - global warming potential (GWP100) | kg CO2-Eq | 190.32605 | 11.02558 | 0.95225 | 68.24511 |
| Eco toxicity: freshwater - freshwater aquatic Eco toxicity (FAETP info) | kg 1,4-DCB-Eq | 25.16185 | 2.30047 | 0.27255 | 18.58223 |
| Eco toxicity: marine - marine aquatic Eco toxicity (MAETP info) | kg 1,4-DCB-Eq | 5.39E+04 | 4284.00626 | 444.37347 | 2.95E+04 |
| Eco toxicity: terrestrial - terrestrial Eco toxicity (TETP info) | kg 1,4-DCB-Eq | 0.37883 | 0.03715 | 0.00416 | 0.27421 |
| energy resources: non-renewable - abiotic depletion potential (ADP): fossil fuels | MJ | 758.52159 | 155.12631 | 13.84844 | 998.77628 |
| eutrophication - eutrophication (fate not incl.) | kg PO4-Eq | 0.12 | 0.00501 | 0.00065 | 0.04267 |

| | | | | | |
|---|---|---|---|---|---|
| human toxicity - human toxicity (HTP info) | kg 1,4-DCB-Eq | 46.8588 | 7.06838 | 0.60742 | 42.32277 |
| material resources: metals/minerals - abiotic depletion potential (ADP): elements (ultimate reserves) | kg Sb-Eq | 0.00022 | 3.63E-05 | 2.40E-06 | 0.00017 |
| ozone depletion - ozone layer depletion (ODP steady state) | kg CFC-11-Eq | 6.79E-07 | 1.98E-07 | 3.98E-08 | 2.88E-06 |
| photochemical oxidant formation - photochemical oxidation (high NOx) | kg ethylene-Eq | 0.02445 | 0.00202 | 0.00016 | 0.01099 |

Table A 2. Absolute value results for M15 Hybrid mixture.

| Impact categories | Unit | A1-M15 Hybrid with Basalt and PP fibres | A2-M15 Hybrid with Basalt and PP fibres | A3-M15 Hybrid with Basalt and PP fibres | B1-M15 Hybrid with Basalt and PP fibres |
|---|---|---|---|---|---|
| acidification - acidification (incl. fate, average Europe total, A&B) | kg SO2-Eq | 0.38184 | 0.01987 | 0.00194 | 0.16935 |
| climate change - global warming potential (GWP100) | kg CO2-Eq | 200.0842 | 11.23932 | 0.95225 | 86.54548 |
| Eco toxicity: freshwater - freshwater aquatic Eco toxicity (FAETP info) | kg 1,4-DCB-Eq | 27.60392 | 2.34507 | 0.27255 | 23.56518 |
| Eco toxicity: marine - marine aquatic Eco toxicity (MAETP info) | kg 1,4-DCB-Eq | 5.90E+04 | 4367.055 | 444.3735 | 3.74E+04 |
| Eco toxicity: terrestrial - terrestrial Eco toxicity (TETP info) | kg 1,4-DCB-Eq | 0.41944 | 0.03787 | 0.00416 | 0.34774 |
| energy resources: non-renewable - abiotic depletion potential (ADP): fossil fuels | MJ | 1034.876 | 158.1336 | 13.84844 | 1266.605 |

| | | | | | |
|---|---|---|---|---|---|
| eutrophication - eutrophication (fate not incl.) | kg PO4-Eq | 0.13148 | 0.00511 | 0.00065 | 0.05412 |
| human toxicity - human toxicity (HTP info) | kg 1,4-DCB-Eq | 54.58419 | 7.20541 | 0.60742 | 53.6719 |
| material resources: metals/minerals - abiotic depletion potential (ADP): elements (ultimate reserves) | kg Sb-Eq | 0.00026 | 3.70E-05 | 2.40E-06 | 0.00021 |
| ozone depletion - ozone layer depletion (ODP steady state) | kg CFC-11-Eq | 9.79E-07 | 2.02E-07 | 3.98E-08 | 3.66E-06 |
| photochemical oxidant formation - photochemical oxidation (high NOx) | kg ethylene-Eq | 0.0273 | 0.00205 | 0.00016 | 0.01394 |

Table A 3. Absolute value results for Nominal mixture 1:2:3

| Impact categories | Unit | A1-Nominal (1:2:3) | A2-Nominal (1:2:3) | A3-Nominal (1:2:3) | B1-Nominal (1:2:3) |
|---|---|---|---|---|---|
| acidification - acidification (incl. fate, average Europe total, A&B) | kg SO2-Eq | 0.40455 | 0.02031 | 0.00196 | 0.14048 |
| climate change - global warming potential (GWP100) | kg CO2-Eq | 220.0778 | 11.48498 | 0.95699 | 71.79374 |
| Eco toxicity: freshwater - freshwater aquatic Eco toxicity (FAETP info) | kg 1,4-DCB-Eq | 27.71514 | 2.39633 | 0.27605 | 19.54848 |
| Eco toxicity: marine - marine aquatic Eco toxicity (MAETP info) | kg 1,4-DCB-Eq | 5.83E+04 | 4462.507 | 451.9594 | 3.10E+04 |
| Eco toxicity: terrestrial - terrestrial Eco toxicity (TETP info) | kg 1,4-DCB-Eq | 0.43525 | 0.0387 | 0.00424 | 0.28846 |
| energy resources: non-renewable - abiotic depletion potential (ADP): fossil fuels | MJ | 869.7043 | 161.5899 | 13.90315 | 1050.711 |

| | | | | | |
|---|---|---|---|---|---|
| eutrophication - eutrophication (fate not incl.) | kg PO4-Eq | 0.13587 | 0.00522 | 0.00066 | 0.04489 |
| human toxicity - human toxicity (HTP info) | kg 1,4-DCB-Eq | 52.0784 | 7.3629 | 0.61318 | 44.52349 |
| material resources: metals/minerals - abiotic depletion potential (ADP): elements (ultimate reserves) | kg Sb-Eq | 0.00024 | 3.78E-05 | 2.42E-06 | 0.00017 |
| ozone depletion - ozone layer depletion (ODP steady state) | kg CFC-11-Eq | 7.85E-07 | 2.06E-07 | 4.00E-08 | 3.03E-06 |
| photochemical oxidant formation - photochemical oxidation (high NOx) | kg ethylene-Eq | 0.02771 | 0.0021 | 0.00016 | 0.01156 |

Appendix B.1. Relative values for M15 Conventional

| Impact categories | Unit | A1-M15 conventional | A2-M15 conventional | A3-M15 conventional | B1-M15 conventional |
|---|---|---|---|---|---|
| acidification - acidification (incl. fate, average Europe total, A&B) | kg SO2-Eq | 100% | 6% | 1% | 38% |
| climate change - global warming potential (GWP100) | kg CO2-Eq | 100% | 6% | 1% | 36% |
| Eco toxicity: freshwater - freshwater aquatic Eco toxicity (FAETP info) | kg 1,4-DCB-Eq | 100% | 9% | 1% | 74% |
| Eco toxicity: marine - marine aquatic Eco toxicity (MAETP info) | kg 1,4-DCB-Eq | 100% | 8% | 1% | 55% |
| Eco toxicity: terrestrial - terrestrial Eco toxicity (TETP info) | kg 1,4-DCB-Eq | 100% | 10% | 1% | 72% |
| energy resources: non-renewable - abiotic depletion potential (ADP): fossil fuels | MJ | 76% | 16% | 1% | 100% |
| eutrophication - eutrophication (fate not incl.) | kg PO4-Eq | 100% | 4% | 1% | 36% |

| | | | | | |
|---|---|---|---|---|---|
| human toxicity - human toxicity (HTP info) | kg 1,4-DCB-Eq | 100% | 15% | 1% | 90% |
| material resources: metals/minerals - abiotic depletion potential (ADP): elements (ultimate reserves) | kg Sb-Eq | 100% | 16% | 1% | 77% |
| ozone depletion - ozone layer depletion (ODP steady state) | kg CFC-11-Eq | 24% | 7% | 1% | 100% |
| photochemical oxidant formation - photochemical oxidation (high NOx) | kg ethylene-Eq | 100% | 8% | 1% | 45% |

Appendix B. 2. Relative values for hybrid mixture

| Impact categories | Unit | A1-M15 hybrid | A2-M15 hybrid | A3-M15 hybrid | B1-M15 hybrid |
|---|---|---|---|---|---|
| acidification - acidification (incl. fate, average Europe total, A&B) | kg SO2-Eq | 100% | 5% | 1% | 44% |
| climate change - global warming potential (GWP100) | kg CO2-Eq | 100% | 6% | 0% | 43% |
| Eco toxicity: freshwater - freshwater aquatic Eco toxicity (FAETP info) | kg 1,4-DCB-Eq | 100% | 8% | 1% | 85% |
| Eco toxicity: marine - marine aquatic Eco toxicity (MAETP info) | kg 1,4-DCB-Eq | 100% | 7% | 1% | 63% |
| Eco toxicity: terrestrial - terrestrial Eco toxicity (TETP info) | kg 1,4-DCB-Eq | 100% | 9% | 1% | 83% |
| energy resources: non-renewable - abiotic depletion potential (ADP): fossil fuels | MJ | 82% | 12% | 1% | 100% |
| eutrophication - eutrophication (fate not incl.) | kg PO4-Eq | 100% | 4% | 0% | 41% |
| human toxicity - human toxicity (HTP info) | kg 1,4-DCB-Eq | 100% | 13% | 1% | 98% |

| | | | | | |
|---|---|---|---|---|---|
| material resources: metals/minerals - abiotic depletion potential (ADP): elements (ultimate reserves) | kg Sb-Eq | 100% | 14% | 1% | 81% |
| ozone depletion - ozone layer depletion (ODP steady state) | kg CFC-11-Eq | 27% | 6% | 1% | 100% |
| Impact categories | Unit | A1-M15 hybrid | A2-M15 hybrid | A3-M15 hybrid | B1-M15 hybrid |

Appendix B.3. Relative results comparison of Nominal 1:2:3 mixture.

| Impact categories | Unit | A1-Nominal (1:2:3) | A2-Nominal (1:2:3) | A3-Nominal (1:2:3) | B1-Nominal (1:2:3) |
|---|---|---|---|---|---|
| acidification - acidification (incl. fate, average Europe total, A&B) | kg SO2-Eq | 100% | 5% | 0% | 35% |
| climate change - global warming potential (GWP100) | kg CO2-Eq | 100% | 5% | 0% | 33% |
| Eco toxicity: freshwater - freshwater aquatic Eco toxicity (FAETP info) | kg 1,4-DCB-Eq | 100% | 9% | 1% | 71% |
| Eco toxicity: marine - marine aquatic Eco toxicity (MAETP info) | kg 1,4-DCB-Eq | 100% | 8% | 1% | 53% |

| | | | | | |
|---|---|---|---|---|---|
| Eco toxicity: terrestrial - terrestrial Eco toxicity (TETP info) | kg 1,4-DCB-Eq | 100% | 9% | 1% | 66% |
| energy resources: non-renewable - abiotic depletion potential (ADP): fossil fuels | MJ | 83% | 15% | 1% | 100% |
| eutrophication - eutrophication (fate not incl.) | kg PO4-Eq | 100% | 4% | 0% | 33% |
| human toxicity - human toxicity (HTP info) | kg 1,4-DCB-Eq | 100% | 14% | 1% | 85% |
| material resources: metals/minerals - abiotic depletion potential (ADP): elements (ultimate reserves) | kg Sb-Eq | 100% | 16% | 1% | 71% |
| ozone depletion - ozone layer depletion (ODP steady state) | kg CFC-11-Eq | 26% | 7% | 1% | 100% |
| photochemical oxidant formation - photochemical oxidation (high NOx) | kg ethylene-Eq | 100% | 8% | 1% | 42% |

Appendix C.1. Hotspot Contribution of Individual Materials (%) in the A1 Stage for Conventional, Hybrid, and Nominal Concrete Mixes.

| | cement % | gravel % | sand % | admixture % | PP % | basalt fibre % |
|---|---|---|---|---|---|---|
| M15 Conventional | 79.57 | 11.81 | 8.62 | | | |
| M15 Hybrid | 73.74 | 10.95 | 7.99 | 3.89 | 2.64 | 0.79 |
| Nominal (1:2:3 | 81.2 | 6.43 | 12.37 | | | |

Appendix C.2. Percentage Contribution of Raw Materials to $GWP_{100}$ in the A1 Stage for Conventional, Hybrid, and Nominal Concrete Mixes.

| | cement % | gravel % | sand % | admixture % | PP % | basalt fibre % |
|---|---|---|---|---|---|---|
| M15 Conventional | 92.41 | 4.55 | 3.04 | | | |
| M15 Hybrid | 87.9 | 4.33 | 2.89 | 2.06 | 1.69 | 1.12 |
| Nominal (1:2:3 | 93.24 | 2.45 | 4.31 | | | |